This is a pre-print of an article published in SPACE SCIENCE REVIEWS.

Plainaki, C., et al. (2018). Towards a Global Unified Model of Europa's Tenuous Atmosphere. SPACE SCIENCE REVIEWS, vol. 214, p. 1-71

The final authenticated version is available online at: https://doi.org/10.1007/s11214-018-0469-6

Questo documento contiene la versione iniziale presentata all'editore dell'articolo

Plainaki, C., et al. (2018). Towards a Global Unified Model of Europa's Tenuous Atmosphere. SPACE SCIENCE REVIEWS, vol. 214, p. 1-71
accettato per la pubblicazione il 7 gennaio 2018.

Space Science Reviews

Towards a global unified model of Europa's tenuous atmosphere

--Manuscript Draft--

Manuscript Number:	
Full Title:	Towards a global unified model of Europa's tenuous atmosphere
Article Type:	Regular review paper
Keywords:	Europa; exosphere; plasma sheet; sputtering
Corresponding Author:	Christina Plainaki Rome, ITALY
Corresponding Author Secondary Information:	
Corresponding Author's Institution:	
Corresponding Author's Secondary Institution:	
First Author:	Christina Plainaki
First Author Secondary Information:	
Order of Authors:	Christina Plainaki
Order of Authors Secondary Information:	
Funding Information:	
Abstract:	Despite the numerous modeling efforts of the past, our knowledge on the radiation-induced physical and chemical processes in Europa's tenuous atmosphere and on the exchange of material between the moon's surface and Jupiter's magnetosphere remains limited. In lack of an adequate number of in situ observations, the existence of a wide variety of models based on different scenarios and considerations has resulted in a fragmentary understanding of the interactions of the magnetospheric ion population with both the moon's surface and neutral gas envelope. Models show large discrepancy in the source and loss rates of the different constituents as well as in the determination of the spatial distribution of the atmosphere and its variation with time. The existence of several models based on very different approaches highlights the need of a detailed comparison among them with the final goal of developing a unified model of Europa's tenuous atmosphere. The availability to the science community of such a model could be of particular interest in view of the planning of the future mission observations (e.g., ESA's JUICE mission, and NASA's Europa Clipper mission). We review the existing models of Europa's tenuous atmosphere and discuss each of their derived characteristics of the neutral environment. We also discuss discrepancies among different models and the assumptions of the plasma environment in the vicinity of Europa. A summary of the existing observations of both the neutral and the plasma environments at Europa is also presented. The characteristics of a global unified model of the tenuous atmosphere are, then, discussed. Finally we identify needed future experimental work in laboratories and propose some suitable observation strategies for upcoming missions.

Towards a global unified model of Europa's tenuous atmosphere

Christina Plainaki[1], Tim A. Cassidy[2], Valery I. Shematovich[3], Anna Milillo[4], Peter Wurz[5], Audrey Vorburger[5], Lorenz Roth[6], André Galli[5], Martin Rubin[5], Aljona Blöcker[7], Pontus C. Brandt[8], Frank Crary[2], Iannis Dandouras[9], Xianzhe Jia[10], Davide Grassi[4], Paul Hartogh[11], Alice Lucchetti[12], Melissa McGrath[13], Valeria Mangano[4], Alessandro Mura[4], Stefano Orsini[4], Chris Paranicas[8], Aikaterini Radioti[14], Kurt D. Retherford[15,16], Joachim Saur[7], Ben Teolis[15]

(1) *Agenzia Spaziale Italiana, Via del Politecnico snc, 00133 Rome, Italy,*
email: christina.plainaki@asi.it; *tel*.:+39 068567253
(2) *Laboratory for Atmospheric and Space Physics, University of Colorado, 3665 Discovery Dr., Boulder, USA*
(3) *Department of Solar system studies, Institute of Astronomy of the Russian academy of sciences, INASAN, 48 Pyatnitskaya str., Moscow 119017, Russian Federation.*
(4) *INAF-IAPS, Via del Fosso del Cavaliere 100, 00133, Rome, Italy*
(5) *Physikalisches Institut, University of Bern, Sidlerstrasse 5, CH-3012 Bern, Switzerland*
(6) *School of Electrical Engineering, KTH Royal Institute of Technology, SE-100 44 Stockholm, Sweden*
(7) *Universität zu Köln, Institut für Geophysik und Meteorologie, Albertus Magnus-Platz, D-50923 Köln, Germany*
(8) *The Johns Hopkins University Applied Physics Laboratory, 11100 Johns Hopkins Road, Laurel, MD 20723, USA*
(9) *IRAP, CNRS and University of Toulouse, 9 Avenue du Colonel Roche, 31400 Toulouse, France*
(10) *Department of Climate and Space Sciences and Engineering, University of Michigan, 2455 Hayward St., Ann Arbor, MI 48109-2143*
(11) *Max Planck Institute for Solar System Research, Justus-von-Liebig-Weg 3, 37077 Göttingen, Germany*
(12) *INAF - Astronomical observatory of Padova, Vic. Osservatorio 5, 35122 Padova PD, Italy*
(13) *SETI Institute, Mountain View, California, USA.*
(14) *Laboratoire de Physique Atmosphérique et Planétaire, Institut d'Astrophysique et de Géophysique, Université de Liège,* 4000 Liege, Belgium
(15) *Southwest Research Institute, San Antonio, Texas, USA*
(16) *Department of Physics and Astronomy, University of Texas at San Antonio, San Antonio, Texas, USA*

12 June 2017

Abstract

Despite the numerous modeling efforts of the past, our knowledge on the radiation-induced physical and chemical processes in Europa's tenuous atmosphere and on the exchange of material between the moon's surface and Jupiter's magnetosphere remains limited. In lack of an adequate number of in situ observations, the existence of a wide variety of models based on different scenarios and considerations has resulted in a fragmentary understanding of the interactions of the magnetospheric ion population with both the moon's surface and neutral gas envelope. Models show large discrepancy in the source and loss rates of the different constituents as well as in the determination of the spatial distribution of the atmosphere and its variation with time. The existence of several models based on very different approaches highlights the need of a detailed comparison among them with the final goal of developing a unified model of Europa's tenuous atmosphere. The availability to the science community of such a model could be of particular interest in view of the planning of the future mission observations (e.g., ESA's JUICE mission, and NASA's Europa Clipper mission). We review the existing models of Europa's tenuous atmosphere and discuss each of their derived characteristics of the neutral environment. We also discuss discrepancies among different models and the assumptions of the plasma environment in the vicinity of Europa. A summary of the existing observations of both the neutral and the plasma environments at Europa is also presented. The characteristics of a global unified model of the tenuous atmosphere are, then, discussed. Finally we identify needed future experimental work in laboratories and propose some suitable observation strategies for upcoming missions.

Keywords: Europa, exosphere, plasma sheet, sputtering

Acknowledgements: The work in this paper has been performed in the context of the activities of the ISSI International Team #322: "Towards a global unified model of Europa's exosphere in view of the JUICE mission" http://www.issibern.ch/teams/exospherejuice/. P.C.B was supported by NASA Grant NNX12AG81G. A.R. is funded by the Belgian Fund for Scientific Research (FNRS). V. Shematovich was supported by the Russian Science Foundation (RSCF).

Table of Contents

1. Introduction

Jupiter's moon Europa possesses a tenuous atmosphere, generated predominantly through the interaction of the plasma environment with the moon's icy surface and characterized by a quasi-collisionless gas (Burger and Johnson 2004; Burger et al. 2010; Coustenis et al. 2010; Johnson et al. 2008; McGrath et al. 2009). There is general consensus that this atmosphere is generated, predominantly, through ion sputtering of the moon's icy surface upon its bombardment by magnetospheric energetic ions, including O^{n+}, S^{n+}, H^{+} with energies from ~10s of keV to several MeV (Ip et al. 1998; Paranicas et al. 2002; Plainaki et al. 2012) and plasma ions with thermal energies of ~100 eV (Ip 1996; Bagenal et al. 2015; Cassidy et al. 2013; Eviatar et al. 1985). Some species in the surface and the atmosphere are the result of radiolysis. Water is expected to be the dominant sputtered species, whereas significant amounts of O_2 and H_2 are released from the surface through a two-step process: water molecules dissociate generating different molecules (e.g. OH, H, H_2, O) which further react chemically to produce, mainly, O_2 and H_2 (Bahr et al. 2001). Moreover, sublimation of water ice in the illuminated hemisphere may result in a locally denser atmosphere (e.g. Smyth and Marconi 2006). Recently, Roth et al. (2014b) suggested that transient water plumes may provide additional material to the atmosphere. Importantly, the morphology of the related UV-photon emission could not be interpreted without some a priori assumptions on the atmosphere and plasma electron spatial distributions derived from previous Galileo and Voyager mission measurements. Photon-stimulated desorption of water-ice might also provide some atmospheric particle contribution, although estimations based on laboratory data show that this mechanism, in general, is not the dominant one (Plainaki et al. 2010). However, increased UV photon fluxes illuminating the icy surface during periods of intense solar activity (i.e., during solar flares) may result in an increased water release from the surface. Meteoroid impact vaporization by high-speed interplanetary dust particles is another possible atmospheric source (Cooper et al. 2001; Koschny and Grün 2001; Schultz 1996).

Based on current knowledge, molecular oxygen is likely the most abundant species in Europa's atmosphere because it does not stick to the surface (like H_2O does), nor does it easily escape the moon's gravity (like H_2 does) (Johnson et al. 2008). The available Hubble Space Telescope (HST) observations (Hall et al. 1995; McGrath et al. 2009; Roth et al. 2016) of UV emissions from O atoms were reported to be consistent with the concept of an atmosphere dominated by O_2. Cassini/UVIS instrument measurements of more extended UV oxygen emissions are diagnostic of escaping oxygen atoms (Hansen et al. 2005). Although the generation mechanisms of atmospheric O_2 have been discussed many times in the past, there is still a considerable uncertainty in the calculation of the atmosphere source/loss rates and the respective density scale heights. For example, the production of Europa's atmosphere and its variation in space and time may be very sensitive to the deflection of thermal ions by the interaction currents – a major feed-back mechanism (Bagenal et al. 2015; Rubin et al. 2015).

The existence of a wide variety of models based on different scenarios (e.g. assuming either the collisional (Shematovich et al. 2005; Smyth and Marconi 2006) or the collisionless (Cassidy et al. 2007; Plainaki et al. 2012) approximation) and different considerations (e.g. spatially uniform (or not) source/loss rates) has resulted in our understanding of Europa's neutral gas environment still being incomplete. In view of the planning of future observations of Europa's atmosphere, the need for an overall revision for the determination of a largely accepted unified model of this environment becomes necessary.

Europa's exosphere, the uppermost region of the atmosphere, is spatially confined only by its lower boundary, the exobase, which is defined as the altitude, h_{exo}, at which the mean free path of a molecule, $\lambda(h_{exo}) = (n(h) \cdot \sigma)^{-1}$, is equal to the scale height, $H(h_{exo}) = k_B T(h_{exo})/mg(h_{exo})$ (thermal gas case). Since h_{exo} is different for different atmospheric species, it is deduced that the exobase is an extended region rather than a thin layer located at a single altitude. Equivalently to the above definition, Europa's exobase is the region where the Knudsen number is equal to ~1, $Kn = \lambda(h)/H(h) \sim 1$, whereas below the exobase it is $Kn < 1$. The particle motion in the tenuous atmosphere of Europa can be described, in general, through the Boltzmann equation of kinetic theory, which is valid for the whole range of Kn. Contrary to other solar system bodies with dense atmospheres, the region between the moon's surface and the exobase at Europa is characterized by a Knudsen number ranging between 0.1 and 1 for O_2 (Figure 1). In this region, the atmospheric molecules have mean free paths of significant length to lead to local energy distributions not being in thermal equilibrium. Due to the relatively high Kn values, this region can be considered as an extended boundary (or Knudsen) layer, where the few collisions are not enough to create thermodynamic equilibrium of the molecules, in contrast to a collision-dominated region where a hydrodynamics regime is valid. This boundary layer (with a width of about a few mean free paths) is of particular interest because it can be considered as an extension of Europa's surface to the actual lower atmospheric boundary and, therefore, an indicator of the surface composition and chemistry. The particle motion in the extended Knudsen layer can be described through Direct Simulation Monte Carlo (DSMC) models (e.g., Shematovich et al. 2005; Smyth and

Marconi 2006), where the solution of the Boltzmann equation for suprathermal atoms and molecules is achieved through the use of Monte Carlo algorithms. In the exospheric region, i.e., $Kn > 1$, a free molecular dynamics regime is valid and collisionless numerical Monte Carlo models can be applied (e.g., Cassidy et al. 2007; Plainaki et al. 2012; Wurz et al. 2014). Analytical models, where the atmosphere density profile is approximated by an exponential form with either given scale height(s) (e.g. Johnson, 1990; Milillo et al. 2016), or depletion length scale (see Saur et al. 1998) are also available.

To distinguish regions of validity of the existing atmospheric models and to attempt to search for convergence among them, it is fundamental to answer the following question: at what altitude is Europa's exobase located and how thick is the Knudsen boundary layer? Such information is fundamental for defining the different regimes of molecular dynamics and for determining the efficiency of the different plasma-neutral interactions. To answer such a question, in the absence of pertaining in situ observations, only modeling, based on the available remote/in situ observations, and laboratory measurements can be made. In the following sections we present the complexity of the different assumptions, given the large number of unknown environment parameters at Europa. We briefly present the problems related to the definition of the structure of Europa's atmosphere, and we perform an in depth comparison of existent atmospheric models. Specifically, we present a summary of the available UV and VIS observations of Europa's atmosphere (Section 2.1), of the plasma, energetic ions and magnetic field observations (Section 2.2), and of the torus of Energetic Neutral Atoms (Section 2.3). In Section 3 we present the current state of modeling of Europa's environment. In Section 3.1 we compare different plasma and MHD models. In Section 3.2 we focus in the environmental modeling and we discuss both the different modeling techniques and their implementation and we perform a detailed comparison among them. Based on this comparison, we define in Section 3.3 the characteristics of a global unified model of Europa's atmosphere and in Section 3.4 we assess possible future lab-experimental work required to constrain the model. In Section 4, in view of future missions to Europa, we suggest some observation strategies that could be useful for the determination of the atmosphere generation mechanism. Finally, in Section 5 we present the conclusions of the current work.

2. Review of the available observations of Europa's neutral and plasma environment

2.1. Summary of the available UV and VIS observations of Europa's atmosphere

Europa's neutral gas environment can so far be directly observed only through atomic emissions or absorption, which have been detected from oxygen (O), sodium (Na), potassium (K) and hydrogen (H). Other than at the neighboring moon Io where several molecular atmospheric species such as SO_2, SO, NaCl and other species have been measured at various wavelengths (e.g., Lellouch et al. 1996; Spencer et al. 2005), no molecules have yet been directly measured in Europa's more tenuous gas environment. In the case of the detected far-ultraviolet O emissions, the measured relative brightness of the optically allowed transition at 1304 Å and the semi-forbidden transition at 1356 Å unambiguously identify dissociative excitation of O_2 from electron impact as a source mechanism. Hence, these observations provide indirect evidence for O_2 in the atmosphere. The presence of a variety of other species is also inferred indirectly, including H_2, H_2O, SO_2, and Cl.

We will first describe the available far-ultraviolet measurements that provide by far the most information on the bulk atmosphere to date and are thus the most important benchmark for the validation of atmosphere modeling efforts. Thereafter, we describe the observations of trace species including some results on modeling efforts to interpret these measurements.

2.1.1 Ultraviolet observations of Europa's oxygen atmosphere

A comprehensive overview of observations of Europa's atmosphere until 2008 was provided by McGrath et al. (2009). Their Table 1 summarizes numerous details of the atmosphere-related observations and the respective publications. Since then, three Hubble Space Telescope (HST) campaigns have been performed with multiple imaging observations by the Space Telescope Imaging Spectrograph (STIS) between November 2012 and April 2015 (Roth et al. 2016). Principally confirming the results and interpretations detailed in McGrath et al. (2009), this HST dataset exceeds the previous data in accuracy of the measured emissions, in the coverage of Europa's longitudes and orbital positions, and often also in spatial resolution.

The first unambiguous detection of Europa's atmosphere (see Figure 2) was achieved through far-ultraviolet observations by the HST Goddard High Resolution Spectrograph (GHRS) (Hall et al. 1995). The spectrum revealed oxygen emissions, which exceed the solar oxygen lines that are reflected from the surface of Europa and which hence originate from Europa's neutral gas environment. Like this first spectrum from 1994 (Hall et al. 1995), two follow-up observations (Hall et al. 1998) consistently measured brighter oxygen emissions from the semi-forbidden oxygen doublet OI ($^5S^0 - {}^3P$) 1356 Å than from the optically allowed oxygen multiplet OI ($^3S^0 - {}^3P$) 1304 Å.

After elimination of all emissions from sources other than Europa like the sometimes bright scattered light from the geocorona, there are several general processes contributing to the observed oxygen signal from Europa:

1) Solar emission lines and continuum photons reflected from the surface
2) Resonance fluorescence scattering of solar lines by atoms in the atmosphere
3) Electron impact excitation of O atoms or dissociative excitation of oxygen bearing molecules such as O_2, H_2O, or CO_2, to produce excited O atoms.

At far-ultraviolet wavelengths the surface albedo and continuum solar incident flux are more than an order of magnitude lower than at visible wavelengths leading to a very faint signal of light reflected off the surface. This is ideal when searching for faint atmospheric emissions. Only at the hydrogen Lyman-α line is the solar flux higher, generating a brighter surface-reflection signal despite the low FUV albedo of 1-2%. The procedure to determine and eliminate the surface-reflection contributions (1) is to adjust a solar spectrum to the measured brightness in a wavelength range where no atmospheric emissions are expected. In the case of the GHRS spectra, the singly ionized carbon emission line at 1335 Å is used to calibrate the solar flux from the surface, which is then subtracted, see Figure 2.

The relative brightness of the remaining oxygen emissions at 1304 Å and 1356 Å effectively constrains the primary atmospheric source process (1 and 2). In the GHRS spectra (as well as in all subsequent observations of the near-surface atmosphere), the OI 1356 Å line was consistently brighter by factor of 1.3-2.2. Because the OI 1356 Å transition is spin-forbidden, most processes produce brighter

OI 1304 Å emissions. Resonant scattering by oxygen atoms (2) is only effective for the 1304 Å emission. In the cases of electron-excited emissions, only dissociation of molecular oxygen, O_2, produces brighter OI 1356 Å emission, while electron impact on other potential atmospheric species like O, H_2O and CO_2 produces brighter OI 1304 Å emission (Ajello et al. 1971; Makarov et al. 2004; Itikawa 2009). The highest cross sections for O excitation are measured for electron impact on O and O_2. The relative excitation rates - calculated with the assumption of Maxwellian distributed electron population around one core temperature (Figure 3) – unambiguously differentiates between a primary O atmosphere with an expected 1356-Å/1304-Å ratio of <0.5, and a primary O_2 atmosphere with an expected ratio of >2. The measured 1356-Å/1304-Å ratio of ~2 and this principal conclusion on the O_2 being the main source still holds to date. A proposed optically thick pure O atmosphere (Shemansky et al. 2014) is in fact neither in agreement with any observation of the near-surface bound atmosphere nor with the theory of optical thickness, and is based on unsubstantiated assumptions about the plasma conditions for electron excitation, see Roth et al. (2016) for more details.

To derive atmospheric abundances, one needs to consider the properties and flow of the exciting electrons. The first approach by Hall et al. (1995; 1998) was to make the simplifying assumption that Europa is surrounded by homogeneous thermal plasma that constantly excites the atmosphere at a rate given by the temperature and the density of the electrons and the collisional excitation rates (Figure 3a). They assume an electron density of 40 cm^{-3} measured by Voyager and a dominant cold component with T = 20 eV, and a T = 250 eV hot component with a mixing ratio between hot and cold of 0.05. For an optically thin atmosphere and constant electron parameters, the measured brightness I in Rayleighs relates to a column density N along the viewing direction through

$$N\,[\mathrm{cm^{-2}}] = 10^{10}\,\frac{I\,[\mathrm{R}]}{n_e\,[\mathrm{cm^{-3}}]\;f(T_e)\,[\mathrm{cm^{3}s^{-1}}]} \qquad (1)\,,$$

with the temperature-dependent electron-impact excitation rate $f\,(T_e)$ and electron density n_e. Based primarily on the OI1356 Å brightness between 70 R and 90 R and the uncertainties in the GHRS spectra, Hall et al. (1998) derived a range of (2.4 – 14) × 10^{14} cm^{-2} for the line-of-sight O_2 column density across Europa's disk.

The first disk-resolved observations of the oxygen 1304 Å and 1356 Å emissions were taken in 1999 by HST/STIS. They revealed an irregular pattern with an emission surplus in the northern anti-Jovian quadrant (McGrath et al. 2004; 2009). This inhomogeneity was speculated to be of atmospheric origin (e.g., Cassidy et al. 2007), but is likely explained by the inhomogeneous and variable plasma environment, as we will elaborate later.

Thereafter, the Ultraviolet Imaging Spectrograph (UVIS) of the Cassini spectrograph measured an extended atomic oxygen atmosphere in addition to the bound molecular oxygen atmosphere (Hansen et al. 2005). The UVIS observations also confirmed the stronger OI 1356 Å emissions in the resolution element covering the moon and the nearest environment and Hansen et al. 2005 also conclude an O_2-dominated bound atmosphere. Additionally, images of visible emissions in eclipse were taken by Cassini's Imaging Science Camera Subsystem (ISS) (Porco et al. 2003). The atmospheric brightness of a few kiloRayleigh in the wavelength range between 200 and 1050 nm can possibly originate from various species including oxygen, but were assigned to electron-excited sodium, see next section.

During the Jupiter flyby of the New Horizons spacecraft in spring 2007, the ALICE UV imaging spectrograph observed Europa several times. UV spectra were obtained from large distances and the disk of Europa was not resolved. High levels of radiation environment induced noise in the detector combined with high levels of instrument stray light in the instrument in several spectra decreased the data quality. The seven best spectra were combined to improve signal to noise and are presented here in Figure 4. This average UV spectrum, together with the individual spectra of more limited quality, confirmed that the measured disk-averaged 1356-Å/1304-Å ratio of ~2 is consistent and as expected. While STIS was not in operation in 2007, several HST campaigns utilized the Advanced Camera for Surveys (ACS) and the Wide-Field Planetary Camera 2 (WFPC2) to observe Europa's UV and visible emissions. WFPC2 images taken in eclipse with several near-UV and visible filters did not reveal measurable atmospheric emissions, and ACS images in and out of eclipse taken in the same program confirmed the known UV oxygen emissions, but were not analyzed quantitatively (Sparks et al. 2010).

A set of four 10-min exposures with the ACS Solar Blind Channel (SBC) F125LP filter was obtained during an eclipse event during the New Horizons Jupiter flyby. These images contain varying levels of foreground Earth airglow background noise. Also the location of Europa within the images is uncertain to within a Europa radius, and a limb brightening morphology in the second image in the series is relied upon for centering the moon disk in their average shown in Figure 5 (middle).

Another ACS program provided again hints for an asymmetric oxygen UV morphology, which was compared to tidal stress pattern on surface cracks to assess the possibility of outgassing for the generation of an atmospheric inhomogeneity (Saur et al. 2011). Furthermore, this analysis pointed out a relation of the UV brightness to Europa's position within the magnetosphere.

The first spectral UV images taken after the repair of STIS held a surprise. They revealed bright localized hydrogen emission near the south pole in addition to the atmospheric oxygen emissions. The localized nature of these emissions and the relative brightness of the coincident OI 1304 Å emission surplus in the same region are consistent with the existence of local water vapor eruptions on the anti-Jovian southern hemisphere (Roth et al. 2014b). Follow-up observations from early 2014 could not confirm an initially hypothesized connection of the detectability of such plume emissions with Europa's orbital position and the changing tidal stresses (Roth et al. 2014a).

During a following observing campaign with STIS, aurora UV images were obtained on 15 days between November 2014 until April 2015 at various orbital positions and geometries (Roth et al. 2016). The analysis of the OI 1304 Å and OI 1356 Å images from all previous STIS campaigns (1999, 2012, 2014, 2015) provided the most comprehensive picture of Europa's oxygen aurora and its dependencies and systematic changes. The emerging picture is a systematically varying aurora that is closely connected to the changing plasma environment. The emissions are brightest in the polar regions where the ambient Jovian magnetic field line is normal to Europa's disk. Near the equator, where bright spots are found at Io, Europa's aurora is faint suggesting a general difference in how the plasma interaction shapes the aurora at Io and Europa.

An unexplained, yet consistently detected characteristic is that the aurora is brighter on the dusk side than on the dawn side. In terms of local time on Europa, the brighter right hemisphere always coincides with the afternoon or dusk region, while the left hemisphere corresponds always with the morning/dawn region. Hence, dependencies of the sources or losses of the atmosphere on the local time through the changing solar illumination could generate such an asymmetry in the atmosphere and aurora. For example, radiolysis rates are temperature dependent hence they possibly differ in the morning and afternoon regions (Plainaki et al. 2013). However, the dusk/dawn asymmetry is not necessarily related to local time effects.

The initially detected 1356Å/1304Å brightness ratios from Hall et al. (1995; 1998) were generally confirmed by the STIS observations with measured ratios between 1.5 and 2.8 and a mean ratio of exactly 2.0 (Roth et al. 2016). The 1356Å/1304Å ratio decreases with increasing altitude in agreement with a more extended atomic O corona (Hansen et al. 2005), but O_2 prevails at least up to altitudes of 900 km. Differing 1356Å/1304Å line ratios on the plasma upstream and downstream hemispheres require differing O mixing ratio in the near-surface O_2 atmosphere as shown in Figure 3(b). While lower ratios on the upstream side are in best agreement with higher O concentration of ~5%, the higher 1356Å /1304Å ratio on the downstream side suggest that hardly any O is present there (1% or less). The difference in abundance is likely related to differences in the production of atomic oxygen. Electron impact dissociation of O_2 is thought to be more efficient on the upstream side, but also longitudinal differences in ion sputtering and radiolysis might have an effect on the O mixing ratio. During several eclipse observations, the aurora does not reveal any signs of systematic changes compared to the sunlit images suggesting no or only weak influence of sunlight on the aurora and an optically thin atmosphere.

Shortly before and following the plume aurora detection another effort to probe Europa's neutral gas environment with the Hubble Space Telescope was made by a group around W. Sparks. During several campaigns the moon was observed in and out of transit to search for anomalies around the limb. The results from these observations indeed provided possible supporting evidence for plumes (Sparks et al. 2016). The imaging method used in these measurements preclude a spectral identification of the absorbing species as water and/or otherwise.

In a recent study, Roth et al. (2017) detected an extended corona of hydrogen, which attenuates Jupiter H Ly-alpha dayglow through resonant scattering. The detected amount of H confirms abundances predicted by Monte Carlo simulations (Smyth & Marconi, 2006).

A recent comprehensive assessment of the Galileo plasma measurements near Europa's orbit by Bagenal et al. (2015) shows that the electron density of 40 cm^{-3} commonly assumed to derive atmospheric abundances is in fact at the lower end of the electron densities measured during the Galileo era (1995-2003). So, if the electron density was underestimated, the atmospheric abundances were potentially overestimated when using the simple conversion after Equation (1). Figure 3(c) shows brightness isolines as a function of both neutral column density and electron density for the approximate range reported by Bagenal et al. (2015). It is important to keep in mind here that the aurora brightness is always a measurement of the product of the two densities. Derived atmosphere abundances are therefore subject to the uncertainty of the plasma environment in addition to the fact that the non-linear processes of the aurora generation and the electro-dynamic interaction of the atmosphere with the magnetosphere (e.g., Kivelson et al. 2004; Saur et al. 1998) are neglected in Equation (1).

2.1.2 Visible observations of trace species

The sodium atmospheric component was discovered in 1996 by Brown and Hill (1996), who detected the emission lines at 5890–5896 Å of an extended escaping component up to 25 R_E. The Na D_2/D_1 ratio of 1.7 was consistent with resonantly scattered sunlight by an optically thin atmosphere from which a surface density of ~70 atoms cm^{-3} was derived. Its origin is still debated, whether it is endogenic, i.e., coming from Europa's subsurface and released from the surface via radiolysis of hydrated salts, or exogenic and coming from Io extended sodium cloud. A column density of ~10^{10} cm^{-2} was derived (Brown 2001).

Potassium in the extended exosphere of Europa was first observed in 1998 (Brown 2001) using Keck/HIRES. Simultaneous observations of potassium and sodium were performed and the Na/K ratio of 25 ± 3 was derived. Vertical profiles in the region between 5 and 15 Europa radii (R_E) were obtained and column densities of (5–15)×10^7 cm^{-2} for K, and (1–4)×10^9 cm^{-2} for Na derived. The Na/K ratio results to be intermediate between values measured elsewhere in the solar system, ranging from 2 in the Earth crust up to almost 200 on Mercury's surface (Potter and Morgan, 1997; Killen et al. 2007), with the solar system value being 15 (Loggers and Fegley 1998), and very close to cosmic abundance value of 20 (Allen 1991). The icy surface of Europa and resurfacing processes with salt deposition and aqueous alteration are surely involved in the Na/K ratio, probably leading to different ratios in the gaseous (exosphere), solid (surface) and liquid (subsurface) components. A recent report by Hörst and Brown (2013) of a search for atmospheric magnesium at the strong 2852 Å resonant scattering emission line using HST/FOS data only provided upper limits. The derived Mg column density upper limits of $2{\cdot}10^{10}$ cm^{-2} at 8.8 R_E and $9{\cdot}10^{9}$ cm^{-2} at 14.4 R_E indicate that the Mg abundance in Europa's atmosphere is lower than meteoritic and cosmic abundances, giving rise to two possible explanations: either Mg is not present in the surface at sufficient abundance, the release process of sputtering is less efficient compared to Na and K, or the Na and K on Europa's surface are enhanced by a contribution from Io.

Modeling of the sodium exosphere (Leblanc et al. 2002) used a 3D Monte Carlo model to reconstruct source processes, energy distribution, and flux of ejected Na. The dominant release process is confirmed to be ion-induced sputtering that, acting on a water ice surface, will produce the inferred and observed column densities of O_2, Na and K. Na is released in the atomic form plus a small component as NaO or NaS; its ejection velocity and spatial distribution depends on the surface regions in terms of the proportion of ices or refractory species. Estimated exospheric loss of Na is (5–10)×10^{6} atoms cm^{-2} s^{-1}. The model reproduces Na cloud asymmetries in both the –orbital plane due to the combined effects of Jupiter and Io, and in the vertical plane due to the combined effect of the centrifugal force and the gravity of Jupiter. Comparison with observed emission profiles at 20 R_E and beyond by Brown (at Keck in 1999 as reported in Leblanc et al. (2002)) help constrain the low energy component, the energetic tail component, and the background component respectively. In particular, an energetic tail occurs when corotating ions (O^+ and S^+ of tens of keV to MeV) and electrons sputter into a material with high excitation density (Johnson 1990). The background component instead can be produced by three possible sources: NaX dissociation, sputtering of dust grains and iogenic Na cloud. The latter is supported by the observed temporal variations. Finally, the sputtered Na flux is calculated to be $3{\cdot}10^{7}$ cm^{-2} s^{-1}, of which 60% returns to the surface (+10% of NaX) and 40% escapes. The net loss rate is (5–10)×10^{6} cm^{-2} s^{-1} and implantation rate for iogenic Na is (0.2–0.8)·10^{6} cm^{-2} s^{-1}; hence, the observed Na is likely of endogenic origin or another source is required to explain such values. The model is improved in Leblanc et al. (2005) by including leading/trailing asymmetry of ejecta, photoionization and heavy ions sputtering by O^{n+} and S^{n+} as source processes, interaction with the O_2 atmosphere and it is compared to an additional set of data.

Cipriani et al. (2008; 2009) update the model to account for non-uniform Na density distribution on the icy surface and for ejection of Na atoms by solar UV photons, and then apply it also to potassium, using the Na/K ratio as measured by Brown (2001). Three regions are identified with different values: beyond 3 R_E where Na/K = 20-25, between 1.5 and 2 where Na/K = 7, and between the two where a steep increase occurs. Depletion of K with increasing altitude is the reason for such profile, for the minimal energy required by Na atoms to reach 3 R_E is half the value needed by K. If Na average source rate is $3 \cdot 10^6$ cm^{-2} s^{-1}, then average K source rate is $1.8 \cdot 10^5$ cm^{-2} s^{-1}. Ionization altitude for Na is 230 km and for K is 200 km; that is 16% Na and 4.5% K are ionized.

2.2. Summary of the plasma and magnetic field observations and of their implications in Europa's exosphere

To investigate the plasma environment of Europa, it is necessary to consider the Io plasma torus and its effect on the environment of Europa. Pioneer 10 in 1973 provided in-situ plasma measurements, which were interpreted in terms of iogenic plasma only after the Voyager flybys (Intriligator and Miller 1981). Voyager 1 (1979) made a closest approach to Jupiter well inside Io's orbit and measured ion and electron properties of the Io plasma torus (Bagenal et al. 1980; Sittler and Strobel 1987). The Unified radio and Plasma Wave Experiment onboard Ulysses spacecraft in 1992 measured electron properties from plasma waves detected as Ulysses made a vertical cut through the Io torus at ~8 R_J (Hoang et al. 1993) and indicated that the torus electrons have supra-thermal tails. The plasma environment between Io and Europa is shown in Figure 7.

In 1995 with the arrival of Galileo spacecraft into orbit around Jupiter, the region around Io and Europa was visited several times. Observations from the Galileo plasma analyser (PLS) during two near encounters with Europa (E4 and E6 orbits) showed that the ions near Europa are a mix of thermalized torus plasma with approximately Maxwellian ion velocity distributions and partially thermalized pickup ions with ring distributions (Paterson et al. 1999). Based on these measurements, plasma moments, ion number densities, bulk flow velocities and ion temperatures were determined.

Bagenal et al. (2015) re-analyzed the PLS data to derive density, azimuthal speed and temperature, assuming that the dominant heavy ion species have an effective mass to charge ratio (M/Q) of 12 (Delamere et al. 2005) and using a forward-modeling technique to model a single isotropic Maxwellian ion species. Figure 8(a) shows the ion temperature as function of electron density derived from Galileo measurements between 8.9 and 9.9 R_J. Measurements within ~2.5 R_E of Europa are excluded, because they could have been affected by the plasma-moon interactions. The temperatures seen in Figure 8(a) are similar to those reported by Paterson et al. (1999). The electron density and ion temperature are inversely correlated, which is indicative of radiative cooling of the torus increasing at higher densities. Before flyby E12, the Plasma Wave Instrument (PWS) (Kurth et al. 2001) measured a particularly high density, while during E12 the magnetic fields were anomalously strong (Kivelson et al. 2009). These transient variations could be related to activity at Europa or to the fact that iogenic plasma passed by Galileo as it approached Europa.

The local electron density, N_e (measured by PWS), and the ion temperature and azimuthal speed (measured by PLS) are shown in the histograms of Figure 8(b). The azimuthal velocity presents a narrow distribution, while the density and temperature distributions have low- and high-energy tails, respectively.

The magnetic field around Europa has been investigated based on Galileo magnetometer measurements. Schilling et al. (2004) investigated the presence of a fixed dipole moment in the interior of the moon, based on data acquired during four passes by Europa. They suggested a small contribution of a permanent dipole moment with an upper limit of 25 nT, which is small compared to the magnitude of the induced magnetic field. Figure (9) shows the observed and modeled field for a Europa flyby, as reported by Schilling et al. (2004)..

Europa's orbital eccentricity (0.0094) produces a ~30 nT variation in the magnetic field magnitude. Figure (10) provides a statistical view of the magnetic field experienced by Europa (Bagenal et al. 2015). The histograms are constructed based on binning of the values of the three model field components B_r, B_{th}, B_{ph} and the magnitude B_{mag} of the internal VIP4 (Connerney et al. 1998) and the Khurana model (Khurana 1997) at Europa's mean orbital distance. Even though the neutral gas environment of Europa is tenuous is still a barrier to magnetospheric ion bombardment. The magnetospheric plasma flow diverts around Europa due to the ionospheric conductivity (Saur et al. 1998).

2.3. ENA observations of Europa's neutral torus

Charge-exchange Energetic Neutral Atoms (ENAs) have been observed in Jupiter's magnetosphere already by Voyager in 1979 (Kirsch et al. 1981a,b; Cheng 1986) and, with more accuracy, by Cassini during the Jupiter flyby in late 2000/early 2001, when the Ion and Neutral Camera INCA, one of three sensors of the Cassini Magnetospheric Imaging Instrument MIMI (Krimigis et al. 2004), obtained the first images of Jupiter's magnetosphere in Energetic Neutral Atoms (ENA) flux (Krimigis et al. 2002).

These ENAs originate from the charge-exchange interactions between the energetic ions in the plasma of the Jovian magnetosphere with the planet's exosphere and the volcanic gases from Io and Europa (Krimigis et al. 2002). The resulting neutrals maintain the species, the energy and the direction of the parent ions and, being not affected anymore by the electromagnetic forces, travel in ballistic orbits reaching large distances from their generation region. The detection of these energetic atoms permits to have a global view of the plasma environment.

INCA is a time-of-flight instrument that separately analyzes the composition and velocity of ENAs. It has a 120° x 90° field of view with an angular resolution of approximately 7° x 7°, depending on particle energy (Krimigis et al. 2004). Measurements show that a continuous flow of fast energetic neutral atoms in the velocity range 10^3 to 10^4 km s^{-1} are emitted within 30 R_J of Jupiter (Figure 11). ENAs are emitted from both polar and equatorial regions of the Jupiter's magnetosphere appearing to be most intense in the vicinity of Io's and Europa's plasma torus.

The closest Cassini distance to Jupiter was around 140 R_J. Given the instrument angular resolution, it was not possible at this distance to ascertain the detailed Jupiter ENA source regions using the raw ENA images. Mauk et al. (2003) removed some instrumental distortions by using a point spread function (PSF) derived using images of Jupiter taken from distances beyond than 800 R_J. Processed 50-80-keV ENA images (15 h of integration time) of Jupiter's magnetosphere from 140 R_J show that a central feature centered on Jupiter, and two outermost features just beyond the orbit of Europa at 9.5 R_J (Mauk et al. 2003) (Figure 12). The brightest emissions come from lines of sight that pass through the largest volume of the emission region. From this image the estimated total emission rate of the torus trans-Europa, 50-80 keV, is 0.8 10^{24} s^{-1} (Mauk et al. 2003). By assuming H^+ on H (or H_2) charge-exchange interactions, given the ion measurements by Galileo (Williams et al. 1996) and the known cross sections, the total number of atoms or molecules in the volume is N = 4.5 10^{33} ± 20%, double of this value if radial symmetry about Europa's orbit (and not only contributions outside of Europa's orbit) is considered. If a volume with a radial extent and a height of 2 R_J is considered, the estimation of neutral gas density is about 40 atoms cm^{-3} (Mauk et al. 2003). This density is by a factor of 50 (Cheng, 1986) to 100 (Mitchell et al. 1996) larger than that expected on the basis of dispersal of neutral gases from Io, but seems in agreement with the estimation derived by Lagg et al. (2003) on the basis of angular distributions of the hot ions at the Europa orbit, affected by the loss due to charge exchange with Europa's neutral torus. By considering the whole energy range of ENAs Mauk et al. (2003) estimated an ENA emission rate of 10^{25} s^{-1}, which even if it is a smaller rate than the one estimated for Io, 10^{28} s^{-1}, it emits a similar energy (Smyth and Marconi, 2000), about 10^{12} W.

The exosphere loss rates from Europa, ranging from $5 \cdot 10^{26}$ s^{-1} (Cooper et al. 2001) to $4 \cdot 10^{27}$ s^{-1} (Saur et al. 1998) are 1–2 orders of magnitude less than the S and O source from Io (Smyth and Marconi 2000). So, either the Io torus loss rates are indeed 1–2 orders of magnitude larger than the loss rates from Europa or the source rates for gases at Europa have been underestimated. On the other hand, charge exchange is not the major loss responsible for ions in the inner Jovian magnetosphere (Europa to Io). During the Voyager epoch, Thorne (1982) argued that ions scattering with EMIC waves in the plasma have much higher potential for generating ion loss than charge exchange. He argued additionally that radial and pitch angle distributions measured by Lanzerotti et al. (1981) favor the predominance of EMIC interactions over charge exchange losses.

These ENA measured by INCA are dominated by hydrogen atoms in the energy range from a few to 100 keV, emitted from the planet's exosphere and neutral gas tori near the inner Galilean satellites (Mitchell et al. 2004). Heavier ions (likely a mixture of oxygen and sulphur) comprise a significant fraction of the ENA flux in the 0.1–1.0 MeV total energy range. During a period of about 80 days, FR^2 (flux*square of the distance) is constant to lowest order (Figure 13(a)), showing that the ENA are radiating from the inner region without any further source or sink (Mitchell et al.

2004). The INCA observed variations were close to the statistical limit of its measurement, thus the Jupiter's magnetosphere was fairly stable in that period. Mitchell et al. (2004) estimated a source rate of ~10^{26}/s H in the 10–100 keV range and $5 \cdot 10^{25}$/s O in the 100–1000 keV energy range.

The derived energy spectra obtained by CASSINI/INCA and by Voyager/LECP are shown in and compared in Figure 13(b). The derived ENA spectrum based on the LECP-data is an upper limit at 100 R_J since the instrument was not able to distinguish between X rays or ENAs (Kirsch et al. 1981). Since ENA species could not be determined from the Voyager data, these upper limits are plotted in figure assuming either pure hydrogen or pure oxygen (see also Cheng, 1986).

In summary, Mauk et al. (2003) located the ENA source peaked at the Europa neutral gas torus, concluding that the Europa source is more powerful than the one at Io. This produces a significant fall-off of energetic ion population moving radially inward from Europa's orbit to Io's one, due to the efficient Charge-exchange collisions with ambient neutrals (Paranicas et al. 2003). Data from Cassini MIMI/INCA suggest that the ENA flux propagate outward without relevant modification (Mitchell et al. 2004).

The ENA images obtained during the Jupiter flyby have been further analyzed for any potential asymmetries by studying images accumulated for 4-5 h during which pointing was stable and therefore consists of a subset of the images analyzed by Mauk et al. (2004). Hydrogen images in the 55-90 keV energy range were analyzed rather than the lower energy channels where the point-spread function of the INCA imager becomes wider. The neutral gas distribution was retrieved by employing a forward-modeling technique using a parametric function to describe the neutral gas and assuming the radial distribution of energetic protons obtained by Galileo/EPD (Mauk et al. 2004). Here, the neutral gas has been assumed to consist of H_2 to be consistent with the calculations of Smyth and Marconi (2006). Note that the ENA image alone cannot be used to differentiate the neutral gas composition. Figure 14 (upper panel, a) displays the observed INCA hydrogen image accumulated over 13:06-17:31 UTC on 2 January 2001. An enhancement over Europa's position can be seen that is about a factor of three higher than that on the opposite side of Jupiter. It has to be emphasized again that the INCA point-spread function at this distance results in a significant blur in the image and that without the instrumental PSF the emission region is significantly smaller.

Figure 14 (upper panel, b) shows the resulting best-fit simulated image constructed by keeping the model energetic proton distribution fixed while adjusting the parametric neutral gas model until the reduced chi-square difference between the observed and simulated images is minimized. The simulation takes in to account the instrumental PSF, the Compton-Getting effect (Gleeson and Axford, 1968) and applies counting noise assuming a Poisson distribution. The resulting neutral gas distribution required for the best fit between the observed and simulated ENA images is presented in Figure 14 (lower panel, left). During the accumulation time, Europa moved a relatively small distance as indicated by the arrow. The first conclusion to be made is that the ENA images in this time range are consistent with an asymmetric Europa gas torus, and consequently the term "torus" is misguided. Note that the center of the neutral gas distribution is approximately 30° ahead Europa in its orbit, which there is no explanation for at this stage. Because the energetic proton distribution is assumed to be relatively confined to the magnetodisc and because the proton intensities fall off rapidly inside of Europa's distance and decrease more gradually beyond Europa's distance, retrievals of the neutral gas using ENA images are most sensitive to the azimuthal asymmetry of the neutral gas distribution around Europa's orbital distance and less sensitive to the exact radial and vertical distributions. To illustrate the effects of the PSF, Figure 14 (lower panel, right) shows the simulated image without the PSF applied or noise applied. As expected, the emission region is a relatively thin region and the azimuthal asymmetry is about one order of magnitude between the line-of-sight (LOS) intersecting Europa's orbit on the right ansa compared to the left ansa.

From these simulations one can also derive the expected temporal variation in the ENA intensities that would come from the magnetodisc wobbling up and down over the Europa gas torus. In the INCA images, this effect would produce a factor of 2-3 variation in the observed intensities, consistent with the observations (Mitchell et al. 2004). However, stronger variations could of course be present due to a temporal variability in the energetic proton intensities because of the large-scale injections thought to occur in the Jovian magnetosphere (Krupp et al. 1998), also pronounced in the Saturnian (Mitchell et al. 2009) and Terrestrial magnetospheres (Brandt et al. 2002).

3. Europa's environment: current state of modeling

3.1 Comparison of Europa plasma and MHD models and possible future improvements

Since the close encounters of the Galileo spacecraft with Europa, a number of numerical models have been developed to understand the plasma interaction with Europa and its atmosphere, and to provide global context for interpreting Galileo observations. These models were based on different assumptions and adopted different approaches. Here we provide an overview of the various plasma models of Europa's plasma interaction focusing on published magnetohydrodynamic (MHD) models and physics-chemistry models.

3.1.1. Plasma and MHD model description and main results

Two-fluid plasma model by Saur et al. (1998)

The main purpose of the model developed by Saur et al. (1998) is to study the interaction of Jupiter's magnetosphere with Europa's atmosphere/ionosphere taking into account a self-consistent treatment of the coupling of the plasma interaction and the atmosphere. The authors also aim to investigate the plasma driven sources and sinks that maintain the neutral atmosphere. The Saur et al. (1998) model is a steady-state, 3D two-fluid (electron and a single ion species O^+) plasma model and is based on the various current systems driven in the interaction. Charge exchange, collisions between the ions and the atmospheric neutrals and electron impact ionization processes are included in the model. The authors estimate that the electron impact ionization is the dominant ionization process in Europa's environment and that photoionization is over an order of magnitude smaller. The model computes self-consistently plasma density, plasma velocity, electron temperature of the thermal and the suprathermal electron population, electric current and electric field in the vicinity of Europa but assumes a spatially constant background magnetic field. The model accounts different source and loss processes of the atmosphere: The pickup loss, atmospheric sputtering, and surface sputtering by torus ions and secondary ions.

Europa's atmosphere is assumed to consist of O_2 molecules. Saur et al. (1998) assume that the atmospheric surface density decreases from the trailing to the leading hemisphere according to the calculations of the normalized flux of ions to the surface of Europa by Pospieszalska & Johnson (1989). Assuming an average scale height of 145 km based on constraints from the HST observations by Hall et al. 1995, they infer a vertical O_2 column density of 5×10^{18} m^{-2} by considering the atmospheric mass balance between surface sputtering and atmospheric loss. The true spatial structure of Europa's atmosphere is likely more complex and affected by various cooling and heating mechanisms, loss and source mechanisms among others. Additionally, Saur et al. *(1998)* apply one independent observational constraint that the atmosphere emits the radiation observed by HST (Hall et al. 1995). For these model parameters the location of the exobase is at 71 km.

Saur et al. (1998) show that Europa's atmosphere and the plasma interaction are strongly coupled and influence each other. The neutral atmosphere is generated, removed, and maintained by sputtering processes, which strongly depend on the electrodynamic conditions at Europa. The Pedersen and Hall conductivities in Europa's ionosphere control the diversion of the plasma flow and allow only about 20% of the upstream plasma to reach the surface of Europa according to the model (shown in Figure 15). At the flanks of the moon the plasma flow is accelerated. The influence of the Hall effect is small and therefore the symmetry of the plasma flow in the ionosphere is only slightly disturbed compared to the unperturbed flow. The distribution of the electron density shows a local maximum with a value of 1000 cm^{-3} at the upstream surface and a global maximum of nearly 9000 cm^{-3}, which is in general agreement with densities derived from radio science measurements by Kliore et al. (1997). Regions with high electron density can be mapped to regions with low electron temperature with a global minimum of 8 eV. A total current of 7×10^5 A is driven in each Alfvén wing.

A balanced neutral atmosphere mass budget for production and loss of O_2 is found for a total O_2 release from the surface of $8.5 \cdot 10^{26}$ s^{-1} corresponding to a net atmospheric loss of 50 kg s^{-1}. The model shows that the atmospheric loss through sputtering dominates pickup loss by about a factor of 10. Primary sputtering by energetic magnetospheric ions strongly exceeds resputtering. Thus sputtering by ionospheric ions is not a major source of Europa's atmosphere. The reason is that the electric field close to the moon is strongly reduced by the electrodynamic interaction.

Consequently, ionospheric ions do not get enough energy from pickup processes to sputter efficiently Europa's surface.

Single-fluid MHD model by Schilling et al. (2007, 2008)

The main purpose of the model developed by Schilling et al. (2007; 2008) is to study self-consistently the effect of the internally induced magnetic field from a subsurface conductive layer on the interaction of Europa's atmosphere with Jupiter's magnetospheric plasma. It is the first model that considers the contribution to induction in Europa's ocean generated by the time-dependent plasma magnetic field. The aim is to constrain the conductivity and thickness of the conductive layer. The Schilling et al. model is a 3D single-fluid MHD model which includes the plasma currents in the atmosphere and the plasma in the vicinity of Europa. Additionally, the model accounts self-consistently for induction in a three-layered conductive shell model in the interior of the moon. The interaction above Europa's surface is described by modified MHD equations that consist of one evolution equation for the plasma density $\boldsymbol{\rho}$, the plasma bulk velocity $\boldsymbol{u}$, the magnetic field $\underline{\boldsymbol{B}}$ and the internal energy $\boldsymbol{E}$. Time-varying background magnetic field of Jupiter and the magnetospheric current sheet B_0, magnetic field caused by the interaction of the magnetospheric plasma with Europa's atmosphere B_P, induced magnetic fields from the interior due to the time-varying background field B_{ind} (B_0) and induced fields due to the time-varying plasma magnetic fields B_{ind} (j_P) are included in the model.

The Schilling et al. model takes into account plasma production P and loss L due to electron impact ionization and dissociative recombination. Moreover, it includes momentum transfer due to collisions between the ions/electrons and the neutrals via collision frequencies ν_{in} and ν_{en}, respectively. The major source for the generation of ionospheric ions is electron impact ionization. Newly created ionospheric electrons are much cooler than the magnetospheric electrons and are not involved into the ionization process. Thus the authors consider the magnetospheric and the newly produced ionospheric electrons separately by assuming a separate continuity equation for the magnetospheric electrons. Thereby they ensure that impact ionization does not change the number of the magnetospheric electrons. The production of ionospheric electrons by electron-impact ionization is strongly temperature dependent. In the model the magnetospheric electron temperature is not calculated self-consistently. To avoid an overestimation of the production rate and to account for the conservation of energy they follow Saur et al. (1998) and describe analytically the spatially dependent electron temperature, so that the electron temperature is decreased strongest close to the surface and on the flanks. They determine the analytical description of the temperature by comparing the model with measurements of Galileo flybys.

Schilling et al. (2007; 2008) use a hydrostatic molecular oxygen atmosphere with a scale height of 145 km and a surface density of $1.7 \cdot 10^7$ cm^{-3} similar to Saur et al. (1998). They adopt the description of the variation of the neutral number surface density in Europa's atmosphere from Saur et al. (1998), with maximum O_2 neutral densities on the trailing side of the moon and lower densities on the leading hemisphere. The simulations were performed with the 3D time-dependent ideal MHD code ZEUS3D.

A consistent description of Europa's interior is given by the concept of virtual plasma. Europa's interior is described by a plasma, which mimics the non-conducting properties of an icy crust. For the description of the upstream magnetospheric plasma Schilling et al. (2007; 2008) apply an average ion mass of 18.5 amu and an effective ion charge of 1.5 (Kivelson et al. 2004). The magnetospheric electrons at Europa consist of a thermal population with a temperature of 20 eV and a supra thermal population with a number density of 2 cm^{-3} at a temperature of 250 eV (Sittler & Strobel 1987). The thermal plasma density varies with the position of Europa in the plasma sheet with a minimum electron number density of 18 cm^{-3} when Europa is outside the plasma sheet and a maximum value of 250 cm^{-3} when Europa is in the center of the plasma sheet. Therefore, they assume the plasma density to fall of with $\exp(-(|z_{CS}|/H)^2)$ perpendicular to the plasma sheet plane, where $H = 0.7\ R_J$ is the scale height of the plasma sheet with Jupiter's radius R_J and z_{CS} is the distance of Europa from the center of the plasma sheet (Thomas et al. 2004; Schilling et al. 2007).

Schilling et al. (2007) show that the spherical harmonics coefficients of the plasma induced magnetic fields are an order of magnitude smaller than the spherical harmonics coefficients of the background magnetic field induced dipole. They conclude that the influence of the fields induced by the time variable plasma interaction is small compared to the induction caused by the time-varying background field. Moreover, they compare their model results with the Galileo Magnetometer data along the trajectories of the flybys E4, E14 and E26. Thereby they concentrate on flybys that occurred when Europa was located outside the current sheet so that the influence of induced fields is strongest. From the comparison with the observed data as shown in Figure 16 they derive constraints on the conductivity and the thickness of Europa’s subsurface ocean. They find for the conductivity of the ocean values of 500 mS/m or larger combined with ocean thicknesses of 100 km and smaller to be most suitable to explain the magnetic flyby data (Schilling et al. 2007).

Schilling et al. (2008) have shown that the Alfvén current system is deformed and displaced due to the influence of the induced fields in the subsurface ocean as shown in Figure 17. These findings are in agreement with theoretical considerations (Neubauer 1999) and observations (Volwerk et al. 2007). They determine a similar total Alfvén wing current through the northern Alfvén wing of $7{\cdot}10^5$ A as Saur et al. (1998). Another effect of the induction is that the plasma wake of Europa is deformed and the enhanced density downstream of Europa is concentrated in a smaller region of the wake. With their model results they are able to explain the high ionospheric densities measured by Kliore et al. (1997) and the ion number densities measured by Paterson et al. (1999) in the wake along the E4 trajectory (Schilling et al. 2008).

The asymmetries in the current and plasma density are time varying. Their results demonstrate that the effect of induced magnetic fields is observable in the Alfven wings and the plasma wake at large distances from Europa where the induced fields are negligible. Therefore a fully self-consistent implementation of the induction into the MHD equations was necessary.

Single-fluid MHD model by Kabin et al. (1999)

Kabin et al. (1999) developed the first MHD model of Europa’s plasma interaction based on the code BATSRUS (Block-Adaptive Tree Solar wind Roe-type Upwind Scheme), which has been described in detail by Powell et al. (1999). The Kabin et al. model was a 3D single-fluid MHD model that solved the ideal MHD equations with a finite-volume, high-order numerical scheme on an adaptively refined unstructured grid that allows resolving the near-Europa region with fine grid resolution while having a simulation domain large enough to include the upstream and wake regions. The model incorporated source and loss terms in the MHD equations to describe various mass-loading processes occurring in Europa’s environment, including ionization, charge-exchange, and recombination with specified constant reactions rates. Furthermore ion-neutral interaction was modeled by a friction force that served as a sink for momentum of the plasma. In applying this model to Europa, the authors also explored different boundary conditions for the inner boundary that represents Europa's surface to examine the sensitivity of model results on boundary conditions and to understand the detailed interaction of the surface with the plasma and the fields.

The MHD model was run for the Galileo E4 flyby conditions with the upstream environment conditions based on measured magnetic field and plasma data. The model results from runs with different inner boundary conditions were then compared with Galileo plasma and fields measurements (Kivelson et al. 1997; Gurnett et al. 1998; Paranicas et al. 1998) along the E4 flyby trajectory. The authors found that a model that included an induced internal dipole and an upstream flow rotated by ~ 20° from the corotation direction appeared to best match the observations. The induced dipole included in the model that reproduced observations had roughly the same orientation as that inferred from magnetometer analysis by Khurana et al. (1998) but with a smaller magnitude. The total mass-loading rate required for the best fit amounted to 3.75 kg/s.

Two-species MHD model by Liu et al. (2000)

Liu et al. (2000) extended the Kabin et al. MHD model by developing a two-species MHD model that included the ambient Jovian plasma (assumed to consist primarily of atomic oxygen ion, O^+) and the molecular oxygen ions (O_2^+) originating from Europa's ionosphere as two separate ion species. Specifically, the two ion species were modeled by separate continuity equations but shared the same momentum and energy equations in the MHD simulation. This treatment allowed to obtain separate distribution of plasmas originating from Jupiter's magnetosphere and Europa's ionosphere, which were merged into one plasma fluid in the previous single-species MHD model by Kabin et al. Other aspects of the Liu et al. model were essentially the same as the Kabin et al. model, such as the inclusion of an induced dipole and the prescription of mass-loading terms in the MHD equations.

The model was also run for the Galileo E4 flyby conditions and compared with Galileo observations. While the general agreement between the model and data is similarly good compared to the previous MHD model, the two-species model did provide additional insights into the plasma interaction at Europa. For instance, it became clear from the comparison with the Galileo PWS observations of electron density (Gurnett et al. 1998) along the E4 flyby that the double peaks in electron density observed near closest approach and the central wake were both caused mainly by O_2^+ originating from Europa. The two-species model also allowed the authors to obtain an estimate of the escape flux of Europa's ionospheric plasma down the tail, which was found to be about $5.6 \cdot 10^{25}$ ions/s or 3 kg/s.

Multi-fluid MHD model by Rubin et al. (2015)

Taking advantage of increased computational resources available and a suite of improvements of the BATSRUS model (Toth et al. 2012) made in recent years, Rubin et al. (2015) developed a multi-fluid MHD model for Europa's plasma environment. Different from the previous two-species MHD model by Liu et al. (2000), the multi-fluid model treats multiple ion species as separate fluids with their own continuity, momentum and energy equations. In addition, the electrons are modeled as a separate fluid. The electron pressure evolution was solved to calculate the electron temperature in a self-consistent manner. The electron heat conduction along magnetic field lines was also considered. These electrons provide an important source of ionization that helps maintaining Europa's ionosphere, as previously suggested by Saur et al. (1998).

In a brief summary, this model included a wide variety of processes, such as ionization due to both photo-ionization and electron impact ionization, charge-exchange, ion-electron recombination, elastic collisions and electron cooling and heating. The model adopted an analytical description for Europa's exosphere, which is a combination of two exponential functions representing the thermal and sputtered components of the exosphere (e.g., Cassidy et al. 2007). Such a setup required a highly resolved grid on the order of 10 km near the surface of Europa. Moreover, in the neutral model the neutral density on the trailing hemisphere was assumed to be higher than that on the leading hemisphere due to increased sputtering. The average column density corresponding to the neutral model used was ~ $1.6 \cdot 10^{16}$ m^{-2}, which is consistent with the column density $(1.5 \pm 0.5) \cdot 10^{19} m^{-2}$ derived from HST observations (Hall et al. 1995). Many of the reaction rates associated with various plasma-neutral interactions were then calculated based on parameters directly derived in the simulation, such as the densities and temperatures of individual species. For instance, the modeled electron temperature was used to calculate the impact ionization rate, the recombination rate, as well as the elastic collision rates of electrons with ions and neutrals. The energy required to ionize a neutral particle has to be provided by the impacting electron, which in turn lowers the electron temperature. Therefore the total mass loading of plasma around Europa is not a pre-defined input but a result of the model calculation.

As an initial application of the multi-fluid model, Rubin et al. (2015) simulated the Galileo E4 and E26 flybys with a three-fluid model. In this simulation, the first fluid consists of oxygen ions (O^+), mostly from Jupiter's magnetosphere with a minor contribution from dissociated and ionized O_2 from Europa's oxygen exosphere. The second fluid represents the molecular oxygen ions (O_2^+) originating from mass-loading through impact ionization, photoionization, and charge-exchange of the plasma ions with the neutral exosphere. The third fluid corresponds to the electrons, which were treated as a charge-neutralizing fluid (MHD). As an example, Figure 18 shows plasma density distribution near Europa for both O^+ and O_2^+. One prominent feature that stands out from the figure is that the multi-fluid MHD model produces some asymmetries in the plasma density distribution. Such asymmetries are consistent with that expected from the physics of the interaction of different plasma populations, i.e., due to the velocity difference between the electron and the ion fluids: on the trailing hemisphere (upstream side) the plasma density of the magnetospheric population is enhanced on the Jupiter facing side (positive EphiO-y side) whereas the density of the pick-up ions is enhanced on the anti-Jovian side.

The model results were in good agreement with the Galileo magnetometer and plasma measurements. The multi-fluid model was able to reproduce Galileo observations without the need of invoking a non-corotation component of the ambient plasma flow, as required in the previous MHD modeling efforts (Kabin et al. 1999). The model self-consistently yielded a total mass-loading rate of 5.4 kg/s for the conditions of the E4 flyby, which is also in line with the two earlier Michigan-based Europa MHD models.

3.1.2. Future Improvements in plasma/MHD models

A detailed comparison among the models described in the previous paragraph is presented in Table 2. Future improvements in modeling could take into consideration the following suggestions.

1. Include possible atmosphere asymmetries

The Saur et al. and the Schilling et al. models describe the O_2 atmosphere with a single scale height and assume a trailing leading asymmetry. Also in the MHD models by Kabin et al. (1999), Liu et al. (2000), Rubin et al. (2015), the spatial distribution of Europa's neutral atmosphere has been assumed as a relatively simplified model. While these models use realistic atmospheric scale heights or/and included asymmetries of the neutral density between the upstream and downstream hemispheres due to ion-induced sputtering (Saur et al. 1998; Schilling et al. 2007; Rubin et al. 2015), other potential asymmetries or inhomogeneities of Europa's neutral atmosphere need to be considered in future simulations. For instance, the recent model by Plainaki et al. (2013) suggested that Europa's exosphere could be highly variable along its orbit around Jupiter depending on both the direction of the incident plasma flow and the direction of solar illumination. The effects of the variability of Europa's neutral atmosphere on its plasma interaction need to investigated and quantified in future plasma modeling.

2. Compute electron temperatures self-consistently

The models by Schilling et al. (2007; 2008) do not compute the electron temperature self-consistently in their model. Heat conduction along magnetic field lines from the plasma torus reheat the newly ionized ions in the atmosphere. This mechanism is extremely effective at Europa (Saur et al. 1998).

3. Consider Europa's surface conductivity

In the MHD models by Kabin et al. (1999), Liu et al. (2000), and Rubin et al. (2015), the inner boundaries were all placed at the surface of Europa. While different boundary conditions were adopted to represent the physical behavior of Europa's surface in interacting with the surrounding plasma environment, such as absorbing and fixed boundary conditions, the properties of Europa's interior were not modeled directly. Given the presence of subsurface conducting layer that produces the observed induced magnetic field at Europa, it is important for future MHD models to directly take into account this aspect of the Europa interaction system. The concept of virtual plasma in Schilling et al. (2007; 2008) is an approximate treatment of the non-conductive surface of Europa and could modify the outcome of the simulations. Duling et al. (2014) derived a consistent description of the inner boundary that takes the non-conducting nature of the surface into account and could be implemented in the Schilling et al. model. Approaches have been developed to incorporate interior layers with different conductivities into global MHD models, and they have been successfully applied to different planetary bodies including Io (Linker et al. 1998; Khurana et al. 2011), Ganymede (Jia et al. 2009) and Mercury (Jia et al. 2015). Future models of Europa's plasma environment may consider implementing such a capability in order to more realistically simulate the effect of Europa's interior on its global interaction.

3.1.3. Physics-chemistry modeling

Dols et al. (2016) explored the "chemistry" of the Europa/magnetosphere interaction focusing on the many reactions between ions, neutrals and electrons, many of which are neglected by models described elsewhere in this paper. This 2D model, which was adapted from Io simulations (Dols et al. 2008, 2012), follows a parcel of magnetospheric plasma as it flows through Europa's atmosphere and tracks the changes in mass and temperature for electrons and 7 ion species including heavy magnetospheric ions (O^{n+}, S^{n+}) and pickup ions (H_2^+, O_2^+). The density distributions provided by the Dols et al. (2016) model give important information of the so called "planetary ion environment" (or "ionized atmosphere") around Europa the characteristics of which are directly related to the atmosphere properties. Given the nature of the model itself, we do not in detail compare its parameters with the ones of the plasma/MHD models in Table 2.

An analytic formula for the flow of an incompressible fluid around a perfectly conducting cylinder was used to track plasma motion around the moon. This is a simplification, but one that captures the basic features reported by other simulations such as the slowing of plasma in front of the moon and speed-up at its flanks. For atmospheric properties they used the 1D (radial) model of Smyth and Marconi (2006), though the O_2 scale height and other properties were varied to explore the sensitivity of the model. Upstream magnetospheric plasma conditions came from the recent reanalysis of Galileo results by Bagenal et al. (2015).

Figure 19 shows the model's results for nominal magnetospheric conditions (median magnetospheric plasma density and temperature as reported by Bagenal et al. 2015). The inflowing magnetospheric ions are mostly diverted around Europa and their densities drop sharply due to loss by charge exchange with atmospheric neutrals.

The pickup ions flow close to the surface and form a dense, narrow wake in accord with Galileo observations (Paterson et al. 1999). The average ion temperature increases near the flanks, where the high plasma flow speed (about 200 km s^{-1}) results in energetic pickup ions.

As the plasma flows through the atmosphere the model also keeps track of the various processes acting upon the neutrals. Dols et al. (2016) assume a scale height of the O_2 atmosphere of 150 km, which assumes it originates entirely from sputtering. However, the main fraction of the O_2 atmosphere will be thermally accommodated with the surface and resulting in a much lower scale height. The authors find a large O_2 sink due to symmetric charge exchange:

$$O_2 + O_2^+ \rightarrow O_2^+ + O_2 \text{ (fast).}$$

This results in the loss of an atmospheric molecule, which either escapes Europa's gravity or impacts the surface. The newly-ionized O_2 is not, as commonly assumed in atmospheric models, immediately lost to the magnetosphere: the pickup ion continues through the atmosphere and becomes the seed of a cascade of charge exchange reactions with other atmospheric O_2 molecules. This continues until the plasma parcel is convected out of the atmosphere. Of course, these ions can only be contained in the atmosphere because it is thick enough to provide enough ion-neutral collisions. With a realistic scale height of the O_2 atmosphere the evacuation of the newly-ionized O_2 the mangetospheric plasma would be much more effective.

Based on these simulation Dols et al. (2016) concluded that this loss process dominates, by a factor of 4 to 40 depending on the simulation parameters used, over the second fastest loss process of electron-impact ionization. This is in accord with the modeling of Saur et al. (1998), whose "atmospheric sputtering" process is broadly similar to the mechanism outlined above. The O_2 loss rates calculated by Saur et al. (1998) also agree quantitatively with Dols et al. (2016) despite very different modeling approaches and assumptions. The result seems to be consistent with other Europa plasma models as well (e.g., Kabin et al. 1999; Schilling et al. 2008), but those papers did not discuss O_2 loss rates explicitly.

This symmetric charge exchange loss process has not been considered by atmospheric modelers, which commonly assume that electron-impact ionization, followed closely by electron-impact dissociation, are the dominant loss processes for O_2. This presents an interesting problem for the atmospheric modeling community: their loss rates seem to be underestimated by an order of magnitude, while at the same time they may have *overestimated* the O_2 source rates (via sputtering) by neglecting the plasma flow diversion found by all Europa plasma modelers.

Another consequence of this symmetric charge exchange cascade is the production of a Jovian neutral O_2 torus. Dols et al. (2016*)* estimated that the fast neutral O_2 leave the charge exchange reaction at an average speed of ~5 km s^{-1}, and at a rate on the order of 100 kg s^{-1}. This is fast enough to escape Europa's gravity and form a broad, and fairly dense, torus around Jupiter. Such a neutral torus could help to explain ambiguous detections of a neutral cloud in the vicinity of Europa's orbit.

3.1.4 Charged Energetic Particles

The radiation environment of Europa is believed to play a role in the weathering of the surface and in the modifications of the atmosphere. Energetic charged particles are generally not impeded by the electromagnetic fields near the body, such as the magnetic induction effect at high magnetic latitudes, so can pass directly into the ice. Electrons that enter the ice can deposit energy to > cm depths and physically alter the ice and non-ice materials that are present. For example, they can change the thermal conductivity (Howett et al. 2011) or lattice structure (Hansen and McCord 2004) of the ice. Energetic electron and ion precipitation can lead to the manufacture of new materials in the ice such as peroxide (Loeffler et al. 2006). Volatile atoms and molecules created in this way can escape from the ice into the atmosphere.

Suprathermal to energetic ions can also modify the ice lattice. In addition, they sputter the ice surface, leading to the creation of newly liberated neutrals. Cassidy et al. (2013) estimated the global sputtering rate of Europa and found 2 x 10^{27} water molecules per s are created, some of which leave the surface as molecular hydrogen and oxygen. These ions can also interact with bound atmospheric neutrals and liberate them into circumplanetary or other orbits. The putative neutral gas torus at Europa's radial distance (e.g., Lagg et al. 2003; Mauk et al. 2004; Kollmann et al. 2016) may be supplied by this interaction between Jovian ions and bound atmospheric neutrals.

3.2. Comparison of atmospheric models and main improvements required

It is a wide consensus that Jupiter's magnetospheric plasma environment is the main agent for the generation of Europa's tenuous atmosphere. Several models based on very different approaches have been developed to describe the tenuous atmosphere of this moon and to better constrain its generation processes. Shematovich et al. (2005) and Smyth and Marconi (2006) used a Monte Carlo multispecies approach to derive the atmospheric O_2, H_2O, H_2, and H, O and OH spatial structure. Cassidy et al. (2007) explored the hypothesis of O_2 surface reactivity and Leblanc et al. (2002; 2005) and Cassidy (2008) studied the structure and evolution of sputtered exospheric trace species using Monte Carlo models. Plainaki et al. (2010; 2012) incorporated sputtering and radiation chemistry information derived from laboratory measurements (Famà et al. 2008; Teolis et al. 2009) into Europan exospheric models, in order to quantify the neutral particle release and to estimate its longitudinal dependence. Considering the O_2 tenuous atmosphere, the study was extended to provide information on the morphology of the environment at different phases of Europa's orbit around Jupiter (Milillo et al. 2016; Plainaki et al. 2013).

In Table 3 and Table 4 we summarize the main characteristics of some of the most recent atmospheric models for Europa, in means of model assumptions and main outputs, respectively. In Section 3.2.1 we will discuss the available techniques applied to existing models whereas in Section 3.2.2 we will make an analytical comparison of some of the existing models on the basis of the parameters presented in Table 3 and Table 4.

3.2.1. Current Modeling Techniques and Assumptions

In the low Knudsen-number atmosphere of Europa (see Figure 1) collision times between molecular species become long compared to transport times and modeling the physics and chemistry imposes some basic assumptions on the environment properties. To describe Europa's thin gas environment, two basic modeling techniques have been proposed in literature based either on the direct solution of the Boltzmann equation or on the discrete modeling of numerous particles by means of Newton’s laws of classical dynamics.

Since there is no general analytical approach to solving the Boltzmann equation, kinetic models are based on the use of numerical methods. The gas flow in the near-surface atmosphere, i.e., in the Knudsen layer and the transition region between collision-dominated and collisionless atmospheric regions (see Figure 1), is best described by a system of the kinetic Boltzmann equations, because of the non-thermal source terms due to both surface sputtering and charge-exchange by the magnetospheric plasma inflow (Shematovich et al. 2005). Such highly non-equilibrium systems are difficult to analyze because of the mathematical complexity of the Boltzmann kinetic equations (nonlinearity and high multiplicity of the collision integrals), requiring new and sophisticated approaches in the field of rarefied gas dynamics.

A very promising approach to study such kinetic systems is the development of discrete mathematical models that use the probabilistic interpretation of collisions in an ensemble of model particles. The DSMC method (Bird, 1994) and its modification for studying non-equilibrium processes in the planetary atmospheres (Marov et al. 1996; Shematovich, 2004) belong to this class of approaches. A stochastic discrete model to investigate the formation, kinetics, and transport of suprathermal particles in the near-surface atmosphere of Europa should take into account the following peculiarities of the atmospheric gas flow: *(i)* the local mean free time and path for suprathermal particles ejected from the icy surface and subsequently dissociated/ionized by the magnetospheric plasma electrons and ions, should be considered, respectively, as the characteristic time and space scale describing the gas state; *(ii)* the parameters of the atmospheric gas change strongly from the collision-dominated regime of gas flow in the Knudsen layer to the virtually collisionless (free-molecule) regime of flow in the exosphere; *(iii)* significant differences between the densities of the suprathermal particles and the ambient atmospheric gas are commonly observed. Therefore, in the numerical models of the near-surface atmosphere, the following approaches must be followed: *(i)* splitting of the solution of the basic kinetic system into simulation steps considering for the suprathermal particle sources collisional thermalization and free molecular transport on a discrete time scale; *(ii)* stochastic simulation of the formation of suprathermal particles and their local kinetics by using analogue Monte Carlo algorithms with statistical weights; *(iii)* calculation of the trajectories of suprathermal particles in the whole exosphere by using finite-difference algorithms.

The direct methods of solving the stochastic (master) kinetic equation consist in setting up and solving a system of equations for the probabilities of all possible paths of the state of a chemically reactive rarefied gas. Unfortunately, this direct procedure can be performed only for a few very simple chemical systems (Van Kampen, 1984) and involves enormous computational difficulties for real systems of chemical reactions. The kinetic Monte Carlo method (see, e.g., Marov et al. 1996;

Shematovich, 2004), which consists in generating a sample of paths for the state of a chemically reactive gas, is an efficient tool for studying complex kinetic systems in the stochastic approximation. The path generation procedure is much simpler - a sequence of transitions between the states of a chemically reactive gas and transition-separating times should be drawn based on the proper probability distributions. Such procedure is an analogue Monte Carlo algorithm for solving the stochastic kinetic equation. In the numerical realizations of the kinetic model the following recent developments in the theory and practice of DSMC method were used (see, e.g. Shematovich 2004; Shematovich et al. 2015): *(i)* an effective approximation of the major frequency, where the collision probability for the chosen pair is estimated from the maximum possible frequencies and is used in choosing the next transition; *(ii)* the multichannel nature of the selected reaction is taken into account for the transition to be realized; this means that the transition is treated as the simultaneous drawing of all possible (elastic, inelastic, and chemically reactive) channels for each one of which the corresponding weight is transferred to the total cross section of the collisional process, proportionally to the ratio of the partial cross section for the given channel; *(iii)* since the algorithmic steps of throwing in suprathermal particles, in accordance with the source functions, and drawing the collisional transitions are accompanied by the formation of new model particles, it is necessary to control the total number of model particles in the numerical model. An efficient method for this control is the so-called clustering of model particles, where groups of model particles with similar parameters are combined into a single particle with weighted parameters.

Test particle Monte Carlo models can be considered as a sub-family of the DSMC models in which the collisions are not considered. Usually each test particle is placed at a random location, e.g. in a cell representing a region of Europa's surface, and is given a random velocity and angular distribution, selected on the basis of the population properties (e.g. species, velocities) and the physical process in action (e.g. surface sputtering, radiolysis, etc.). Then the particle trajectories are integrated taking into account, in general, the gravitational fields of both Europa and Jupiter, as well as Europa's rotation. The integration time step can be set equal to $dt = \frac{dx}{vn_c}$ where n_c is the number of particles inside the cell, and v is the velocity of the emerging particle and dx is the dimension of each cell.

3.2.2. Differences in the implementation

Most models agree that the H_2O, H_2 and O_2 atmospheres of Europa are created by ion bombardment of the surface plus possible contributions from plumes and sublimation.

Ip (1996) proposed a model for the atmosphere of Europa based on the sputtering rates estimated for the case of icy surfaces (Shi et al. 1995) assuming a simple model for the plasma effects. The atmosphere was considered to be globally homogeneous with respect to surface sources.

The 1-D kinetic model of Shematovich and Johnson (2001) for O_2 and the improved 1-D kinetic model of Shematovich et al. (2005) for both O_2 and H_2O provided the velocity distribution for these species in the near-surface region. These models were the first kinetic models of Europa's near-surface atmosphere with collisions. In the 1D kinetic model of Shematovich and Johnson (2001), the following physical processes were taken into account: a) collisions between all atmospheric species in the near-surface (Knudsen) layer; b) O_2 dissociation by solar UV-photons and by magnetospheric electrons; c) charge-exchange (often referred to as atmospheric sputtering) between neutrals and plasma ions; d) adsorption; e) thermalization; f) rapid desorption in the collisions of O_2 molecules with Europa's icy surface. The stochastic version (Marov et al. 1996) of the DSMC method was used in a one-dimensional approximation to calculate the chemical and thermal structure of the atmosphere and the production rate of oxygen atoms in the reactions of dissociation of the parent molecule O_2, ejected into the atmosphere upon radiolysis of the moon's icy surface. It was shown that the primary loss process of oxygen is its ionization by the magnetospheric electrons and the secondary loss process is atomic oxygen escape. The latter provides an important source of neutral gas to the neutral torus forming along the satellite's orbit. A modified model was further developed (Shematovich et al. 2005; Shematovich, 2006) to study the formation of both the near-surface atmosphere and hot oxygen corona induced by the thermal and nonthermal sources of atoms and molecules due to the radiolysis of Europa's icy surface. The dissociation and ionization of parent H_2O and O_2 molecules by magnetospheric electrons and solar UV-radiation as well as the charge-exchange between vapour molecules (water and oxygen) and low-energy magnetospheric ions, were considered in that model. The spatial distribution of the near-surface neutral atmosphere and its thermal structure were calculated. It was shown that oxygen molecules predominantly populate the near-surface atmosphere which is surrounded by an extended and rarefied hot corona of atomic oxygen (see Figure 20).

The estimated O_2 atmosphere scale was of the order of ~20 km at small altitudes; the energy distribution of O_2 is thermal with a high-energy tail. Nagy et al. (1998) had previously noted that Europa must have a corona of hot atomic oxygen formed in the dissociative recombination reaction of the molecular ion O_2^+ with ionospheric electrons. The observations by *Cassini* during the flyby of the Jovian system (Hansen et al. 2004) showed that the atomic oxygen population is more widely distributed in the exosphere of Europa compared to the predominantly near-surface O_2 distribution predicted by the models by Shematovich et al. (2005) and Shematovich (2006).

Interestingly, the O_2 scale height of about 20 km in the model by Shematovich et al. (2005), is consistent with a gas in thermal equilibrium with Europa's ~100 K surface. This suggests that the plasma impingement on the atmosphere does little to heat the bulk of the atmosphere and the magnetospheric ions pass the thin atmosphere mostly unaffected. This may be at odds with observations, such as those by Kliore et al. (1997) of an ionosphere with a scale height one order of magnitude larger, or the Roth et al. (2016) vertical profiles of atmospheric emission likewise suggestive of scale heights much larger than 20 km. Addressing these discrepancies requires modeling both the ionosphere and atmosphere self consistently, something that has not been attempted yet.

The kinetic model by Smyth and Marconi (2006) includes all the water group species, namely H_2O, H_2, O_2, OH, O, and H. The results of this model showed that O_2 is the dominant species near the surface while H_2 is somewhat less abundant but is the dominant species at higher altitudes and has by far the largest escape rate. In this model, the heavy O_2 molecule is lost from the atmosphere either as hot O generated by the electron impact and ion-collisional dissociation of O_2 or as O_2^+ generated through electron impact ionization of O_2 (direct ion sweeping). The model predicts that the escaping O atoms have velocities near the escape velocity (equal to 2.02 km/s) and therefore they are expected to be distributed near Europa's orbit and to form an important gas torus. Due to its small mass, H_2 escapes easily the moon's gravity and, similarly to the O case, is distributed around the moon near its orbit forming a gas torus. One part of the H_2 population is also lost as hot H generated through electron impact dissociation. These H atoms are distributed over a large volume of the Jupiter system. The model by Smyth and Marconi (2006) predicts for the rest of the atmospheric species column abundances much smaller (by an order of magnitude) than the one of H_2. It is evidenced that in the model by Smyth and Marconi (2006) shows that the assumed atmospheric source rates for the various species are determined by partitioning the O_2 source rate, the value of which is chosen so as to reproduce the O UV brightness reported by Hall et al. (1995) using the electron-impact excitation cross-sections of Kanik et al. (2003).

The collisionless model by the University of Bern was originally developed for Mercury's exosphere (Wurz and Lammer, 2003; Wurz et al. 2010) and extended for the Moon (Wurz et al. 2007). It has been used for many planetary objects, most recently also for the icy moons of Jupiter (Wurz et al. 2014; Vorburger et al. 2015). The model is a Monte Carlo calculation of a collisionless neutral environment (often referred to as an exosphere). Particles are released either from the surface or from the exobase through several release processes: thermal release, sublimation, photo-stimulated desorption, micro-meteorite impact vaporization, and sputtering. For the latter, sputtering of ice and minerals are treated differently. For each release process the 3D velocity distribution at the surface is considered. Trajectories are calculated in 2D by using Kepler's laws. Modifications to the trajectory for photon pressure are performed where necessary, e.g. for Na. Ionization and fragmentation of molecules along the trajectory are calculated using ionization and fragmentation rates for photons and electrons for the Jupiter system. Released particle fluxes from the surface are calculated ab initio, e.g. by using the chemical and mineralogical composition of the surface and applying the physical laws of particle removal for the different release processes. Recently, Vorburger et al. (2015) presented a similar model for Callisto's exosphere. The main outputs of the code are density profiles, radial and transverse column densities, for all species and release processes. In addition, velocity distributions at a certain altitude, loss rates, escape fluxes are also provided.

The Europa Global model of Exospheric Outgoing Neutrals (EGEON) is a numerical single-particle Monte Carlo model simulating the generation of Europa's neutral atmosphere (Plainaki et al. 2010; 2012; 2013; Milillo et al. 2016). As physical sources the model includes ion sputtering and radiolysis and as loss processes, the sticking to the surface capability of the H_2O molecules, the electron-impact ionization and the gravitational escape for all the considered species (H_2O, O_2, H_2). The source rates used as an input in EGEON were calculated on the basis of the known Jupiter's magnetospheric energy spectrum of ions (Paranicas et al. 2002), the literature sputtering yields (Famá et al. 2008) and the moon's surface temperature map (Spencer et al. 1999). The resulting atmospheric density was compared, a posteriori, to the observations (where existent) in order to validate the model. This particular approach provided an opportunity to discuss aspects of sputtering and radiolysis modeling that had not been in detail treated in detail in the past. For example, using the precise formula for the sputtering yield of Famá et al. (2008), the different release mechanisms leading to the generation of the moon's exosphere were distinguished, and, their dependence on the specific properties of the impacting ions (e.g. species, energy) and on the icy surface temperature was attributed. As a main output, EGEON provides the 3-D density distribution of the main atmospheric constituents (i.e. the radiolytically produced H_2 and O_2 and the sputtered H_2O, see Figure 21). The possibility to estimate these distributions for different orbital phases also exists in EGEON. Milillo et al. (2016) used the EGEON densities to define a parameterized equation giving the O_2 density as a function of altitude, latitude and longitude at different orbital positions of Europa. This analytical model for the tenuous O_2 atmosphere is proposed as a tool for the interpretation of future observations to be performed either with JUICE payload instruments or with space telescopes (Milillo et al. 2016). In Figure 22, we show the expected O_2 density distribution at different orbital phases. It is evidenced that at low altitudes (i.e. below ~150 km), no detailed (but only integrated) information on the density distribution can be extracted from EGEON due to the model's spatial resolution (~0.1 R_E). Moreover, EGEON allows investigating the trailing/leading and sunlit/dark hemisphere asymmetries and the escape rate from the moon as a function of the surface release mechanisms. Recently, the model results were used for the interpretation of the first observations of the Europa plumes (Roth et al. 2014b).

Cassidy et al. (2007, 2008, 2009) used a collisionless atmospheric model to simulate the O_2 atmosphere (2007), Na exosphere (2008), and trace species (2009) such as CO_2 and SO_2. The first of these models explored the sensitivity of the atmosphere to surface reactivity, which was later found to be important to the O_2 and CO_2 exospheres of Saturn's icy moons (Teolis et al. 2016). The 2008 paper concluded that visible emissions from Europa in eclipse observed by Cassini are likely from electronic excitation of atomic sodium. Both papers proposed hypotheses to explain the non-uniformity of photon emissions from the atmosphere, but further observations (Roth et al. 2016) show that the emission patterns are not explained by any published model. The implementation of Cassidy's model was kept as simple as possible. As with many other atmospheric models, there was little consideration for plasma physics: the electron-impact ionization lifetime, for example, was a constant despite the variable electron temperatures and densities (see Section 3.1). It also, along with other atmospheric models, did not consider a possible major loss process identified by Dols et al. (2016).

Sputtering due to surface bombardment by magnetospheric ions represents only one of the exogenic processes influencing the generation of Europa's atmosphere. Both the kinetic models by Shematovich et al. (2005) and Smyth and Marconi (2006) provided important results based on the chemistry between the various atmospheric constituents in the first atmospheric layers near the surface. Both of these models do not consider different configurations between Jupiter, Europa and the Sun (corresponding to different orbital phases) and the effect that they could have on the atmosphere's spatial distribution and the escape rate of the neutral particles. To account for such a possible effect, Plainaki et al. (2013) applied the EGEON model for different configurations between the moon, Jupiter and the Sun and investigated the trailing/leading and sunlit/dark hemisphere asymmetries in the spatial distribution of the atmosphere O_2 density. They showed that the O_2 atmosphere is explicitly time-variable due to the time-varying relative orientations of solar illumination and the incident plasma direction (see Figure 22). Solar illumination of Europa by the Sun and preferable plasma impact direction together are the key agents determining the spatial distribution of the generated O_2 exosphere and the O_2 release efficiency. The density of the released O_2 molecules becomes maximal when the trailing hemisphere coincides is sunlit resulting in a surface density of $\sim 10^{14}$ m^{-3} (Plainaki et al. 2013, yields review (Milillo et al. 2016) included). The EGEON results on the O_2 column densities were consistent with the surplus of OI emission at the 90^0 west longitude (leading hemisphere) observed by HST (Saur et al. 2011). According to EGEON, solar illumination prevails over the more intense bombardment of the trailing hemisphere by energetic ions in determining the efficiency of the O_2 release. The escape rate from the moon of O-atoms produced by the dissociation of exospheric O_2 molecules was maximal when trailing hemisphere coincides with sunlit hemisphere. In this case, the rate of supply of O-atoms to the torus is estimated to be 2.1 10^{25}/s (Plainaki et al. 2013, yields review included). Although the O_2 column density calculated with EGEON was, in general, consistent with the observations of the OI emission from the trailing hemisphere of Europa, the longitudinal asymmetry (at 230–250^0 west longitude) was not reproduced by the model. Such asymmetry, however, was re-produced in the model by Cassidy et al. (2017), allowing O_2 molecules to react with Europa’s visibly dark surface material and assuming at the same time a uniform electron excitation of O_2 over the trailing hemisphere.

One of the most important differences among the existing Europa's atmosphere models is the considered pattern for the plasma ion precipitation to the moon's icy surface. This is a fundamental point in modeling that determines significantly the properties of the generated neutral environment. Since the ejection of surface material due to the impact of magnetospheric ions to Europa's icy surface is the dominant agent for the release of both sputtered and radiolyitical products, the considered ion precipitation pattern becomes a critical parameter for each model. Pospieszalska and Johnson (1989) were the first to estimate the ion bombardment pattern. Specifically, Pospieszalska and Johnson (1989) showed that 30 keV sulphur ions from Jupiter’s magnetosphere can eventually reach almost all points on the satellite surface and result in a near linear angle-dependence of the relative ion flux, with the maximum flux at the trailing hemisphere apex and with the minimum at the opposite point (180°). Cassidy et al. (2007) and Plainaki et al. (2012) considered a preferential neutral ejection from the trailing hemisphere, using a similar exit-angle distribution as the one proposed by Pospieszalska and Johnson (1989), that is a cosine flux on the trailing hemisphere due to either the corotating plasma or hot electrons. Paranicas et al. (2001) showed also that most energetic electrons impact Europa’s trailing hemisphere, primarily at low latitudes. Subsequent estimations on the magnetiospheric ion flux by Paranicas et al. (2002) based on information obtained with Galileo were taken as a proxy for sputtering rate (e.g., Tiscareno and Geissler 2003; Cassidy et al. 2008). However, Cassidy et al. (2013) argued that that ion flux and sputtering rate are quite distinct. In particular, Cassidy et al. (2013) discussed the ion motion at Europa's environment and distinguished the effect of different ion energies on the ion bombardment patterns. They showed that at the typical energy of the cold ion population (~100 eV), sulphur ions have very small gyroradii and the ion speed is small compared to the corotation drift speed. The corotation drift carries the ions onto the trailing hemisphere, resulting in the bullseye pattern centered on the trailing apex (see Cassidy et al. (2013), Fig. 8, upper left). A similar bullseye pattern found in the UV surface reflectance was attributed to absorption by SO_2 in the surface (Hendrix et al. 2011). At higher ion energies (10^3 eV), the ion speed becomes comparable to the corotation drift speed, though the gyroradii are still small compared to Europa's radius. With increasing ion speed the corotation drift remains unchanged hence the average ion speed in the corotation direction remains unchanged too. The ion motion parallel to the magnetic field faces is not influenced and at high energies the ions increasingly reach Europa's surface from the North or South. As a result, at even higher energies (~10^5 eV), the precipitating ion flux peaks at the poles whereas at ~10^6 eV the gyroradius is comparable to Europa's radius and the ions can access Europa's surface from all directions.

Considering the plasma flow diversion, the existing models of the magnetosphere-moon interaction have generally assumed either the atmosphere-centric approach or the plasma-centric approach. The atmosphere-centric approach calculates ion fluxes by treating Europa as electromagnetically inert. The modelers assume that Europa's interaction is lunar-like, that is a completely absorbing barrier. However, this is not consistent with the observations (Paranicas et al. 1998; Paterson et al. 1999) that show plasma diversion around Europa as a consequence of mass loading and ionospheric conductivity (Saur et al. 1998). To address the balance between mass loading and loss, realistic scale heights for the different exospheric species should be identified. The plasma-centric approach assumes a static atmosphere that diverts the plasma flow around Europa. According to these models plasma has limited access to Europa's surface. The shortcoming in this approach is that it neglects to consider self-consistency.

Figure 23 shows the O_2 source rates from the literature going back to the first estimate by Johnson et al. (1982). There is a big discrepancy among the results of different models because of the different assumptions and parameters that go into such models (see Table 3). The differences can be ascribed to a number of key assumptions that differ from paper to paper. One such assumption is the choice of charged particle population responsible for radiolysis and sputtering (indicated by colors in Figure 23). The particles bombarding the surface range from thermal plasma (eV-keV) to energetic non-thermal (keV-MeV) populations and include electrons, protons, oxygen and sulphur ions of a variety of charge states. The surface is also bombarded by pickup ions (primarily O_2^+) from the atmosphere (Ip, 1996; Rubin et al. 2015) and energetic neutral O_2 (Dols et al. 2016). The bombarding flux, bombardment pattern, and sputtering yields all vary as a function of species and energy (e.g., Cassidy et al. 2013; Galli et al. 2016) and models generally do not include all of these species and energies. Eviatar et al. (1985), for example, only considered O_2 production by low-energy thermal plasma ions, while Cooper et al. (2001) only considered energetic non-thermal electrons and ions. Neither paper includes a justification for these assumptions. The lack of agreement on this matter is the main reason for the range of results shown in Figure 23.

Loss processes are another source of disagreement. All models agree, roughly, on the electron-impact loss process rates (see summary in Johnson et al. 2009). But many plasma simulation models include a loss process left out of the atmospheric models: charge exchange between atmospheric O_2 and the pickup ion O_2^+, that is a cascade of symmetrical charge exchanges between O_2^+ ions and neutral O_2. This mechanism takes place because once an atmospheric oxygen molecule is ionized by an electron or photon it is first picked up by the flow and entrained through the atmosphere. A cascade of symmetrical charge exchanges with other atmospheric O_2 neutrals along the whole path of the flow through the atmosphere takes place (Dols et al. 2016). Each charge exchange ejects a fast neutral until the ultimate ion is eventually convected out of the atmosphere. This process was firstly identified as a major loss process by Saur et al. (1998), who called it "atmospheric sputtering". Kinetic models (e.g. Shematovich etal. (2005)) have indeed included its effects by considering a constant rate for the respective reaction. More recently Lucchetti et al. (2016) examined the effects of the consideration of such a loss process in atmosphere modeling. Dols et al. (2016) showed that the total production rate of ejected neutrals could be an order of magnitude larger than the production of ions. To address the relative weight of each loss process, the identification of a realistic scale height of O_2 is necessary.

The energy distribution of each atmospheric constituent is an important parameter of the Europa atmosphere models. The assumptions used in modeling are in principle based on the existing laboratory measurements though the conditions at the moon's surface may differ significantly. Single particle Monte Carlo models assume standard energy distribution functions describing the respective release process (e.g. sputtering, sublimation). On the contrary, DSMC models estimate dynamically the energy distribution function of the atmosphere dynamically as at each simulation step collisions and chemical reactions change the energetics of the molecules.

3.3. Definition of a global unified model of Europa's atmosphere

A global model of Europa's tenuous atmosphere should take into account the following important physical properties.

1. Position of Europa with respect to Jupiter's plasma sheet

Due to the tilt of Jupiter's magnetic field relative to Europa's orbit plane, the plasma environment changes as the dipole spins. The cold plasma density maximizes at the 'centrifugal equator', the equilibrium surface lying between the magnetic equator and the rotational equator. However, as Europa orbits around Jupiter it moves above and below this plane by ~ 1 Jupiter radius (R_J). The cold plasma decreases in density as exp$(-(z/H)^2)$ above the centrifugal equator with a scale height of H ~1 R_J (Bagenal, 1994), resulting in an average cold ion density of 0.75 times the centrifugal value above (Cassidy et al. 2013). The hot ions do not decrease much in density above the centrifugal equator owing to their uniform pitch angle distribution (Roederer, 1970). In a global atmosphere model, a plasma model considering different conditions of the Jupiter plasma sheet, such as the one by Bagenal et al. (2015), should be taken into account. We note that the consideration of a plasma model embedded in the atmosphere model is necessary for constraining both primary (see Cassidy et al. 2013) sources and secondary (see Saur et al. (1998)) sources and losses (see Dols et al. (2016); Lucchetti et al. (2016)) of the atmosphere.

2. Ion precipitation to the surface

The spatial density and energy distribution of Europa's tenuous atmosphere is likely conditioned from the properties of the magnetospheric ion precipitation to the surface. The critical parameter determining the efficiency of the release of material at each surface point (characterized by a specific surface temperature) is the product of the intensity of the ion flux energy spectrum at a specific energy with the release yield (for this ion energy). In a global atmosphere model, the ion precipitation patterns at different energies should be taken into account in such an estimation. An overall release taking into consideration both the directional properties of the ion impact and the actual efficiency of the release of surface material integrated in ion energy should be estimated. This consideration is particularly important for the atmosphere constituents generated through direct sputtering (e.g. H_2O) and with small probability of multiple bouncing on ice (i.e. sticking~1).

3. Release processes and yields

A spatially-dependent calculation of Europa's sputtered and radiolyiotically produced atmosphere should be based on the use of up-to-date plasma parameters and sputtering yields. The effect of both hot and cold ion populations on the surface material release should be estimated independently. Possible dependence of the sputtering rate on the regolith grain size as argued by Cassidy et al. (2013) should be examined too.

Knowledge of the physics of ice in the high radiation environment of Europa is a major component in understanding both the surface composition of this moon and the release of material to its tenuous atmosphere. Decades of laboratory experimentation on water ice, aimed at providing such knowledge, have now enabled a comprehensive, self-consistent and quantitative model for the yields of the major radiolysis products: O_2, H_2 and H_2O_2. Recent work by Teolis et al. (2017) revealed an inverse projectile range dependence in the yields (per unit deposited energy) of O_2 and H_2 from ice, but not in H_2O_2. This result suggests - unlike H_2O_2 which may be synthesized by hydroxyl reactions all along the particle tracks as they penetrate into the solid - that O_2 and H_2 are generated preferentially at the ice surface in an atomic scale layer ~30 Å in thickness. Preferential hydrogen escape from the surface-layer oxygenates the surface stoichiometry, altering the chemical pathways in favor of the formation of O_2 over H_2O_2. The analytical expressions approximating the energy and temperature dependence of the radiolysis yields, enabling accurate estimates of equilibrium H_2O_2 abundances in the surfaces, and sputtered source rates of H_2 and O_2 into the tenuous atmospheres, are fundamental components of future models of Europa's neutral environment. The applicability of these to Europa's icy surface is contingent on surface impurity concentrations, depending on the endogenic surface composition, and the degree of preferential sputtering, escape, and fallback of sputtered or cryovolcanic water vapor. Therefore, the future modeling efforts should take into account the constraints in the efficiency of surface release dependent on the abundance of surface impurities.

Water ice sublimation should be examined through the consideration of different surface composition patterns including impurities that can significantly diminish the efficiency of this mechanism. In addition, possible thermal anomalies on the surface should be incorporated in such estimations in order to define realistic rates of sublimated water outgassing at different surface points and during different moon orbital phases.

Moreover, the role of micrometeoroid impact vaporization as well as plume outgassing should be evaluated in more detail in the future with the scope to provide an upper limit in the atmosphere surplus due to these transient source process.

3. Particle re-impact to the surface

Considering the particle re-impact to the ice, the following considerations should be taken into account in a global model:

- sticking and thermal accommodation based on the properties of each particle species;
- gas diffusion through the porous regolith;
- cold trapping near the poles;

4. Particle circulation, interactions and loss

In the near-surface Knudsen layer, collisions and plasma ion chemistry should be taken into account in a global model. In an ideal case, the reaction cross sections considered in the model should be energy dependent, although such an assumption would require much longer calculation times. A collisionless approach can be assumed at regions where $Kn>1$. The modeling of the plasma flow around Europa is another important parameter determining the characteristics of the loss processes. Simplified approaches including the description of the flow as an incompressible flow around a conducting obstacle should be replaced by more accurate ones requiring the use, at least in the form of input, of quantities derived directly from MHD models (e.g. plasma energy and density at the borders of the atmosphere simulation box).

Finally, a three-dimensional model including all the water group species (e.g. H_2O, H_2, O_2, OH, O, H, H_2O_2), their ionization, dissociation and charge-exchange reactions, and their photochemistry would be required. The calculations based on a model with these characteristics can be of use when calibrating the instruments for the currently developed space missions to explore Jupiter's icy satellites—the ESA's JUICE (Grasset et al. 2013) and NASA's Mission to Europa (Pappalardo et al. 2015).

3.4. Possible future laboratory experiments to constrain the models

There are two groups of experiments and experimenters who deal with plasma interactions with water ice surfaces relevant to the icy moons: those who study irradiation processes in the ice (e.g., Loeffler et al. 2006; Strazzulla et al. 2007; Shi et al. 2011; Hand and Carlson 2011) and those who examine particle release from the ice (e.g., (Famá et al. 2008; Galli et al. 2016; Muntean et al. 2016)). In this chapter we will concentrate on the second group of experiments since the surface-release products are the source-components of Europa's atmosphere. So far, most experiments to quantify release processes were performed with water ice films on a microbalance to achieve a high measurement accuracy. However, these types of ice samples cannot be used for the study of the alteration processes inside the ice (e.g., weathering) as the required dimensions and physical (porosity and density) and chemical properties are quite far away from the realistic ones in ice regolith surfaces.

For Europa, the dominant process to release particles from the surface to the atmosphere is sputtering, whereas for Ganymede and Callisto sublimation may play an important role, too (Shematovich et al. 2005; Plainaki et al. 2015; Vorburger et al. 2015). Sublimation of ices as a function of temperature can easily be measured in a vacuum chamber. Two recent meta-studies on sublimation pressures of ices, were presented by Andreas (2007) and Fray and Schmitt (2009).

To accurately describe the sputtering process on Europa's icy surface, the quantity, the elemental composition, and the velocity distribution of all ejecta should be measured and determined as a function of the impactor's species (e^-, H^+, O^+, and S^+ being the dominant species (Paranicas et al. 2002)) and energy (eV to MeV), the ice temperature and the surface's physical properties. The effect of ion irradiation of water ice is described by the physical quantity of the sputtering yield, i.e., the number of molecules ejected from the ice per incident ion. A commonly used experimental technique to assess sputtering yields consists of vapour depositing a thin film (100 – 1000 nm) of compact (density ≈ 0.9 g cm^{-3}) amorphous ice onto a quartz microbalance (Famá et al. 2008; Shi et al. 2012). The ice film is then gradually sputtered and the observed frequency change of the quartz crystal allows to deduce the sputtering yield. For these thin ice films, surface charging effects usually do not bias sputtering yields as the surface potential is too weak to deflect the impinging energetic ions.

Galli et al. (2016) experimented with a different approach to study sputtering properties of water ice. They created thick and porous ice samples of micrometer-sized water ice grains covered by a frost layer, which is much more representative for the regolith surface of icy moons. Since a thick and porous ice layer cannot be attached to a microbalance they had to resort to a different method of measuring the sputtering yield: the measurement of the pressure rise in the vacuum chamber caused by sputtering. Moreover, the thick and cold ice samples are excellent insulators (electric conductivity ~10^{-15} S m^{-1} even with NaCl impurities), resulting in a strong and long-enduring electrical charging of the ice during ion bombardment.

The description of most sputtering experiments with ices before 2010 and of their outputs is included in an online database by the University of Virginia[1]. The impacting species include H, noble gases up to Xe, C, N, O, and F, and noble gases up to Xe, with energies ranging from roughly 1 keV to 25 MeV. There is also reference to one study (Heide, 1984) about 100 keV electrons sputtering water ice molecules. Noble gas ions are often used as impactors for practical rather than for scientific reasons. Noble gases are easy to acquire and they do not react with surfaces and valves inside vacuum chambers contrary, for example, to sulphur. Argon is sometimes used in sputtering experiments as a proxy for sulphur because it has similar mass. Additional experimental studies not listed by Johnson and Liu (2010) were done by Farenzena et al. (2006) who shot 65 MeV Ba^{15+} ions at various ice species and by Shi et al. (2012) who used Ar ions to study electrical properties of irradiated water ice. Recent sputtering experiments with water ice on microbalances are presented by Muntean et al. (2016) (singly and doubly charged ions of solar wind energy) and by Galli et al. (2017) (Ar^+, Ar^+, O^+, O^+, O_2^+, and electrons).

For ion energies below 1 keV, the sputtering yield of ions in water ice can be described by a cascade of elastic collisions, whereas at higher energies, the so-called electronic sputtering dominates. Famá et al. (2008) derived a semi-empirical formula for the sputtering yield for the sum of both contributions, based on laboratory experiments with water ice films:

---

1 http://www.people.virginia.edu/~rej/sputter_surface.html

$$Y(\mathrm{E},\mathrm{m}_1,\mathrm{Z}_1,\theta,\mathrm{T}) = \frac{1}{U_0}\left(\frac{3}{4\pi^2 C_0}\alpha \mathrm{S}_n + \eta \mathrm{S}_e^2\right)\left(1 + \frac{Y_1}{Y_0}\exp\left(\frac{-E_a}{\mathrm{kT}}\right)\right)\cos^{-f}(\theta) \quad \text{Eq. (2)}$$

Equation (2) quantifies the sputtering yield as a sum of elastic and electronic sputtering, described by the nuclear stopping power S_n and the electronic stopping power S_e. The sputtering yield depends on energy E, mass of impactor m_1, atomic number of impactor Z_1, the incidence angle θ from the 90 surface normal, and temperature T. For U_0, the sublimation energy of water (0.45 eV) is assumed, C_0 = 1.3 Å^2, E_a = 0.06 eV, and Y_1/Y_0 = 220 are constants. The temperature-independent fraction in Equation (2) is due to the direct ejection of H_2O molecules. The temperature-dependent term with the activation energy E_a becomes dominant above T = 120 K and is due to the release of H_2 and O_2 (Johnson et al. 2004; Famá et al. 2008; Teolis et al. 2009). Water radicals inside the irradiated ice react to form mainly H_2 and O_2, which are then released by sputtering (O_2) or diffusion (H_2). Given the angular dependence of the yield in Equation (2), one expects an order of magnitude higher sputtering yields at ion incidence angles between 60° and 80° than for perpendicular ion impacts. The condition is that the ice sample is microscopically smooth. Küstner et al. (1998) studied graphite surfaces of varying roughness on a μm scale and found that the sputtering yield increased only by a factor of 2.5 when the ion incidence angle increased from 0° to 80°. For a smooth graphite surface, they confirmed that the yield increases by more than a decade.

Cassidy et al. (2013) examined the data compiled by Johnson and Liu (2010) and found that the semi-empirical sputtering Equation (2) fits data well for energies below 100 keV. At higher energies, the formula by Johnson et al. (2009) for electronic sputtering is more accurate. In Figure 24, we juxtapose the total sputtering yield caused by O^+ ions (predicted with the formulae given by Famá et al. (2008) and by Johnson et al. (2009) for energies below and above 100 keV, respectively) to the yield of O_2 alone according to Teolis et al. (2010). The O_2 yield is more important for atmospheric modeling than the total yield, as the latter is dominated by H_2O molecules that will stick to the surface again. Figure 24 illustrates that the O_2 yield is not a fixed fraction of the total sputtering yield, the ratio is highest for ion energies around 10 keV.

Impacting electrons are not expected to directly eject water molecules out of the ice, nevertheless, they contribute to the production of O_2, H_2, and H_2O_2 (Hand and

Carlson, 2011). In their review paper, Teolis et al. (2016) presented O_2 sputtering yields and penetration depths as a function of electron energy based on theory and experiments at low energies (Orlando and Sieger 2003). The first experiments at electron energies above 100 eV indicated that the yield does increase until 1 keV but the expected decrease above 1 keV cannot be reproduced yet (Galli et al. 2017).

For atmospheric models, the energy distribution of the sputtered ejecta is as important as the sputtering yield. The characteristic energy of sputtered particles is orders of magnitudes lower than the energy of the impactors. Cassidy and Johnson (2005) modeled the sputter product energy distribution from any regolith target as the sum of the "planar binding" sputter product energy distribution (Boring et al. 1984) and a Maxwell energy distribution for the part of volatiles (O_2 and H_2) that interact and thermalize with neighbouring regolith grains before escaping:

$$f(E) = \mathrm{Y}_1 \frac{2\mathrm{UE}}{(\mathrm{E+U})^3} + \mathrm{Y}_2 \frac{E}{(\mathrm{kT})^2} \exp\left(\frac{-E}{\mathrm{kT}}\right) \quad \text{Eq. (3)}$$

The predicted energy of the thermalized O_2 and H_2 reaches only kT= 0.008 eV at regolith temperatures of 90 K. On the other hand, the median energy of ejected water molecules for 6 keV ions sputtering water ice was observed by Haring et al. (1984) to range between 0.15 and 0.19 eV. This implies that U in the first term of Equation (3) approximates the sublimation energy. The surface binding energy of water would be a decade smaller (U = 0.054 eV). Interestingly enough, a similar energy (0.05 eV) was found in experiments by Haring et al. (1984) for the bulk of O_2 released from water ice.

From measurements of the angular distribution of sputtered H_2O from amorphous water ice films, Vidal et al. (2005) concluded that the angular distribution of water molecules follows $\sim\cos^{1.3}\phi$ at an ice temperature of 100 K. In this case, 2/3 of the sputtered molecules leave the ice in a cone of $\phi = 40^0$ around the surface normal. In the most extreme case of H_2O ejected uniformly to all angles, ϕ would increase from 40° to 60°.

The ion sputtering yield from laboratory measurements agrees between different groups within a factor of two (Johnson et al. 2004; Famá et al. 2008) for similar experiment set-ups, that is, for a thin film of pure water ice with densities > 0.9 g cm^{-3} (Famá et al. 2008) and low temperatures (T < 100 K). This uncertainty per se would not be troublesome for atmosphere models of Europa, as other parameters are not more accurately known, either. Among other reasons, different studies take porosity into account by enhancing laboratory yields by a factor of 1–4 (Marconi, 2007). Unfortunately, it is unclear if the subsequent release of radiolysed H_2 and O_2 is included in all publications the same way (see Teolis et al. (2016) for a recent overview).

Galli et al. (2016) tackled the questions related to porosity by creating a 0.9 cm thick and porous sample of water ice grains. Their first results indicate sputtering yields similar to previous lab experiments performed with water ice films sputtered off a microbalance. These results are thus consistent with the notion that sputtering from porous regolith ice is similar to dense monolayers of water ice. But more experiments at various energies, incidence angles, and different ion species are required to make a stronger statement. An inherent problem of experimenting with thick porous layer is the accuracy of the measurement methods (see Galli et al. 2017 for a quantitative assessment).

The sticking probability (or duration) is linked to the uncertainty introduced by porosity. Generally the H_2O is assumed to stick to the ice again, whereas O_2 and H_2 do not permanently stick. This is justified, as experiments by Gibson et al. (2011) showed that for 0.3 and 0.7 eV energies, 98% to 99% of ejected water molecules stick to crystalline water ice. Because of that sticking probability, a sputtered water molecule is less probable to escape from within a porous ice layer. In contrast, the amount of O_2 and H_2 ejected is controlled only by the details of the radiation chemistry. Cassidy and Johnson (2005) therefore concluded from a Monte Carlo model that the reduction of the H_2O sputtering yield from water ice due to porosity is on the order of 70% compared to the sputtering from a dense and smooth ice surface.

However, Cassidy et al. (2013) assumed that in reality the reduction due to porosity is compensated by the sputtering yield increase due to the irregular surface. Contrary to a smooth surface, ions will hit the grains in a rough surface at a wide distribution of impact angles, thus the average sputtering yield for a perpendicular incidence angle will be closer to the yield observed at a 45° incidence angle. This effect of porosity on angular dependence is only expected for the regime of single elastic collisions up to few keV energies of impacting ions.

If experimental results from coarse graphite surfaces (Küstner et al. 1998) also apply to water ice, the yield from porous ice varies only by a factor of 2 or 3 for the full range of incidence angles in contrast to the order of magnitude expected from $\sim\cos^{-f}(\theta)$ (Equation (2)). To decide whether this affects atmospheric models one has to integrate the sputter yield over the whole angular range of the ion distribution. A spatially uniform ion distribution would result in a two times lower sputtering production if we adopt the flat angular dependence instead of the cosine-law of Equation (2). But more experimental results, in particular for water ice, are needed (see Section 4) before discussing potential effects on atmospheric models.

Another element of uncertainty is the charge state of the ions. In their alternative interpretation of Europa's atmosphere, Shemansky et al. (2014) proposed that sputtering was dominated by multiply charged O and S ions with charge state of 3 and higher. Aumayr and Winter (2004) showed that for perfect insulator surfaces such as NaCl and LiF the sputtering yield increases with recombination energy and thus with the charge state of the impacting ion (see also reviews of this topic in Kallio et al. 2008 and Wurz et al. 2010). Aumayr and Winter (2004) did not study ice targets. Cooper and Tombrello (1984) found that the sputtering yield from a water ice film doubled when they switched from F^{4+} to F^{8+} in the MeV range, but these charge states and energies are not representative for Europa's plasma environment. In more recent experiments, Muntean et al. (2016) and Galli et al. (2017) found no significant difference in sputtering yields between singly and doubly charged C, N, O, and Ar for energies between 1 and 50 keV

Other areas where little or no experimental results exist include the release yield due to high energy electrons and due to impacting molecules (Equation (2) applies only to single atoms). The case of impacting O_2 or O_2^+ is of particular interest for Europa (Dols et al. 2016): Galli et al. 2017 found that the sputtering yield due to O_2^+ in the electronic sputtering regime is two times higher than expected, but no general framework exists yet to accommodate these data. The sputtering yield due to electrons may be orders of magnitude smaller than for ions of the same energy (Galli et al. 2017). Nevertheless, electron irradiation would still play an important role for Europa's surface: due to their much deeper penetration depth, energetic electrons from the Jovian magnetosphere can irradiate the top centimeters of ice layers, whereas ions of that energy are stopped within the top 10-100 μm (Hand and Carlson 2011).

Since the open issues discussed above cannot be quantified with first-principle analyses or numerical methods only (Johnson, 1989; Cassidy and Johnson, 2005), the role of laboratory work becomes substantial for providing information in the following directions:

1. Identify the ways in which porosity affects sputtering

Porosity, ion incidence angle, and surface roughness should be varied independently from each other in laboratory tests similar to the ones described in Galli et al. (2016) to see if sputtering yield, energy distribution, and angular distribution are similar for deep porous ice and ice films.

2. Study radiolysis products from porous water ice and understand for how long do H_2 and O_2 remain trapped inside such types of ice

If the atmospheric O_2 is the direct release product, looking at the O_2 atmosphere we are mostly sensitive to the dayside surface close to the equator and, in particular, to the subsolar point (Plainaki et al. 2013).

3. Determine how the chemical composition of the sputtered ejecta relates to that of the surface; determine the timescale for space-weathering

Sputtering does not give a 1:1 stoichiometric representation of the surface composition as we know from sputtering experiments with Moon and Mercury analogues (Dukes et al. 2011) that volatiles (e.g. Na) are preferentially released from irradiated silicates. As a result, the surface composition will change with respect to the bulk composition (the so-called "space weathering") until it reaches a new steady state. As a result, the elements less efficiently sputtered will be enhanced in a thin surface layer compared to the bulk composition, whereas the composition of the ejecta will reflect the bulk composition. Is the timescale to reach this steady state similar to the very short timescales (typically ~years for the uppermost μm) derived for sputtering, radiolysis, and regolith growth (Cooper et al. 2001; Johnson et al. 2004)?

4. Determine the O_2 release yield due to high-energy electrons

Very little is known about sputtering yield (direct or via radiolysis) from electron precipitation (Heide, 1984; Orlando and Sieger, 2003). The recent review paper by Teolis et al. (2016) makes predictions for the O_2 yield from electrons irradiating water ice including energies > 100 eV, which have never been studied in laboratory. This gap should be filled.

5. Study scattered particles, and in particular O^+ and S^+ ions reflected from the surface; study the sputtering yield from multiply charged ions

These magnetospheric ions can be back-scattered as ions, neutrals (Wieser et al. 2016), or possibly negative ions.

6. Expand the description of the sputtering yield to molecular species.

It is of interest to understand the effects of molecules impacting water ice.

4. Definition of suitable observation strategies for future missions to Europa

Europa's tenuous atmosphere represents the actual interface between the icy surface of this moon and the giant planet's environment. In this perspective, its characterization is of key importance to achieve a fully understanding of the alteration processes induced on the icy surfaces by the radiation environment. A few examples illustrating this point are:

- The deposition of neutral species from the tenuous atmosphere onto the moon's surface will spectrally mask the weathering products (deposition of H_2O) or directly start new chemical patterns (e.g.: oxidation by oxygen-bearing species)
- The efficiency of weathering and particle release from the surface may be reduced by the ionosphere.

It is, therefore, clear that a full interpretation of surface data and an in depth understanding of the surface evolution history, has as a necessary prerequisite the accurate determination of the role of the tenuous atmosphere in the interactions between the icy moons and the Jupiter's magnetospheric environment. Moreover to understand the mass and energy exchange between Europa and Jupiter's magnetosphere, the detailed characterization of the tenuous atmosphere as a boundary region between the moon and the giant planet's magnetosphere, is fundamental. Many factors determining the characteristics of the tenuous atmosphere are not obviously assessed a priori (e.g. the actual flux of charged particles impacting the surface; the density of the ionosphere). Therefore, the understanding of the generation and dissipation mechanisms of Europa's tenuous atmosphere requires a long term monitoring of several parameters, with comparable coverage and sampling in time and space. The achievement of the related science objectives of future missions to

Europa will be feasible only through an interdisciplinary approach characterized by coordinated observation scenarios and joint campaigns in payload operations. Namely, it is of key importance to measure - in the larger possible extent allowed by the details of the flybys phase - the following quantities:

- Density of neutral species
- Density of ionosphere and charged particles fluxes
- Efficiency of interactions of the tenuous atmosphere with particle and photon radiation fields

While the JUICE payload elements have the potential to assess these phenomena, it should be stressed that each dataset alone can not fully assess the moon's atmosphere behavior; the highly dynamical nature of the involved processes requires a joint analysis to properly interpret the data correlation in a vast extent. Through the planning of potential synergies between different datasets to be obtained during the two Europa flybys, a contribution to the achievement of the JUICE scientific objectives related to Europa will be provided (see Table 5). In particular, the measurements related to the moon's tenuous atmosphere will help to answer the following JUICE science objectives:

- Determine the composition of the non-ice material at Europa, especially as related to habitability;
- Search for liquid water under the most active sites at Europa;
- Study the recently active processes at Europa;
- Understand the moons as sources and sinks of Jupiter's magnetospheric plasma;

It is clear that such considerations, intimately of interdisciplinary nature, are of significant importance while planning the JUICE mission observations since the latter can dramatically increase our knowledge on the involved physical phenomena. In this concept, the following inter-disciplinary science goals can be defined:

- Characterization of the atmospheric environment of Europa
- Investigation of the interactions between the tenuous atmosphere of Europa and the Jovian magnetosphere, with respect to the relation between the time-scales of their variations
- Study of the moon atmosphere - surface coupling as a main agent for both the atmosphere generation and the surface weathering

Each one of the proposed goals can be further structured in one or more specific interdisciplinary science objectives (see Table 5) with respect to their compatibility to the mission resources and instrument requirements. In Table 5 we also demonstrate that each one of the proposal's science objectives is directly related to one or more JUICE mission Science Objectives. It is furthermore emphasized that in order to accurately plan such synergies, the use of a global model for the tenuous atmosphere of Europa (see Section 3.3) is strongly required.

Below we provide an example of possible interdisciplinary research related to the Europa's tenuous atmosphere to be done once the JUICE s/c has arrived at the moon. Given the variability of the environment around the icy moon, such studies can be considered to refer to the more general thematic of planetary space weather (Lilensten et al. 2014; Plainaki et al. 2016). In Figure 25, a snapshot corresponding to the JUICE s/c arrival to Europa is shown. The JUICE s/c will be at a distance of ~ 22,745 km from Europa with a phase angle of ~ 87.4^0. On the same figure, the expected spatial distribution of the O_2 tenuous atmosphere, for this exact configuration between Jupiter, Europa and the Sun, as derived from the EGEON model (Plainaki et al. 2012; 2013), is overlaid. During approach, JUICE will cover the regions above the trailing terminator. This configuration favors also the direct search for the occurrence of possible plumes (Huybrighs et al. 2017) also in the northern hemisphere as well as the detection of plume-material (possibly scattered from condensates) originating from the southern hemisphere, with UVS, SWI, JANUS, MAJIS and PEP-JNA (the latter at distances smaller than ~12,000 km) (science objective G1.2 in Table 1). Detailed studies of the chemical composition of Europa's exosphere will be performed with PEP-NIM (Wurz et al. 2014). This configuration allows also the detection in the dayside of non-LTE emissions from minor components (CO_2, CO, Na, H_2O) and airglow emissions as well; at the nightside the detection of airglow emissions from water and O_2 products (O, OH, H) can be attempted since the existence of long-lived species in excited states cannot be ruled out in the almost collisionless environment of Europa. Moreover, this configuration is favorable for the determination of the tenuous atmosphere morphology above both the illuminated and non-illuminated hemispheres allowing the identification of possible inhomogeneity (science objective G1.2) and, consequently, a direct comparison with the spatial distributions provided by the existing atmosphere models. It is stressed that current models predict different spatial distributions for the O_2 tenuous atmosphere of Europa. The EGEON model assumes a strong dependence of the release yields on surface temperature, resulting in the O_2 density asymmetry seen in Figure 25. Conversely, other authors consider this dependence negligible, implying a more symmetric tenuous atmosphere (Cassidy et al. 2013). Therefore, the observation geometry in Figure 25 allows one to evaluate the role of surface temperature in the generation of the O_2 tenuous atmosphere. Instruments such as SWI and PEP-JNA can map before the flyby the densities above subsolar and antisolar points, allowing a clean discrimination between the two scenarios.

5. Conclusions

Europa's tenuous atmosphere is a complex field of active ongoing research. Although the existing observations of Europa's exosphere have provided important constraints for determining its generation and loss rates, a direct measurement of the main exospheric species (i.e. H_2O, O_2, H_2) has not been performed yet and the limited available observations are just proxies of these bulk constituents. In the absence of an adequate number of in situ observations, modeling becomes a fundamental tool for understanding the nature of Europa's neutral environment and for planning future space observations.

Sputtering and radiolysis are key source processes for the atmosphere of Europa provoking also the alteration of the moon surface, in terms of composition, reflectance, volatility and porosity. Understanding the structure and the emission properties of Europa's rarefied atmosphere allows to infer about the relative composition of the parent molecules released from the moon’s icy surface due to its bombardment by Jupiter’s magnetospheric plasma. At the same time, the correct interpretation of surface data requires necessarily the accurate determination of the tenuous atmosphere in the plasma-icy moon interactions. Being also the tenuous atmosphere the boundary region between Jupiter's magnetosphere and the icy surface, it becomes the laboratory for studying the mass and energy exchange between the moon and the giant planet. The science of the Europa environment, therefore, becomes a critical and interdisciplinary aspect of the study of the whole Jovian system.

In the current paper, in a larger view approach that involves different disciplines, we reviewed the available in situ and telescope observations and compared a large part of the existing plasma and atmosphere models. We discussed different controversial issues among models and presented the advantages and disadvantages of different modeling techniques. Based on our review, we defined the required characteristics for a community-unified atmospheric model in means of main physical phenomena to be included, acceptable assumptions and approximations. We conclude that there is an urgent need to implement such a global model for the environment around Europa, paying special attention to its spatial and temporal variability. Such a project would be very important for planning correctly the observations that will address the main science goals during future missions to the Europa moon.

References

M. Allen, Nature354, 272 (1991). DOI 10.1038/354272a0

E.L. Andreas, Icarus186, 24 (2007). DOI 10.1016/j.icarus.2006.08.024

J.M. Ajello, The Journal of Chemical Physics 55(7), 3169 (1971). DOI 10.1063/1.1676564

F. Aumayr, H. Winter, Philosophical Transactions of the Royal Society of London A: Mathematical, Physical and Engineering Sciences 362(1814), 77 (2004). DOI 10.1098/rsta.2003.1300. http://rsta.royalsocietypublishing.org/content/362/1814/77

F. Bagenal, J.D. Sullivan, G.L. Siscoe, Geophys. Res. Lett.7, 41 (1980). DOI 10.1029/GL007i001p00041

F. Bagenal, E. Sidrow, R.J. Wilson, T.A. Cassidy, V. Dols, F.J. Crary, A.J. Ste, P.A. Delamere, W.S. Kurth, W.R. Paterson, Icarus261, 1 (2015). DOI 10.1016/j.icarus.2015.07.036

F. Bagenal, J. Geophys. Res.99, 11043 (1994). DOI 10.1029/93JA02908

D.A. Bahr, M. Famá, R.A. Vidal, R.A. Baragiola, J. Geophys. Res.106, 33285 (2001). DOI 10.1029/2000JE001324

Bird, G.A., (1994). Molecular Gas Dynamics and the Direct Simulation of Gas Flows. Clarendon Press, Oxford, England.

A. Blöcker, J. Saur, L. Roth, Journal of Geophysical Research (Space Physics) 121, 9794 (2016). DOI 10.1002/2016JA022479

J.W. Boring, J.W. Garrett, T.A. Cummings, R.E. Johnson, W.L. Brown, Nuclear Instruments and Methods in Physics Research B 1, 321 (1984). DOI 10.1016/0168-583X(84)90087-9

P.C. Brandt, D.G. Mitchell, Y. Ebihara, B.R. Sandel, E.C. Roelof, J.L. Burch, R. Demajistre, Journal of Geophysical Research (Space Physics) 107, 1359 (2002). DOI 10.1029/2001JA000084

M.E. Brown, Icarus151, 190 (2001). DOI 10.1006/icar.2001.6612

M.E. Brown, R.E. Hill, Nature380, 229 (1996). DOI 10.1038/380229a0

M.H. Burger, R.E. Johnson, Icarus171, 557 (2004). DOI 10.1016/j.icarus.2004.06.014

M.H. Burger, R. Wagner, R. Jaumann, T.A. Cassidy, Space Sci. Rev.153, 349 (2010). DOI 10.1007/s11214-010-9645-z

T.A. Cassidy, R.E. Johnson, O.J. Tucker, Icarus201, 182 (2009). DOI 10.1016/j.icarus.2008.12.033

T.A. Cassidy, R.E. Johnson, Icarus176, 499 (2005). DOI 10.1016/j.icarus.2005.02.013

T.A. Cassidy, C.P. Paranicas, J.H. Shirley, J.B. Dalton, III, B.D. Teolis, R.E. Johnson, L. Kamp, A.R. Hendrix, Planet. Space Sci.77, 64 (2013). DOI 10.1016/j.pss.2012.07.008

T.A. Cassidy, R.E. Johnson, P.E. Geissler, F. Leblanc, Journal of Geophysical Research (Planets) 113, E02005 (2008). DOI 10.1029/2007JE002955

T.A. Cassidy, R.E. Johnson, M.A. McGrath, M.C. Wong, J.F. Cooper, Icarus191, 755 (2007). DOI 10.1016/j.icarus.2007.04.033

A.F. Cheng, J. Geophys. Res.91, 4524 (1986). DOI 10.1029/JA091iA04p04524

F. Cipriani, F. Leblanc, O. Witasse, R.E. Johnson, Geophys. Res. Lett.36, L12202 (2009). DOI 10.1029/2009GL038636

F. Cipriani, F. Leblanc, O. Witasse, R.E. Johnson, Geophys. Res. Lett.35, L19201 (2008). DOI 10.1029/2008GL035061

J.E.P. Connerney, M.H. Acuña, N.F. Ness, T. Satoh, J. Geophys. Res.103, 11929 (1998). DOI 10.1029/97JA03726

B.H. Cooper, T.A. Tombrello, Radiation E_ects 80(3-4), 203 (1984). DOI 10.1080/00337578408216464

J.F. Cooper, R.E. Johnson, B.H. Mauk, H.B. Garrett, N. Gehrels, Icarus149, 133 (2001). DOI 10.1006/icar.2000.6498

A. Coustenis, T. Tokano, M.H. Burger, T.A. Cassidy, R.M. Lopes, R.D. Lorenz, K.D. Retherford, G. Schubert, Space Sci. Rev.153, 155 (2010). DOI 10.1007/s11214-009-9615-5

P.A. Delamere, F. Bagenal, A. Ste_, Journal of Geophysical Research (Space Physics) 110, A12223 (2005). DOI 10.1029/2005JA011251

V.J. Dols, F. Bagenal, T.A. Cassidy, F.J. Crary, P.A. Delamere, Icarus264, 387 (2016). DOI 10.1016/j.icarus.2015.09.026

V. Dols, P.A. Delamere, F. Bagenal, W.S. Kurth, W.R. Paterson, Journal of Geophysical Research (Planets) 117, E10010 (2012). DOI 10.1029/2012JE004076

V. Dols, P.A. Delamere, F. Bagenal, Journal of Geophysical Research (Space Physics) 113, A09208 (2008). DOI 10.1029/2007JA012805

C.A. Dukes, W.Y. Chang, M. Famá, R.A. Baragiola, Icarus212, 463 (2011). DOI 10.1016/j.icarus.2011.01.027

S. Duling, J. Saur, J. Wicht, Journal of Geophysical Research (Space Physics) 119, 4412 (2014). DOI 10.1002/2013JA019554

A. Eviatar, A. Bar-Nun, M. Podolak, Icarus61, 185 (1985). DOI 10.1016/0019-1035(85)90100-9

Famà, M., Shi, J., Baragiola, R.A., Surf. Sci. 602, 156–161, (2008) DOI:10.1016/j.susc.2007.10.002

L.S. Farenzena, P. Iza, R. Martinez, F.A. Fernandez-Lima, E.S. Duarte, G.S. Faraudo, C.R. Ponciano, M.G.P. Homem, A.N. de Brito, K. Wien, E.F. da Silveira, Earth Moon and Planets 97, 311 (2005). DOI 10.1007/s11038-006-9081-y

N. Fray, B. Schmitt, Planet. Space Sci.57, 2053 (2009). DOI 10.1016/j.pss.2009.09.011

A. Galli, A. Vorburger, A. Pommerol, P. Wurz, B. Jost, O. Poch, Y. Brouet, M. Tulej, N. Thomas, Planet. Space Sci.126, 63 (2016). DOI 10.1016/j.pss.2016.03.016

L.J. Gleeson, W.I. Axford, Ap&SS2, 431 (1968). DOI 10.1007/BF02175919

O. Grasset, M. Dougherty, A. Coustenis, E. Bunce, C. Erd, D. Titov, M. Blanc, A. Coates, P. Drossart, L. Fletcher, H. Hussmann, R. Jaumann, N. Krupp, J.P. Lebreton, O. Prieto-Ballesteros, P. Tortora, F. Tosi, H.T. Van, PLANETARY AND SPACE SCIENCE 78, 1 (2013). DOI 10.1016/j.pss.2012.12.002.

D.A. Gurnett, W.S. Kurth, A. Roux, S.J. Bolton, E.A. Thomsen, J.B. Groene, Geophys. Res. Lett.25, 237 (1998). DOI 10.1029/97GL03706

H.G. Heide, Ultramicroscopy 14(3), 271 (1984). DOI 10.1016/0304-3991(84)90095-0.

D.T. Hall, P.D. Feldman, M.A. McGrath, D.F. Strobel, ApJ499, 475 (1998). DOI 10.1086/305604

D.T. Hall, D.F. Strobel, P.D. Feldman, M.A. McGrath, H.A. Weaver, Nature373, 677 (1995). DOI 10.1038/373677a0

K.P. Hand, R.W. Carlson, Icarus215, 226 (2011). DOI 10.1016/j.icarus.2011.06.031

C.J. Hansen, D.E. Shemansky, A.R. Hendrix, Icarus176, 305 (2005). DOI 10.1016/j.icarus.2005.02.007

G.B. Hansen, T.B. McCord, Journal of Geophysical Research (Planets) 109, E01012 (2004). DOI 10.1029/2003JE002149

R. Haring, Chemical sputtering induced by keV ion bombardment. Ph.D. thesis, PhD Thesis, Univ. of Leiden, Holland, (1984)

A.R. Hendrix, T.A. Cassidy, R.E. Johnson, C. Paranicas, R.W. Carlson, Icarus212, 736 (2011). DOI 10.1016/j.icarus.2011.01.023

S. Hoang, N. Meyer-Vernet, M. Moncuquet, A. Lecacheux, B.M. Pedersen, Planet. Space Sci.41, 1011 (1993). DOI 10.1016/0032-0633(93)90105-B

S.M. Hörst, M.E. Brown, ApJ764, L28 (2013). DOI 10.1088/2041-8205/764/2/L28

C.J.A. Howett, J.R. Spencer, J. Pearl, M. Segura, Journal of Geophysical Research (Planets) 116, E03003 (2011). DOI 10.1029/2010JE003718

H.L. Huybrighs, Y. Futaana, S. Barabash, M. Wieser, P. Wurz, N. Krupp, K.H. Glassmeier, B. Vermeersen, Icarus 289, 270 (2017)

D.S. Intriligator, W.D. Miller, Geophys. Res. Lett.8, 409 (1981). DOI 10.1029/GL008i004p00409

W.H. Ip, D.J. Williams, R.W. McEntire, B.H. Mauk, Geophys. Res. Lett.25, 829 (1998). DOI 10.1029/98GL00472

W.H. Ip, Icarus120, 317 (1996). DOI 10.1006/icar.1996.0052

Y. Itikawa, Journal of Physical and Chemical Reference Data 38(1) (2009)

X. Jia, J.A. Slavin, T.I. Gombosi, L.K.S. Daldor_, G. Toth, B. Holst, Journal of Geophysical Research (Space Physics) 120, 4763 (2015). DOI 10.1002/2015JA021143

X. Jia, R.J. Walker, M.G. Kivelson, K.K. Khurana, J.A. Linker, Journal of Geophysical Research (Space Physics) 114, A09209 (2009). DOI

10.1029/2009JA014375

R.E. Johnson, Icarus 78, 206-210, (1989)

R.E. Johnson, Energetic Charged-Particle Interactions with Atmospheres and Surfaces (1990)

R.E. Johnson, Physics and Chemistry in Space 19 (1990)

R.E. Johnson, M.R. Combi, J.L. Fox, W.H. Ip, F. Leblanc, M.A. McGrath, V.I. Shematovich, D.F. Strobel, J.H. Waite, Space Sci. Rev.139, 355 (2008). DOI 10.1007/s11214-008-9415-3

R.E. Johnson, R.M. Killen, J.H. Waite, Jr., W.S. Lewis, Geophys. Res. Lett.25, 3257 (1998). DOI 10.1029/98GL02565

R.E. Johnson, L.J. Lanzerotti, W.L. Brown, Nuclear Instruments and Methods in Physics Research 198, 147 (1982). DOI 10.1016/0167-5087(82)90066-7

R.E. Johnson, R.W. Carlson, J.F. Cooper, C. Paranicas, M.H. Moore, M.C. Wong, Radiation e_ects on the surfaces of the Galilean satellites (2004), pp. 485-512

R.E. Johnson, M.H. Burger, T.A. Cassidy, W.H. Smyth, M.L. Marconi, (2009). Modeling Europa’s tenuous atmosphere. In: Pappalardo, R.T., McKinnon, W.B., Khurana, K.K. (Eds.), Europa.

K. Kabin, M.R. Combi, T.I. Gombosi, A.F. Nagy, D.L. DeZeeuw, K.G. Powell, J. Geophys. Res.104, 19983 (1999). DOI 10.1029/1999JA900263

E. Kallio, P. Wurz, R. Killen, S. McKenna-Lawlor, A. Milillo, A. Mura, S. Massetti, S. Orsini, H. Lammer, P. Janhunen, W.H. Ip, Planet. Space Sci.56, 1506 (2008). DOI 10.1016/j.pss.2008.07.018

I. Kanik, C. Noren, O.P. Makarov, P. Vattipalle, J.M. Ajello, D.E. Shemansky, Journal of Geophysical Research (Planets) 108, 5126 (2003). DOI 10.1029/2000JE001423

K.K. Khurana, M.G. Kivelson, D.J. Stevenson, G. Schubert, C.T. Russell, R.J. Walker, C. Polanskey, Nature395, 777 (1998). DOI 10.1038/27394

K.K. Khurana, J. Geophys. Res.102, 11295 (1997). DOI 10.1029/97JA00563

K.K. Khurana, X. Jia, M.G. Kivelson, F. Nimmo, G. Schubert, C.T. Russell, Science 332, 1186 (2011). DOI 10.1126/science.1201425

R. Killen, G. Cremonese, H. Lammer, S. Orsini, A.E. Potter, A.L. Sprague, P. Wurz, M.L. Khodachenko, H.I.M. Lichtenegger, A. Milillo, A. Mura, Space Sci. Rev.132, 433 (2007). DOI 10.1007/s11214-007-9232-0

E. Kirsch, S.M. Krimigis, W.H. Ip, G. Gloeckler, Nature292, 718 (1981a). DOI 10.1038/292718a0

E. Kirsch, S.M. Krimigis, J.W. Kohl, E.P. Keath, Geophys. Res. Lett.8, 169 (1981b). DOI 10.1029/GL008i002p00169

M.G. Kivelson, K.K. Khurana, S. Joy, C.T. Russell, D.J. Southwood, R.J. Walker, C. Polanskey, Science 276, 1239 (1997). DOI 10.1126/science.276.5316.1239

M.G. Kivelson, F. Bagenal, W.S. Kurth, F.M. Neubauer, C. Paranicas, J. Saur, Magnetospheric interactions with satellites, in Jupiter: The Planet, Satellites and Magnetosphere, ed. by F. Bagenal, T.E. Dowling, W.B. McKinnon (Cambridge University Press, Cambridge, 2004), pp. 513–536

M.G. Kivelson, K.K. Khurana, M. Volwerk, Europa's interaction with the Jovian magnetosphere, in Europa, ed. by R.T. Pappalardo, W.B. McKinnon, K.K. Khurana, University of Arizona Press, Tucson, 2009, p. 545

A.J. Kliore, D.P. Hinson, F.M. Flasar, A.F. Nagy, T.E. Cravens, Science 277, 355 (1997). DOI 10.1126/science.277.5324.355

P. Kollmann, C. Paranicas, G. Clark, E. Roussos, A. Lagg, N. Krupp, Geophys. Res. Lett.43, 9425 (2016). DOI 10.1002/2016GL070326

D. Koschny, E. Grün, Icarus154, 402 (2001). DOI 10.1006/icar.2001.6708

S.M. Krimigis, D.G. Mitchell, D.C. Hamilton, S. Livi, J. Dandouras, S. Jaskulek, T.P. Armstrong, J.D. Boldt, A.F. Cheng, G. Gloeckler, J.R. Hayes, K.C. Hsieh, W.H. Ip, E.P. Keath, E. Kirsch, N. Krupp, L.J. Lanzerotti, R. Lundgren, B.H. Mauk, R.W. McEntire, E.C. Roelof, C.E. Schlemm, B.E. Tossman, B. Wilken, D.J. Williams, Space Sci. Rev.114, 233 (2004). DOI 10.1007/s11214-004-1410-8

S.M. Krimigis, D.G. Mitchell, D.C. Hamilton, J. Dandouras, T.P. Armstrong, S.J. Bolton, A.F. Cheng, G. Gloeckler, K.C. Hsieh, E.P. Keath, N. Krupp, A. Lagg, L.J. Lanzerotti, S. Livi, B.H. Mauk, R.W. McEntire, E.C. Roelof, B. Wilken, D.J. Williams, Nature415, 994 (2002). DOI 10.1038/415994a

N. Krupp, J. Woch, A. Lagg, B. Wilken, S. Livi, D.J. Williams, Geophys. Res. Lett.25, 1249 (1998). DOI 10.1029/98GL00863

W.S. Kurth, D.A. Gurnett, A.M. Persoon, A. Roux, S.J. Bolton, C.J. Alexander, Planet. Space Sci.49, 345 (2001). DOI 10.1016/S0032-0633(00)00156-2

M. Küstner, W. Eckstein, V. Dose, J. Roth, Nuclear Instruments and Methods in Physics Research B 145, 320 (1998). DOI 10.1016/S0168-583X(98)00399-1

A. Lagg, N. Krupp, J. Woch, D.J. Williams, Geophys. Res. Lett.30, 1556 (2003). DOI 10.1029/2003GL017214

L.J. Lanzerotti, C.G. Maclennan, T.P. Armstrong, S.M. Krimigis, R.P. Lepping, N.F. Ness, J. Geophys. Res.86, 8491 (1981). DOI 10.1029/JA086iA10p08491

F. Leblanc, A.E. Potter, R.M. Killen, R.E. Johnson, Icarus178, 367 (2005). DOI 10.1016/j.icarus.2005.03.027

F. Leblanc, R.E. Johnson, M.E. Brown, Icarus159, 132 (2002). DOI 10.1006/icar.2002.6934

E. Lellouch, D.F. Strobel, M.J.S. Belton, M.E. Summers, G. Paubert, R. Moreno, ApJ459, L107 (1996). DOI 10.1086/309956

J. Lilensten, A.J. Coates, V. Dehant, T. Dudok de Wit, R.B. Horne, F. Leblanc, J. Luhmann, E. Woodfield, and M. Barthélemy. Astron. and Astrop. Rev., 22, 79, doi:10.1007/s00159-014-0079-6, 2014

J.A. Linker, K.K. Khurana, M.G. Kivelson, R.J. Walker, J. Geophys. Res.103, 19867 (1998). DOI 10.1029/98JE00632

W. Liu, D.R. Schultz, ApJ530, 500 (2000). DOI 10.1086/308367

M.J. Loe_er, U. Raut, R.A. Vidal, R.A. Baragiola, R.W. Carlson, Icarus180, 265 (2006). DOI 10.1016/j.icarus.2005.08.001

M.J. Loe_er, R.L. Hudson, Icarus219, 561 (2012). DOI 10.1016/j.icarus.2012.03.023

A. Lucchetti, C. Plainaki, G. Cremonese, A. Milillo, T. Cassidy, X. Jia, V. Shematovich, Planet. Space Sci.130, 14 (2016). DOI 10.1016/j.pss.2016.01.009

O.P. Makarov, J.M. Ajello, P. Vattipalle, I. Kanik, M.C. Festou, A. Bhardwaj, Journal of Geophysical Research (Space Physics) 109, A09303 (2004). DOI 10.1029/2002JA009353

M. Marconi, Icarus 190(1), 155 (2007). DOI 10.1016/j.icarus.2007.02.016.

M.Y. Marov, V.I. Shematovich, D.V. Bisicalo, Space Sci. Rev.76, 1 (1996). DOI 10.1007/BF00240583

B.H. Mauk, D.G. Mitchell, R.W. McEntire, C.P. Paranicas, E.C. Roelof, D.J. Williams, S.M. Krimigis, A. Lagg, Journal of Geophysical Research (Space Physics) 109, A09S12 (2004). DOI 10.1029/2003JA010270

B.H. Mauk, D.G. Mitchell, S.M. Krimigis, E.C. Roelof, C.P. Paranicas, Nature421, 920 (2003). DOI 10.1038/nature01431

M.A. McGrath, C.J. Hansen, A.R. Hendrix, Observations of Europa's Tenuous

Atmosphere (2009), p. 485

M.A. McGrath, E. Lellouch, D.F. Strobel, P.D. Feldman, R.E. Johnson, Satellite atmospheres (2004), pp. 457_483

A. Milillo, C. Plainaki, E. De Angelis, V. Mangano, S. Massetti, A. Mura, S. Orsini, R. Rispoli, Planet. Space Sci.130, 3 (2016). DOI 10.1016/j.pss.2015.10.011

D.G. Mitchell, S.M. Krimigis, C. Paranicas, P.C. Brandt, J.F. Carbary, E.C. Roelof, W.S. Kurth, D.A. Gurnett, J.T. Clarke, J.D. Nichols, J.C. Gérard, D.C. Grodent, M.K. Dougherty, W.R. Pryor, Planet. Space Sci.57, 1732 (2009). DOI 10.1016/j.pss.2009.04.002

D.G. Mitchell, C.P. Paranicas, B.H. Mauk, E.C. Roelof, S.M. Krimigis, Journal of Geophysical Research (Space Physics) 109, A09S11 (2004). DOI 10.1029/2003JA010120

D.G. Mitchell, S.M. Krimigis, A.F. Cheng, S.L. Hsieh, S.E. Jaskulek, E.P. Keath, B.H. Mauk, R.W. McEntire, E.C. Roelof, C.E. Schlemm, B.E. Tossman, D.J. Williams, (1996), vol. 2803, pp. 154_161. DOI 10.1117/12.253415.

E.A. Muntean, P. Lacerda, T.A. Field, A. Fitzsimmons, W.C. Fraser, A.C. Hunniford, R.W. McCullough, MNRAS462, 3361 (2016). DOI 10.1093/mnras/stw1855

A.F. Nagy, J. Kim, T.E. Cravens, A.J. Kliore, Geophys. Res. Lett.25, 4153 (1998). DOI 10.1029/1998GL900139

F.M. Neubauer, J. Geophys. Res.104, 28671 (1999). DOI 10.1029/1999JA900217

T. Orlando, M. Sieger, Surface Science 528(1_3), 1 (2003). DOI 10.1016/S0039-6028(02)02602-X. Proceedings of the Ninth International Workshop on Desorption Induced by Electronic Transitions

R.T. Pappalardo, D.A. Senske, L.M. Prockter, B. Paczkowski, S. Vance, B. Goldstein, T. Magner, B. Cooke, in Lunar and Planetary Science Conference, Lunar and Planetary Science Conference, vol. 46 (2015), Lunar and Planetary Science Conference, vol. 46, p. 2673

C. Paranicas, B.H. Mauk, R.W. McEntire, T.P. Armstrong, Geophys. Res. Lett.30, 1919 (2003). DOI 10.1029/2003GL017682

C. Paranicas, J.M. Ratli_, B.H. Mauk, C. Cohen, R.E. Johnson, Geophys. Res. Lett.29, 1074 (2002). DOI 10.1029/2001GL014127

C. Paranicas, R.W. Carlson, R.E. Johnson, Geophys. Res. Lett.28, 673 (2001). DOI 10.1029/2000GL012320

C. Paranicas, A.F. Cheng, D.J. Williams, J. Geophys. Res.103, 15001 (1998). DOI 10.1029/98JA00961

W.R. Paterson, L.A. Frank, K.L. Ackerson, J. Geophys. Res.104, 22779 (1999). DOI 10.1029/1999JA900191

C. Plainaki, A. Milillo, A. Mura, J. Saur, S. Orsini, S. Massetti, Planet. Space Sci.88, 42 (2013). DOI 10.1016/j.pss.2013.08.011

C. Plainaki, A. Milillo, A. Mura, S. Orsini, S. Massetti, T. Cassidy, Icarus218, 956 (2012). DOI 10.1016/j.icarus.2012.01.023

C. Plainaki, A. Milillo, A. Mura, S. Orsini, T. Cassidy, Icarus210, 385 (2010). DOI 10.1016/j.icarus.2010.06.041

C. Plainaki, J. Lilensten, A. Radioti, M. Andriopoulou, A. Milillo, T.A. Nordheim, I. Dandouras, A. Coustenis, D. Grassi, V. Mangano, S. Massetti, S. Orsini, S., and A. Lucchetti. Space Weather Space Clim.6, doi:10.1051/swsc/2016024, (2016).

C.C. Porco, R.A. West, A. McEwen, A.D. Del Genio, A.P. Ingersoll, P. Thomas, S. Squyres, L. Dones, C.D. Murray, T.V. Johnson, J.A. Burns, A. Brahic, G. Neukum, J. Veverka, J.M. Barbara, T. Denk, M. Evans, J.J. Ferrier, P. Geissler, P. Helfenstein, T. Roatsch, H. Throop, M. Tiscareno, A.R. Vasavada, Science 299, 1541 (2003). DOI 10.1126/science.1079462

M.K. Pospieszalska, R.E. Johnson, Icarus78, 1 (1989). DOI 10.1016/0019-1035(89)90065-1

A.E. Potter, T.H. Morgan, Planet. Space Sci.45, 95 (1997). DOI 10.1016/S0032-0633(96)00100-6

Powell, K. G., Roe, P. L., Linde, T. J., Gombosi, T. I., & DeZeeuw, D. L. 1999, J. Comput. Phys., 154, 284

J.G. Roederer, Physics and Chemistry in Space 2 (1970). DOI 10.1007/978-3-642-49300-3

L. Roth, K.D. Retherford, N. Ivchenko, N. Schlatter, D.F. Strobel, T.M. Becker, C. Grava, AJ153, 67 (2017). DOI 10.3847/1538-3881/153/2/67

L. Roth, N. Ivchenko, K.D. Retherford, N.J. Cunningham, P.D. Feldman, J. Saur, J.R. Spencer, D.F. Strobel, Geophys. Res. Lett.43, 2465 (2016). DOI 10.1002/2015GL067451

L. Roth, K.D. Retherford, J. Saur, D.F. Strobel, P.D. Feldman, M.A. McGrath, F. Nimmo, Proceedings of the National Academy of Science 111, E5123 (2014a).

DOI 10.1073/pnas.1416671111

L. Roth, J. Saur, K.D. Retherford, D.F. Strobel, P.D. Feldman, M.A. McGrath, F. Nimmo, Science 343, 171 (2014b). DOI 10.1126/science.1247051

M. Rubin, X. Jia, K. Altwegg, M.R. Combi, L.K.S. Daldor_, T.I. Gombosi, K. Khurana, M.G. Kivelson, V.M. Tenishev, G. Tóth, B. Holst, P. Wurz, Journal of Geophysical Research (Space Physics) 120, 3503 (2015). DOI 10.1002/2015JA021149

J. Saur, D.F. Strobel, F.M. Neubauer, J. Geophys. Res.103, 19947 (1998). DOI 10.1029/97JE03556

J. Saur, P.D. Feldman, L. Roth, F. Nimmo, D.F. Strobel, K.D. Retherford, M.A. McGrath, N. Schilling, J.C. Gérard, D. Grodent, ApJ738, 153 (2011). DOI 10.1088/0004-637X/738/2/153

N. Schilling, K.K. Khurana, M.G. Kivelson, Journal of Geophysical Research (Planets) 109, E05006 (2004). DOI 10.1029/2003JE002166

N. Schilling, F.M. Neubauer, J. Saur, Icarus192, 41 (2007). DOI 10.1016/j.icarus.2007.06.024

N. Schilling, F.M. Neubauer, J. Saur, Journal of Geophysical Research (Space Physics) 113, A03203 (2008). DOI 10.1029/2007JA012842

P.H. Schultz, J. Geophys. Res.101, 21117 (1996). DOI 10.1029/96JE02266

D.E. Shemansky, Y.L. Yung, X. Liu, J. Yoshii, C.J. Hansen, A.R. Hendrix, L.W. Esposito, ApJ797, 84 (2014). DOI 10.1088/0004-637X/797/2/84

V.I. Shematovich, Solar System Research 40, 175 (2006). DOI 10.1134/S0038094606030014

V.I. Shematovich, R.E. Johnson, J.F. Cooper, M.C.Wong, Icarus173, 480 (2005). DOI 10.1016/j.icarus.2004.08.013

V.I. Shematovich, Solar System Research 38, 178 (2004). DOI 10.1023/B:SOLS.0000030857.87194.11

V.I. Shematovich, R.E. Johnson, Advances in Space Research 27, 1881 (2001). DOI 10.1016/S0273-1177(01)00299-X

V.I. Shematovich, D.V. Bisikalo, D.E. Ionov, Suprathermal Particles in XUV-Heated and Extended Exoplanetary Upper Atmospheres (Springer International Publishing, Cham, 2015), pp. 105_136. DOI 10.1007/978-3-319-09749-76

J. Shi, M. Famá, B.D. Teolis, R.A. Baragiola, Phys. Rev. B 85, 035424 (2012). DOI

10.1103/PhysRevB.85.035424.

J. Shi, U. Raut, J.H. Kim, M. Loe_er, R.A. Baragiola, The Astrophysical Journal Letters 738(1), L3 (2011).

M. Shi, R.A. Baragiola, D.E. Grosjean, R.E. Johnson, S. Jurac, J. Schou, Journal of Geophysical Research: Planets 100(E12), 26387 (1995). DOI 10.1029/95JE03099.

E.C. Sittler, D.F. Strobel, J. Geophys. Res.92, 5741 (1987). DOI 10.1029/JA092iA06p05741

W.H. Smyth, M.L. Marconi, J. Geophys. Res.105, 7783 (2000). DOI 10.1029/1999JA000308

W.H. Smyth, M.L. Marconi, Icarus181, 510 (2006). DOI 10.1016/j.icarus.2005.10.019

W.B. Sparks, M. McGrath, K. Hand, H.C. Ford, P. Geissler, J.H. Hough, E.L. Turner, C.F. Chyba, R. Carlson, M. Turnbull, International Journal of Astrobiology 9, 265 (2010). DOI 10.1017/S1473550410000285

J.R. Spencer, E. Lellouch, M.J. Richter, M.A. López-Valverde, K. Lea Jessup, T.K. Greathouse, J.M. Flaud, Icarus176, 283 (2005). DOI 10.1016/j.icarus.2005.01.019

J.R. Spencer, L.K. Tamppari, T.Z. Martin, L.D. Travis, Science 284, 1514 (1999). DOI 10.1126/science.284.5419.1514

G. Strazzulla, G.A. Baratta, G. Leto, O. Gomis, Icarus192, 623 (2007). DOI 10.1016/j.icarus.2007.08.004

B. Teolis, J. Shi, R. Baragiola, The Journal of chemical physics 130(13), 134704 (2009)

B.D. Teolis, C. Plainaki, A.T. Cassidy, U. Raut, JGR-Planets, under review, (2017)

B.D. Teolis, J.H. Waite, Icarus272, 277 (2016). DOI 10.1016/j.icarus.2016.02.031

B.D. Teolis, G.H. Jones, P.F. Miles, R.L. Tokar, B.A. Magee, J.H. Waite, E. Roussos, D.T. Young, F.J. Crary, A.J. Coates, R.E. Johnson, W.L. Tseng, R.A. Baragiola, Science 330, 1813 (2010). DOI 10.1126/science.1198366

N. Thomas, F. Bagenal, T. Hill, J. Wilson, Jupiter. The planet, satellites and magnetosphere 1, 561 (2004)

R.M. Thorne, J. Geophys. Res.87, 8105 (1982). DOI 10.1029/JA087iA10p08105

M.S. Tiscareno, P.E. Geissler, Icarus161, 90 (2003). DOI 10.1016/S0019 1035(02)00023-4

G. Tóth, B. Van der Holst, I.V. Sokolov, D.L. De Zeeuw, T.I. Gombosi, F. Fang,

W.B. Manchester, X. Meng, D. Najib, K.G. Powell, et al., Journal of Computational Physics 231(3), 870 (2012)
N.G. van Kampen, Â Elsevier Science PublishersÂ, New York (1992)
R. Vidal, B. Teolis, R. Baragiola, Surface science 588(1), 1 (2005)
M. Volwerk, K. Khurana, M. Kivelson, Annales Geophysicae 25, 905 (2007). DOI 10.5194/angeo-25-905-2007
A. Vorburger, P. Wurz, H. Lammer, S. Barabash, O. Mousis, Icarus262, 14 (2015). DOI 10.1016/j.icarus.2015.07.035
M. Wieser, Y. Futaana, S. Barabash, P. Wurz, Icarus269, 91 (2016). DOI 10.1016/j.icarus.2015.12.043
D.J. Williams, B.H. Mauk, R.E. McEntire, E.C. Roelof, T.P. Armstrong, B. Wilken, J.G. Roederer, S.M. Krimigis, T.A. Fritz, L.J. Lanzerotti, Science 274, 401 (1996). DOI 10.1126/science.274.5286.401
P. Wurz, J.A. Whitby, U. Rohner, J.A. Martín-Fernández, H. Lammer, C. Kolb, Planet. Space Sci.58, 1599 (2010). DOI 10.1016/j.pss.2010.08.003
P. Wurz, U. Rohner, J.A. Whitby, C. Kolb, H. Lammer, P. Dobnikar, J.A. Martín-Fernández, Icarus191, 486 (2007). DOI 10.1016/j.icarus.2007.04.034
P. Wurz, H. Lammer, Icarus164, 1 (2003). DOI 10.1016/S0019-1035(03)00123-4
P. Wurz, K. Altwegg, H.R. Balsiger, S. Gasc, A. Galli, M. Rubin, A. Jäckel, L. Le Roy, U. Calmonte, C.Y. Tzou, U.A. Mall, A. Korth, B. Fiethe, J.M. De Keyser, J.J. Berthelier, H. Rème, T.I. Gombosi, S. Fuselier, AGU Fall Meeting Abstracts (2014)
P. Wurz, A. Vorburger, A. Galli, M. Tulej, N. Thomas, Y. Alibert, S. Barabash, M. Wieser, H. Lammer, European Planetary Science Congress 2014, EPSC Abstracts, Vol. 9, id. EPSC2014-504 9, EPSC2014-504 (2014).

Figure Captions

Figure 1: An example of the Knudsen number profile in the O_2-dominant near-surface atmosphere of Europa. Here, the O_2 density profile (Shematovich et al. 2005) has been used. For the calculation of the O_2 mean free path the elastic collision cross section with mean value of 3 10^{-15} cm^2 have been taken. Vertical and horizontal dashed lines indicate the formal definition of the exobase.

Figure 2: First detection of Europa’s oxygen atmosphere in an HST/GHRS spectrum from 1994 (bottom) and two follow-up spectra from 1996 (Hall et al. 1998)

Figure 3: (**A**) Excitation rates producing the OI 1304 Å and OI 1356 Å emissions from electron-impact on O and O_2. (**B**) Theoretical 1356-Å/1304-Å brightness ratio for pure O (solid) and pure O_2 (dashed) atmospheres based on the rates in (a). In addition, mixed O-O_2 atmosphere cases are shown that match the observed ratios (dotted, dashed-dotted). (**C**) Contour plot showing the relation of the measured brightness to electron density and atmospheric column density.

Figure 4: Europa's UV spectrum composite of the 7 highest quality NH Pluto-Alice spectra. The OI 1356 Å line is ×2 brighter than OI 1304 Å, which is consistent with previous observations and an O_2 excitation source.

Figure 5: Left: Cassini ISS NAC visible image with clear filters of Europa in eclipse (Cassidy et al. 2008, their Fig. 2b with enhanced contrast) shows a strong emission surplus in the sub-Jovian northern quadrant. Middle: A local emission surplus is similarly detected in a composite HST/ACS/SBC F125LP image of four exposures of Europa's OI 130.4 nm and OI 135.6 nm aurora in eclipse. Right: HST/ACS/SBC PR130L observations of the OI 1356 Å aurora in eclipse (Sparks et al. 2010, reprocessed image). Europa's location is relatively uncertain in the ACS figures.

Figure 6: Sketch of the systematic changes of the aurora morphology and the relation of Europa's position in the magnetosphere (after Roth et al. (2016)). Some images show a less clear and sometimes differing behavior, but a rough correlation is still seen in most of the images.

Figure 7: Plasma environment between Io and Europa. From Bagenal et al. (2015).

Figure 8: **(a)** Ion temperature (Plasma Science instrument) vs. electron density (Plasma Wave instrument) derived from Galileo measurements between 8.9 and 9.9 R_J, excluding the region within 2.5 R_E of Europa. Color corresponds to measurement dates. The solid, dashed and dotted lines show the median, quartiles, 10th- and 90th-percentile values respectively. The double-headed arrows show the variation in density with latitude for high and low ion temperatures. The straight line is drawn by eye to give a simple power-law relation between temperature and density (top, right corner). Galileo's 1 Europa flyby is labeled by E12. Figure taken from Bagenal et al. 2015. **(b).** Histograms of electron density, measured by Galileo PWS data, ion temperature and azimuthal velocity measured by Galileo PLS data. From Bagenal et al. 2015.

Figure 9: Observed and modeled field for the Europa flyby E4 in the Cartesian Coordinate System. The measured field is shown by red. The background field is shown by thin black. The predicted field for the internal permanent dipole plus induction for external field is shown by green. Blue, black and cyan stand for the predicted field by using the Alfven wing model to describe the external local currents for internal sources: induction only, induction plus dipole and induction plus dipole plus quadrupole, respectively. Adapted from Schilling et al. 2004.

Figure 10: Histogram of magnetic field values at Europa's average radial distance of 9.38 R_J for the VIP4 and Khurana magnetic field model. From Bagenal et al. 2015

Figure 11: ENA image (energy range 50-80 keV/nuc) of the Jupiter environment obtained by CASSINI/INCA (Krimigis et al. 2002).

Figure 12: Deconvolved 50-80 keV ENA image (counts in 15h) of the Jupiter environment obtained by CASSINI/INCA at 140 RJ (Mauk et al. 2003)

Figure 13: Upper panel. ENA flux*$(R/100)^2$ versus Cassini distance to Jupiter for different energy ranges (Mitchell et al. 2004). **Lower panel.** ENA energy spectrum obtained by Cassini/INCA (Mitchell et al. 2004).

Figure 14: Upper panel (a). Observed INCA hydrogen ENA image in the 55-90 keV range obtained by Cassini during its distant flyby of Jupiter. **Upper panel (b).** Best fit simulated ENA image assuming a H_2 neutral gas distribution displayed in the lower panel of this figure. **Lower panel (a).** Resulting neutral gas distribution required to obtain the best-fit simulated ENA image of the figure's upper panel. **Lower panel (b).** Same format as in the figure's upper panel, but without the instrumental PSF and geometrical factor applied to the image.

Figure 15: Lines of equal electric potential (in V), which are also streamlines of electron flow. The plasma flows from the left. The electric field is decreased and modified in the close vicinity of Europa in a way that the electrons are slowed down and mostly swept around Europa (Saur et al. 1998).

Figure 16: Observed and modeled magnetic field for the E4 flyby in the EPhiO coordinate system. Red line shows the measurements of *Kivelson et al.* (1997); dashed black line shows the modeled field with no induced field in the interior; Blue, green, and black line show the model results including induction in a 100-km-thick ocean located beneath a crust of 25 km for ocean conductivities of 100, 250, and 500 mS/m, respectively. From *Schilling et al.* (2007).

Figure 17: Left. Alfvenic current in 10^{-7} A/m^2 in a cross section through the northern Alfven wing for the E4 flyby conditions and without induction. Right. Same as left panel but with induction (Schilling et al. 2008).

Figure 18: Plasma density distribution around Europa during the Galileo E4 flyby as modeled by Rubin et al. (2015). (a) $\mathbf{O^+}$ mass density distribution in the equatorial plane in EphiO coordinates. The trailing hemisphere facing the inflow of the magnetospheric plasma is on the left hand side. The positive EphiO y-direction points towards Jupiter. The black line shows Galileo's trajectory projected onto this plane. (b) $\mathbf{O^+}$ mass density in the close vicinity of Europa in three perpendicular cuts. Panels (c) and (d) show the same for $\mathbf{O_2^+}$. Both species show an asymmetry about the upstream flow direction.

Figure 19: Contours of densities and temperatures for ions in Europa's equatorial plane. The densities of three species are shown on the left: O_2^+, which is the primary pickup ion from Europa's atmosphere, and sulphur and oxygen species from the jovian magnetosphere. The average temperature of these ions is shown on the right.

Figure 20: Height distributions of the number density *n* (panel (a)), and average thermal energy *T*m (panel (b)) of molecular (solid lines) and atomic (dashed lines) oxygen in model (Shematovich, 2006) of Europa's atmosphere. The dashed–dotted line in panel (a) shows the distribution of the number density of molecular oxygen from model by Saur et al.(1998).

Figure 21: H_2O density distribution around Europa according to the EGEON model. The release yields used in EGEON were updated according to the description provided in Milillo et al. (2016). Positive X-axis points to Europa's orbital direction, Z-axis to the spin direction.

Figure 22: O_2 density distribution around Europa at different orbital phases, according to the EGEON model.

Figure 23: O_2 source rates from Europa atmosphere models. There is a long-standing debate over both the source rate and source process: colors indicate the charge-particle population responsible for producing most O_2 in each model. "Energetic" refers to non-thermal ions with energies of >10s of keV, "thermal" refers to the Io plasma torus (T ~100 eV), "O_2^+ pickup" refers to ionized O_2 from Europa's atmosphere.

Figure 24: Predictions of the total sputtering yield (Famá et al. 2008; Johnson et al. 2009) (upper curves) versus the O_2 yield alone (Teolis et al. 2010) for oxygen ions irradiating water ice at 100 K.

Figure 25: JUICE mission phase 2.b. Europa's trailing hemisphere as viewed from the JUICE s/c while approaching the moon at a distance of ~ 22,735 km, on 13 Feb 2031 at 1h40m prior to the closest approach. In transparency, the O_2 tenuous atmosphere densities on the sagittal plane, for this exact configuration between Jupiter, Europa and the Sun, as derived from the EGEON model (Plainaki et al. 2013). The diffuse high-altitude component shows a clear asymmetry between the illuminated and non-illuminated hemispheres. Simulations performed using the CELESTIA open-source software with the SPICE kernels for JUICE and Solar System bodies.

Table Captions

Table 1: Overview of the observations of Europa's tenuous atmosphere

Table 2: Comparison among the plasma model assumptions

Table 3: Comparison among the atmosphere model assumptions

Table 4: Comparison among the atmosphere model outputs

Table 5: Interdisciplinary science goals, objectives and requirements related to the Europa atmospheric science

figure 01 Click here to download figure Figure_01.tiff

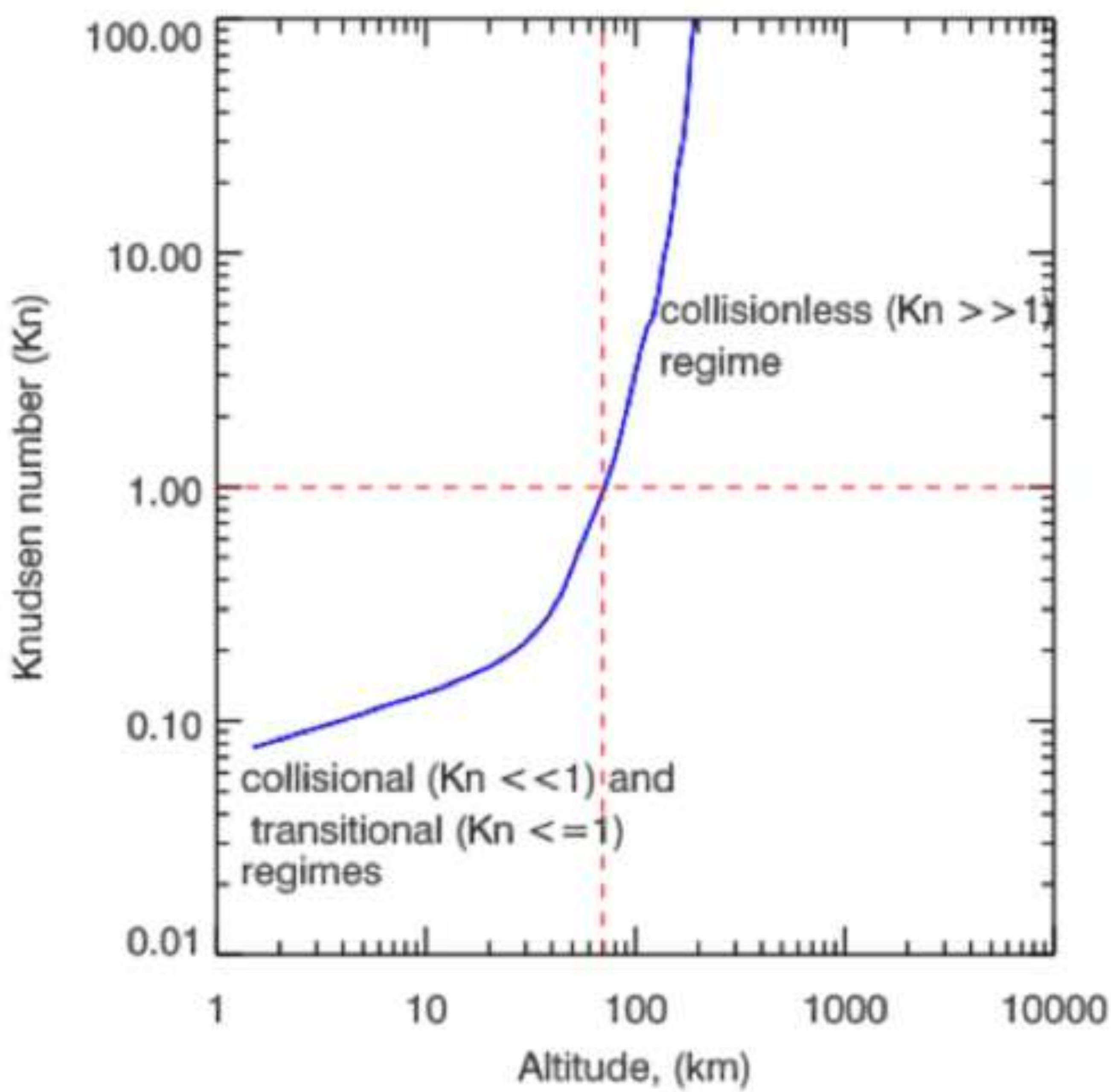

figure 02

Click here to download figure Figure_02.tiff

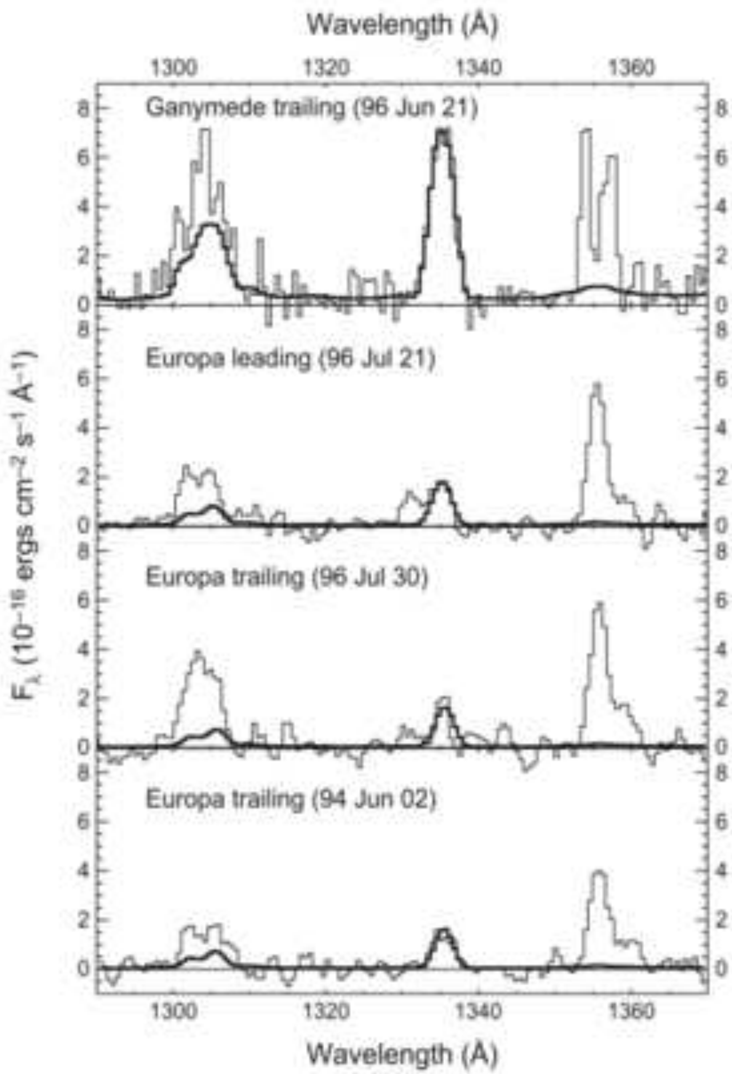

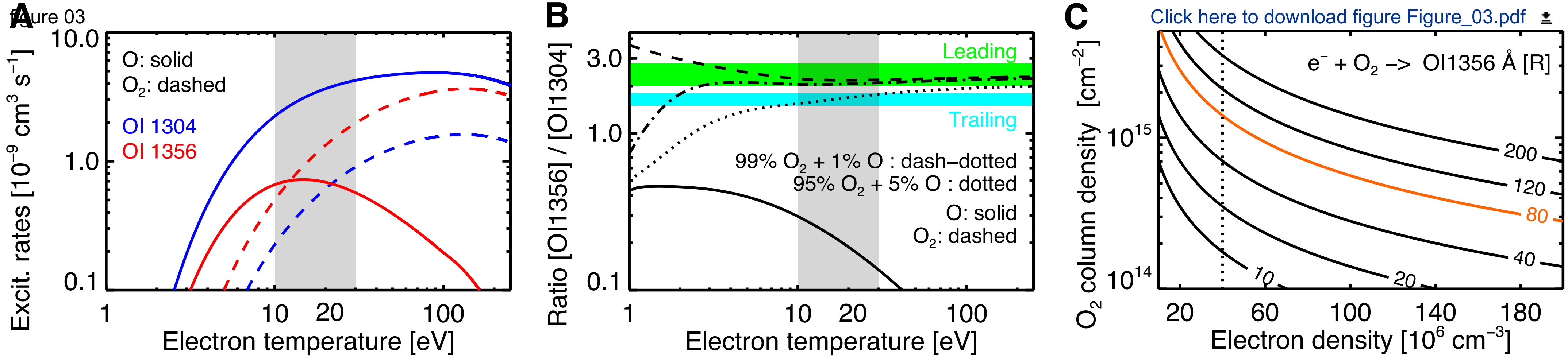
A
Excit. rates [10^{-9} cm^3 s^{-1}]
O: solid
O$_2$: dashed
OI 1304
OI 1356
10.0
1.0
0.1
1
10
20
100
Electron temperature [eV]
B
Ratio [OI1356] / [OI1304]
Leading
Trailing
99% O$_2$ + 1% O : dash–dotted
95% O$_2$ + 5% O : dotted
O: solid
O$_2$: dashed
3.0
1.0
0.1
1
10
20
100
Electron temperature [eV]
C
O$_2$ column density [cm^{-2}]
e$^-$ + O$_2$ –> OI1356 Å [R]
10^{15}
10^{14}
200
120
80
40
20
10
20
60
100
140
180
Electron density [10^6 cm^{-3}]

figure 04 Click here to download figure Figure_04.tiff

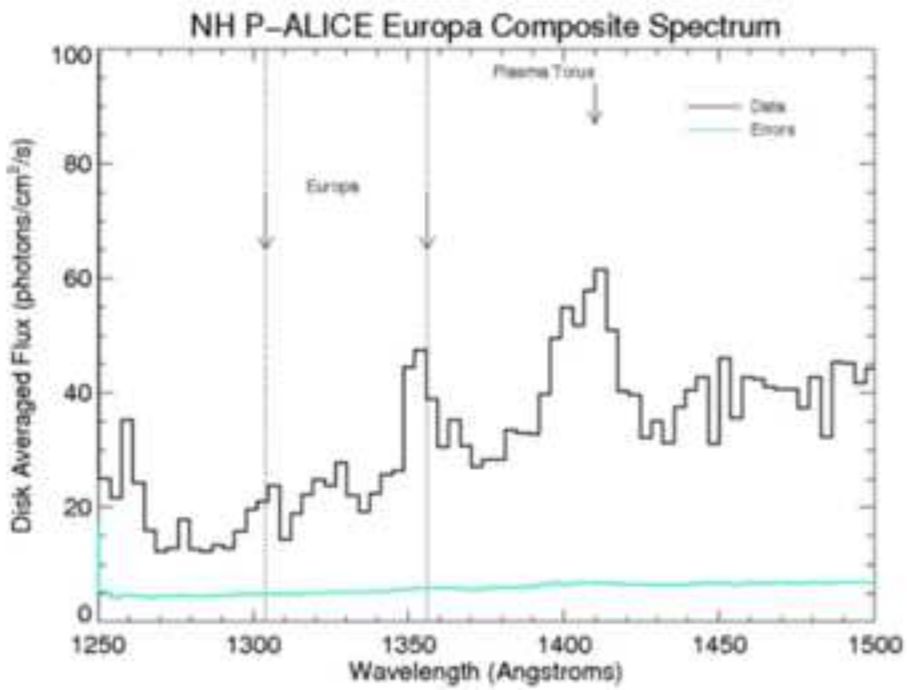

figure 05

Click here to download figure Figure_05.tiff

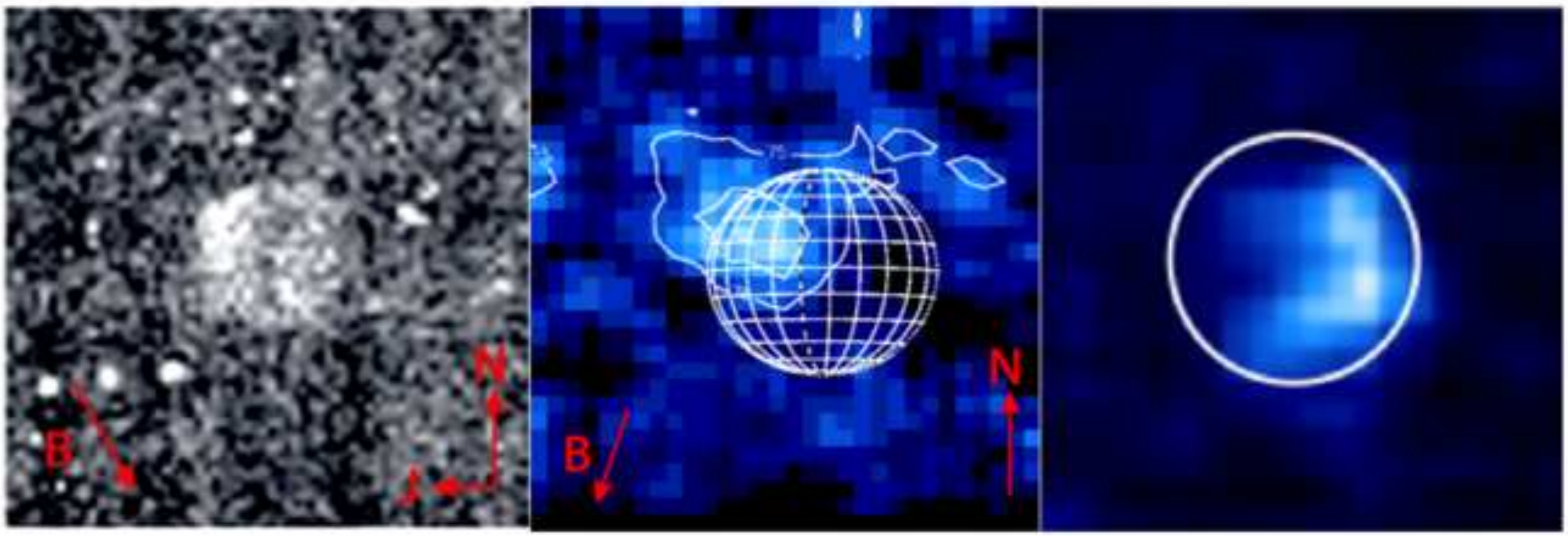

figure 06

Click here to download figure Figure_06.tiff

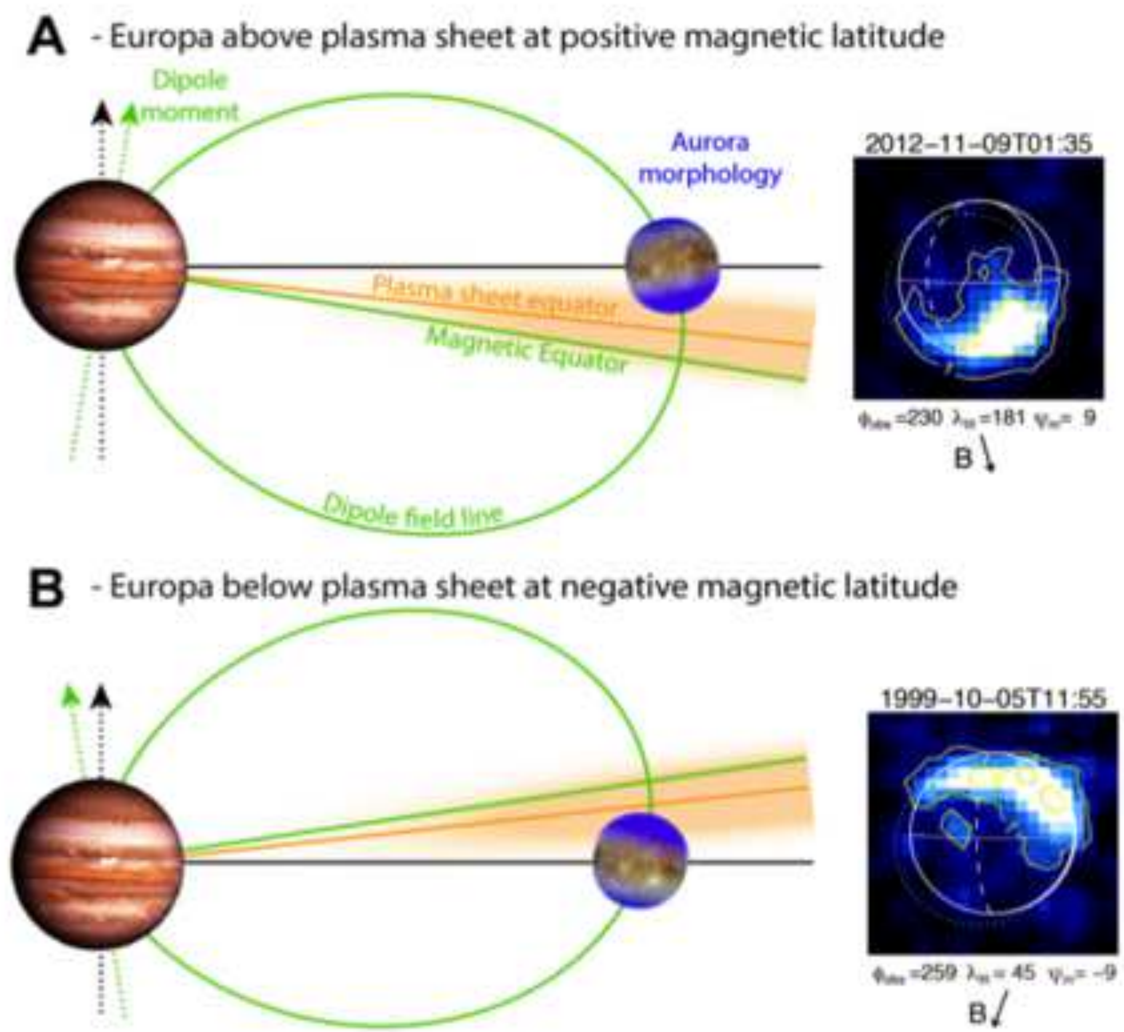

figure 07

Click here to download figure Figure_07.tiff

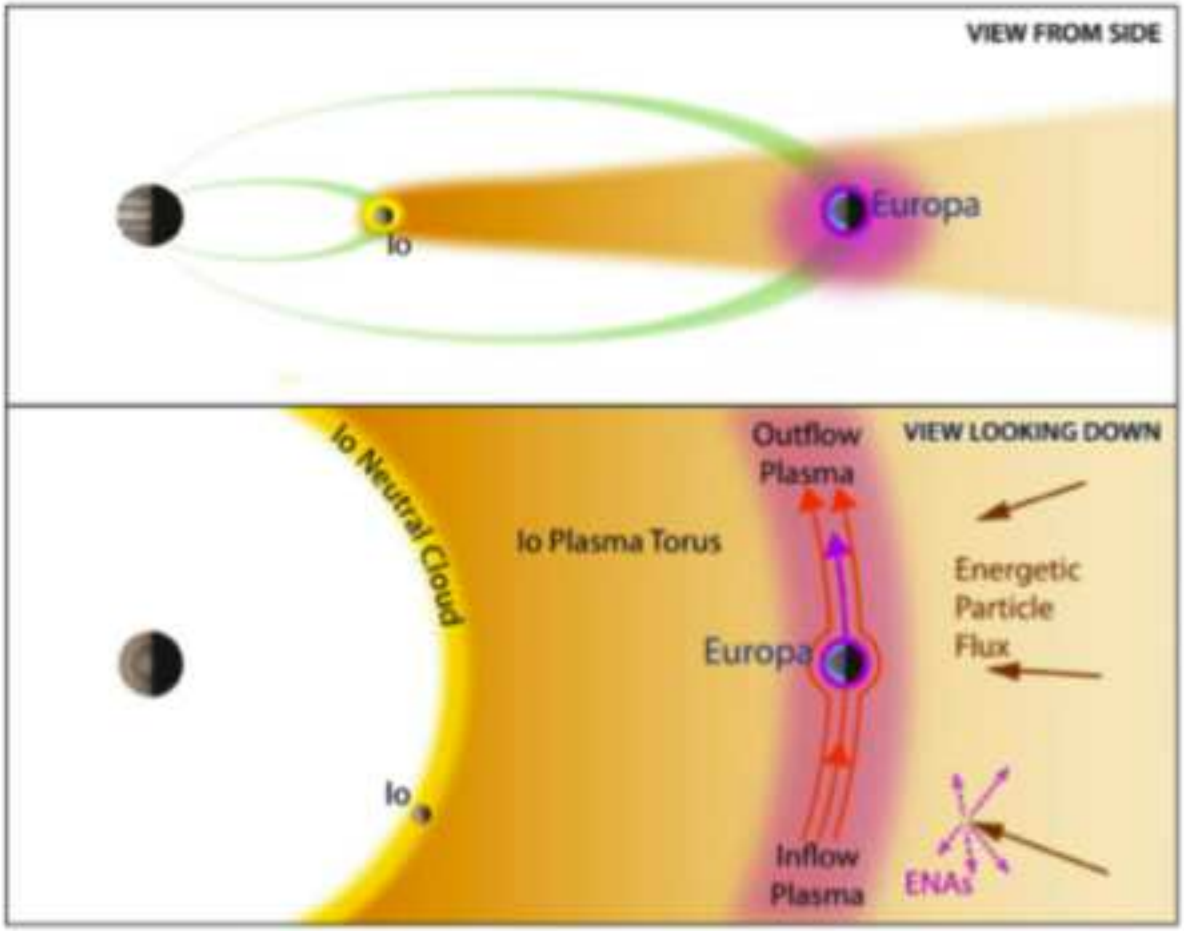

figure 08

Click here to download figure Figure_08.tiff

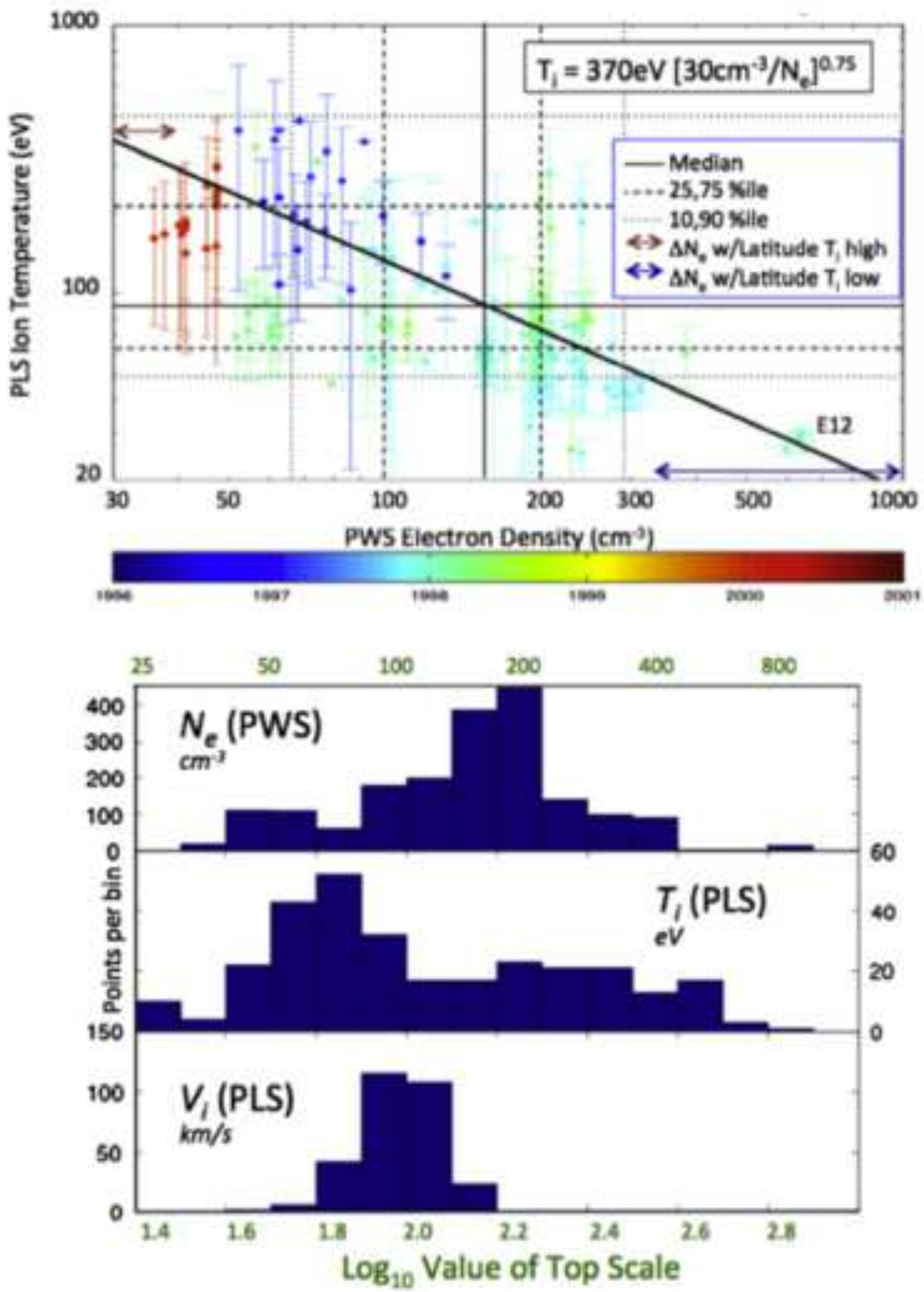

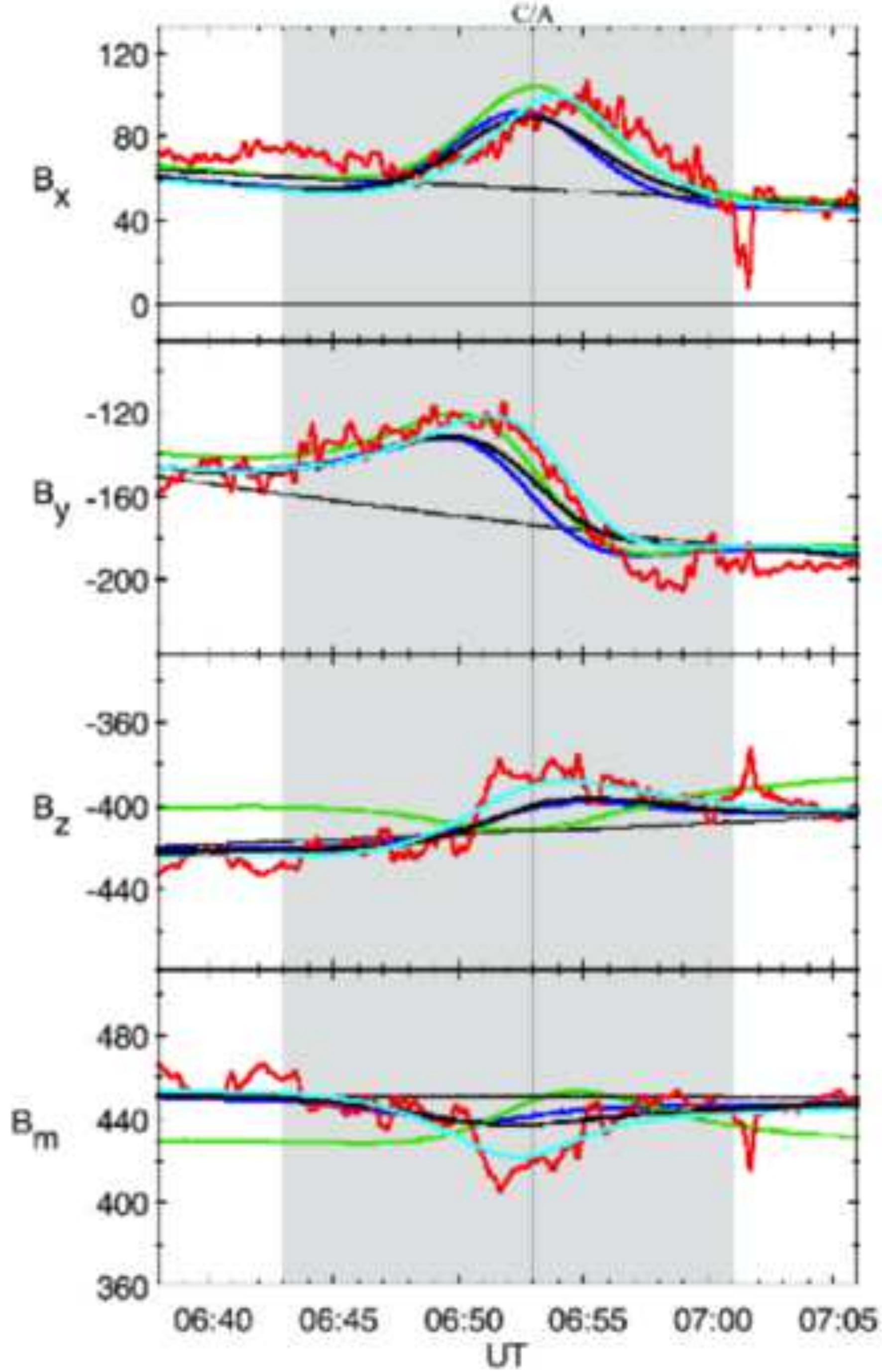
C/A
120
80
40
0
B_x
-120
-160
-200
B_y
-360
-400
-440
B_z
480
440
400
360
B_m
06:40
06:45
06:50
06:55
07:00
07:05
UT

figure 10

Click here to download figure Figure_10.tiff

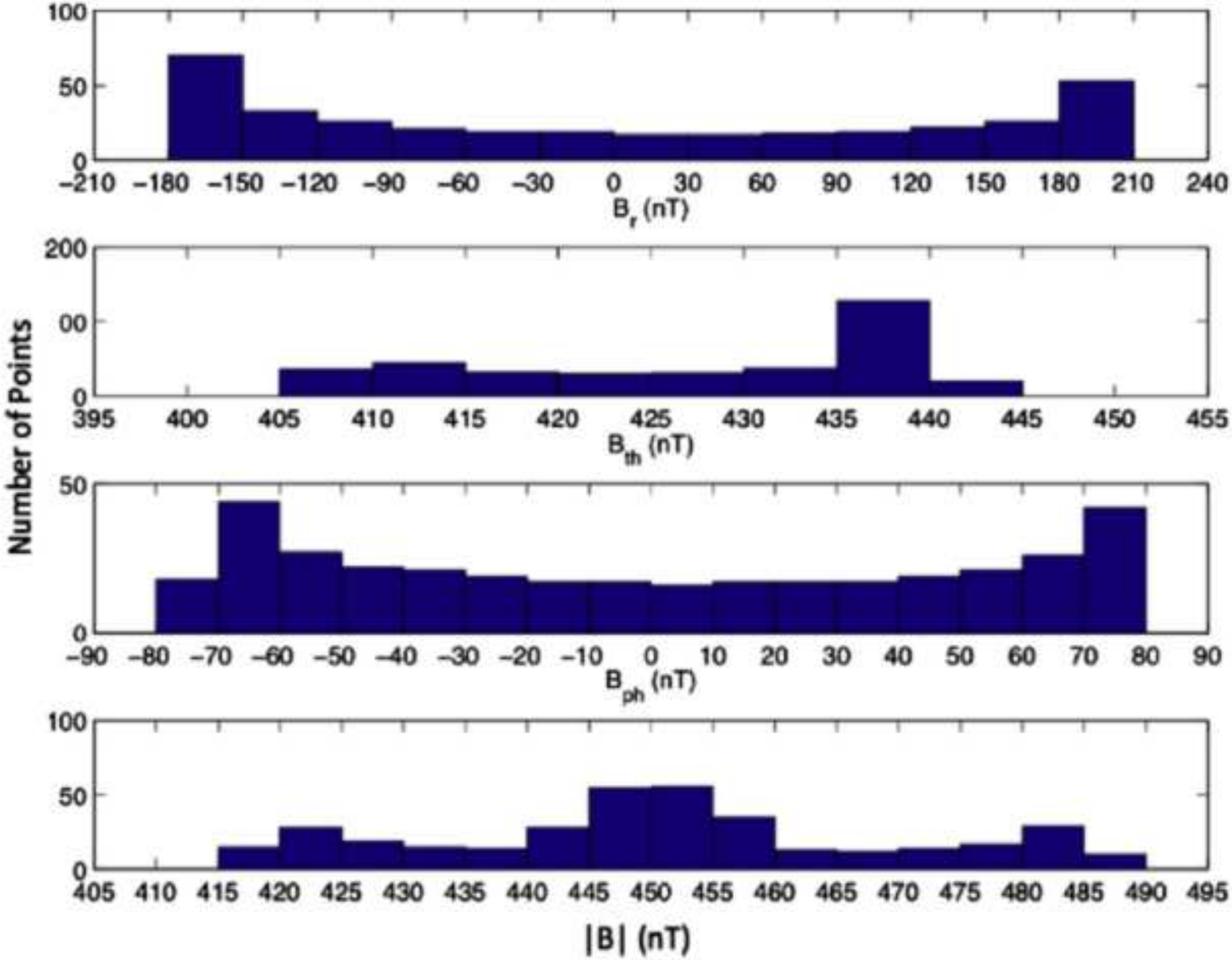

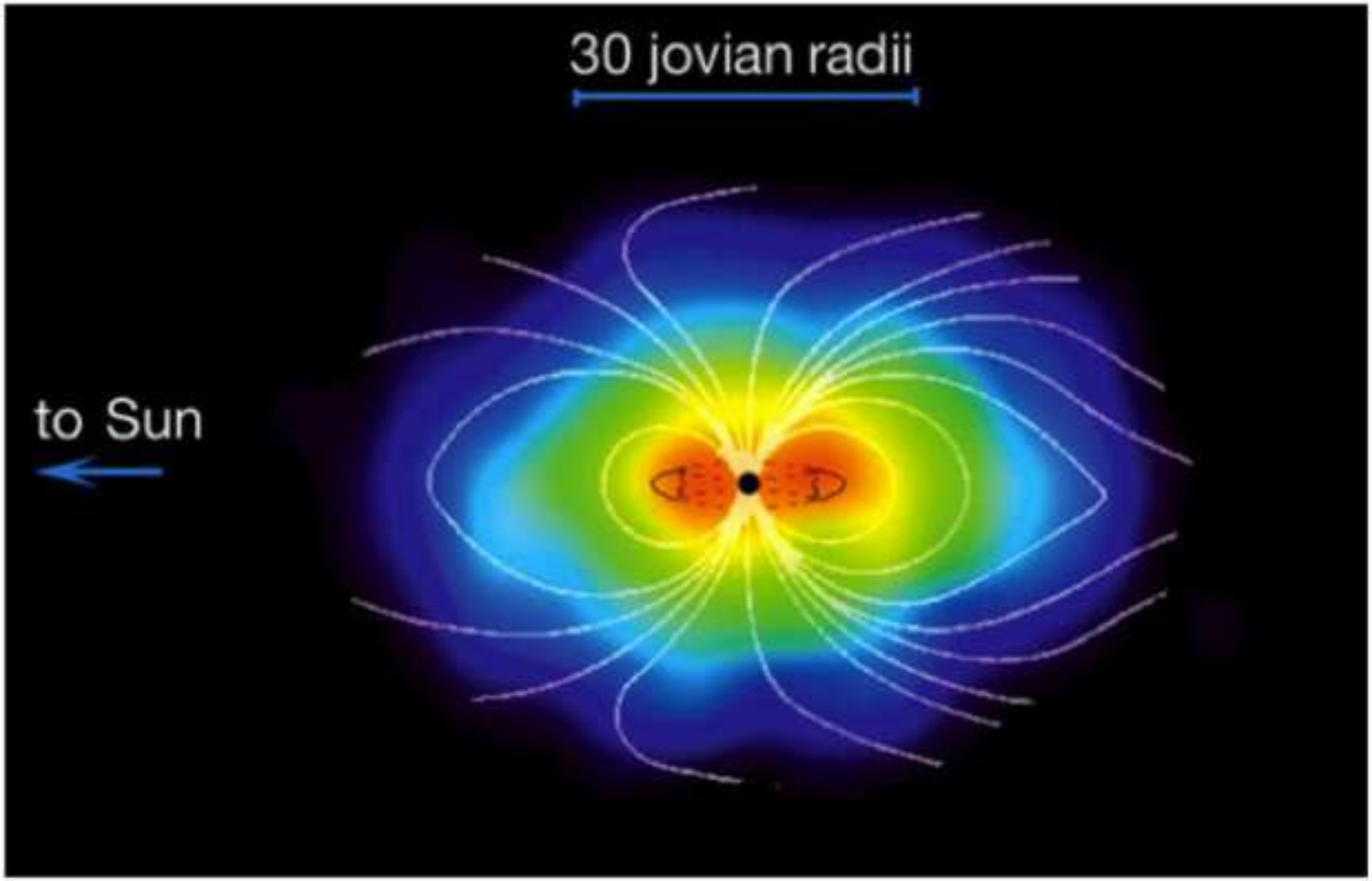
30 jovian radii
to Sun

figure 12

Click here to download figure Figure_12.tiff

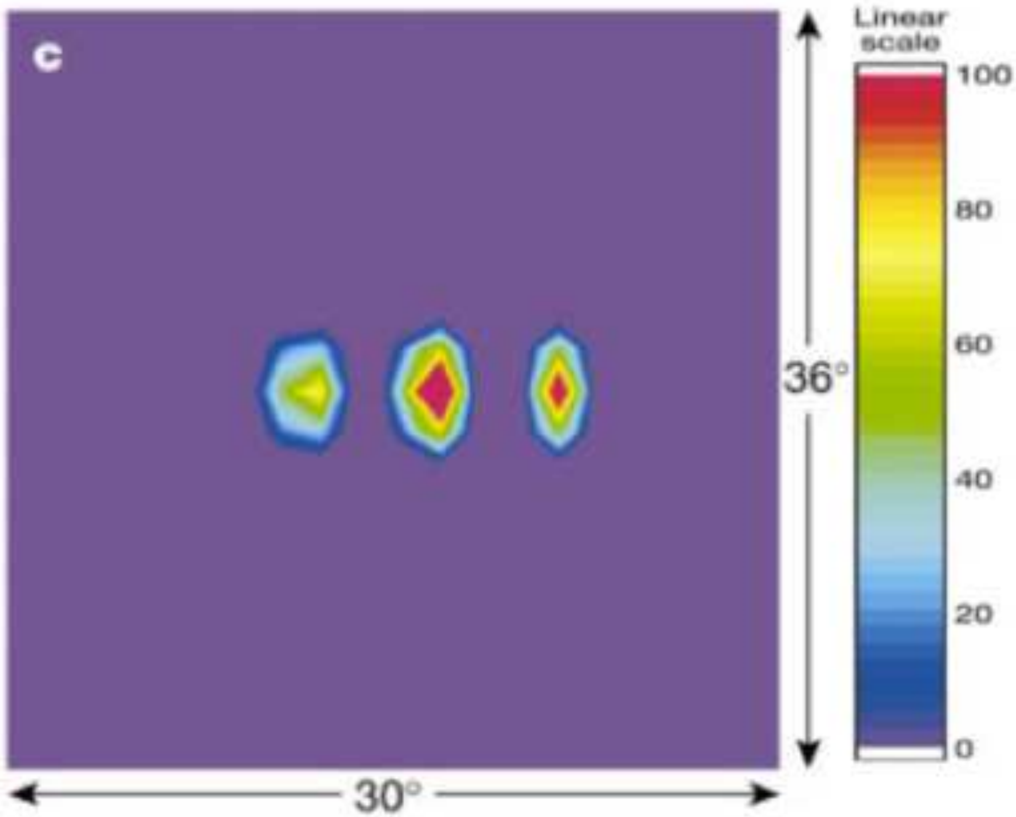

figure 13 Click here to download figure Figure_13.tiff

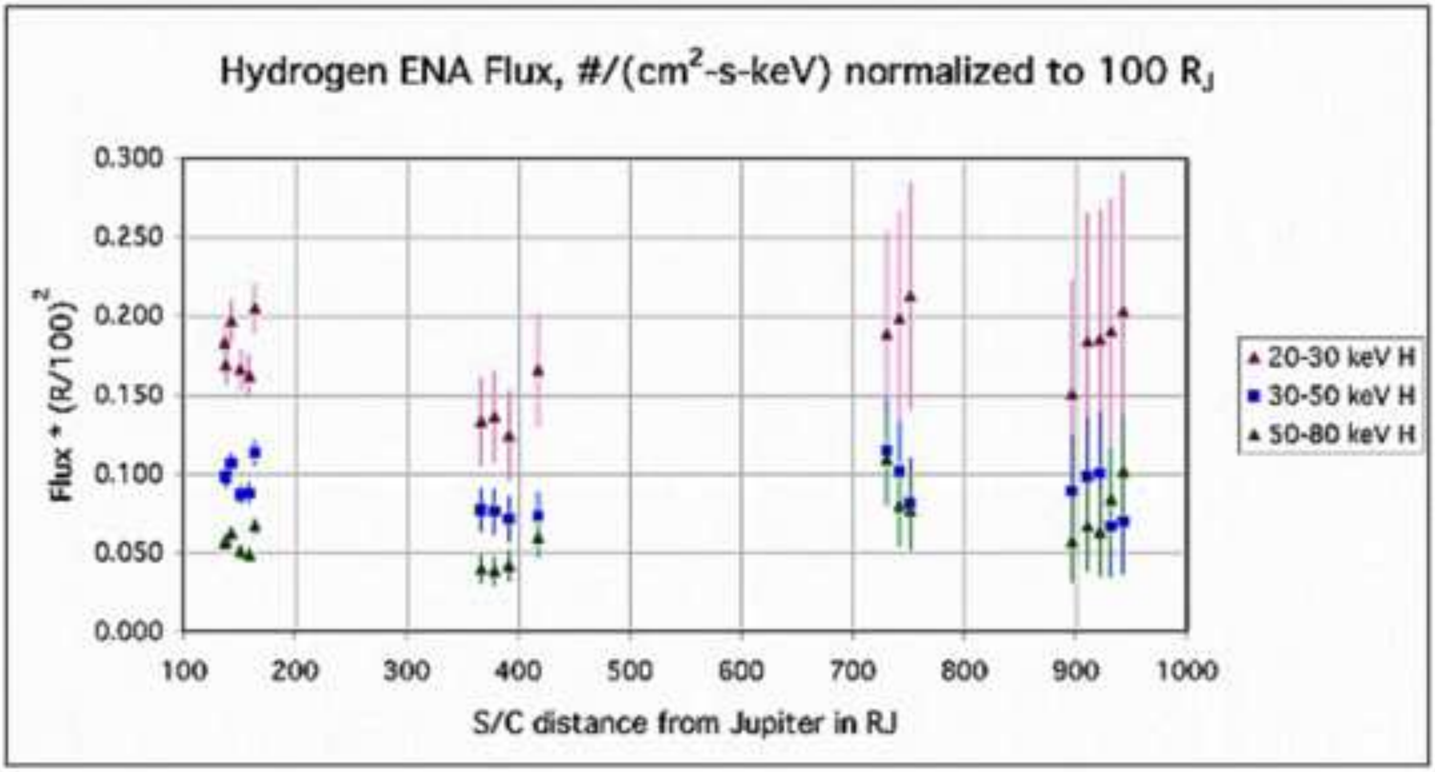

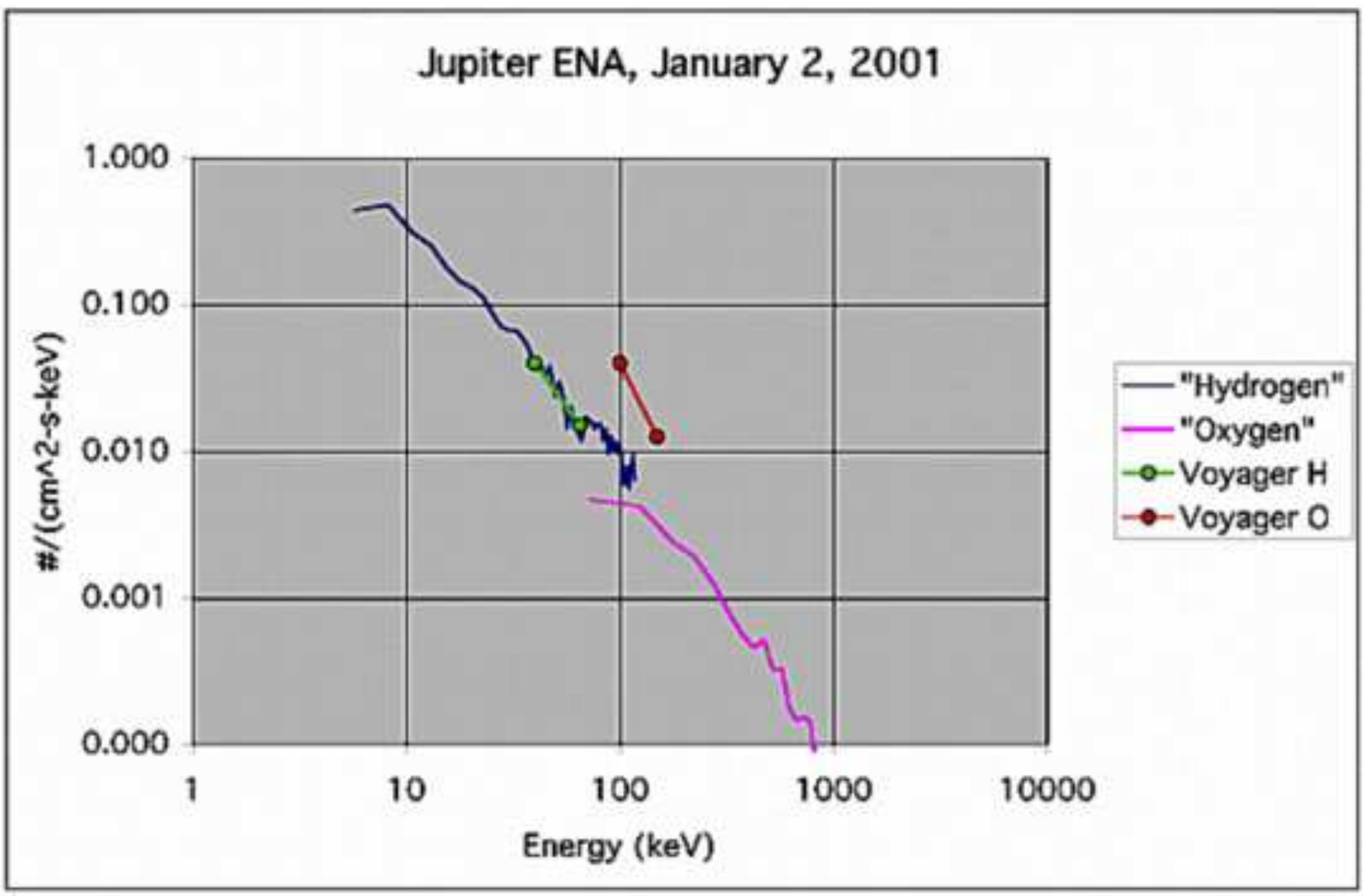

figure 14

Click here to download figure Figure_14.tif

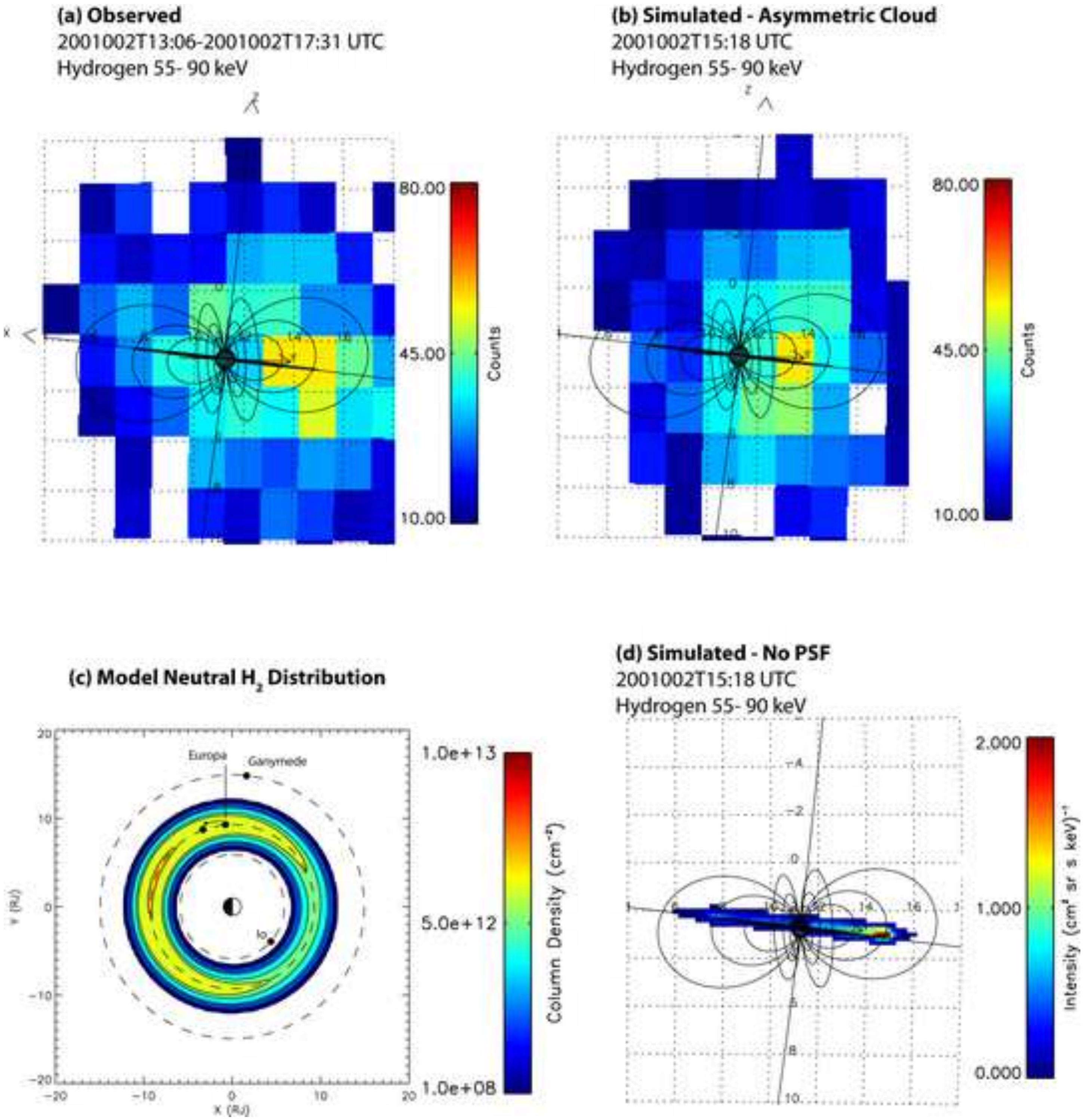

figure 15

Click here to download figure Figure_15.tiff

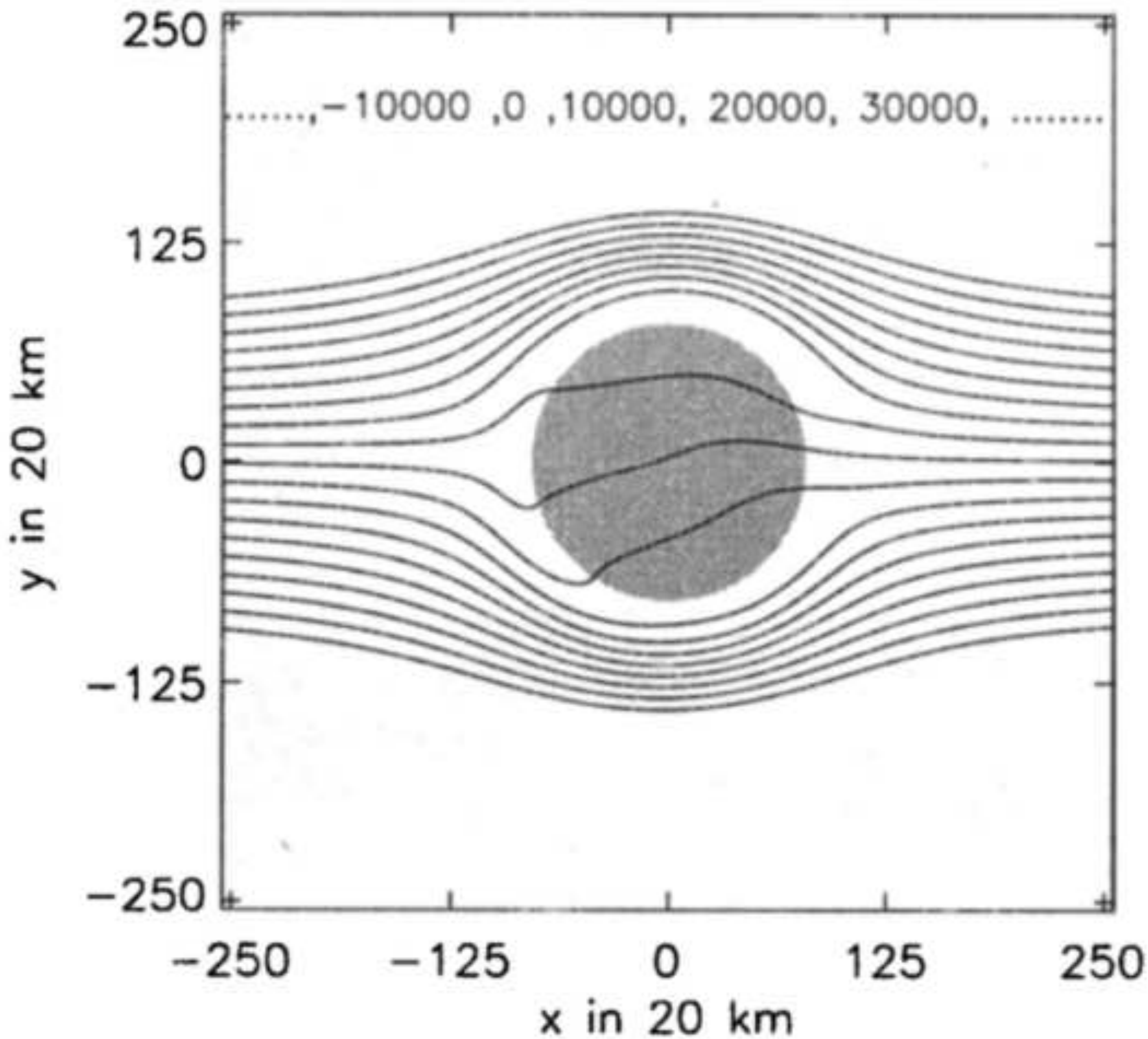

figure 16

Click here to download figure Figure_16.tiff

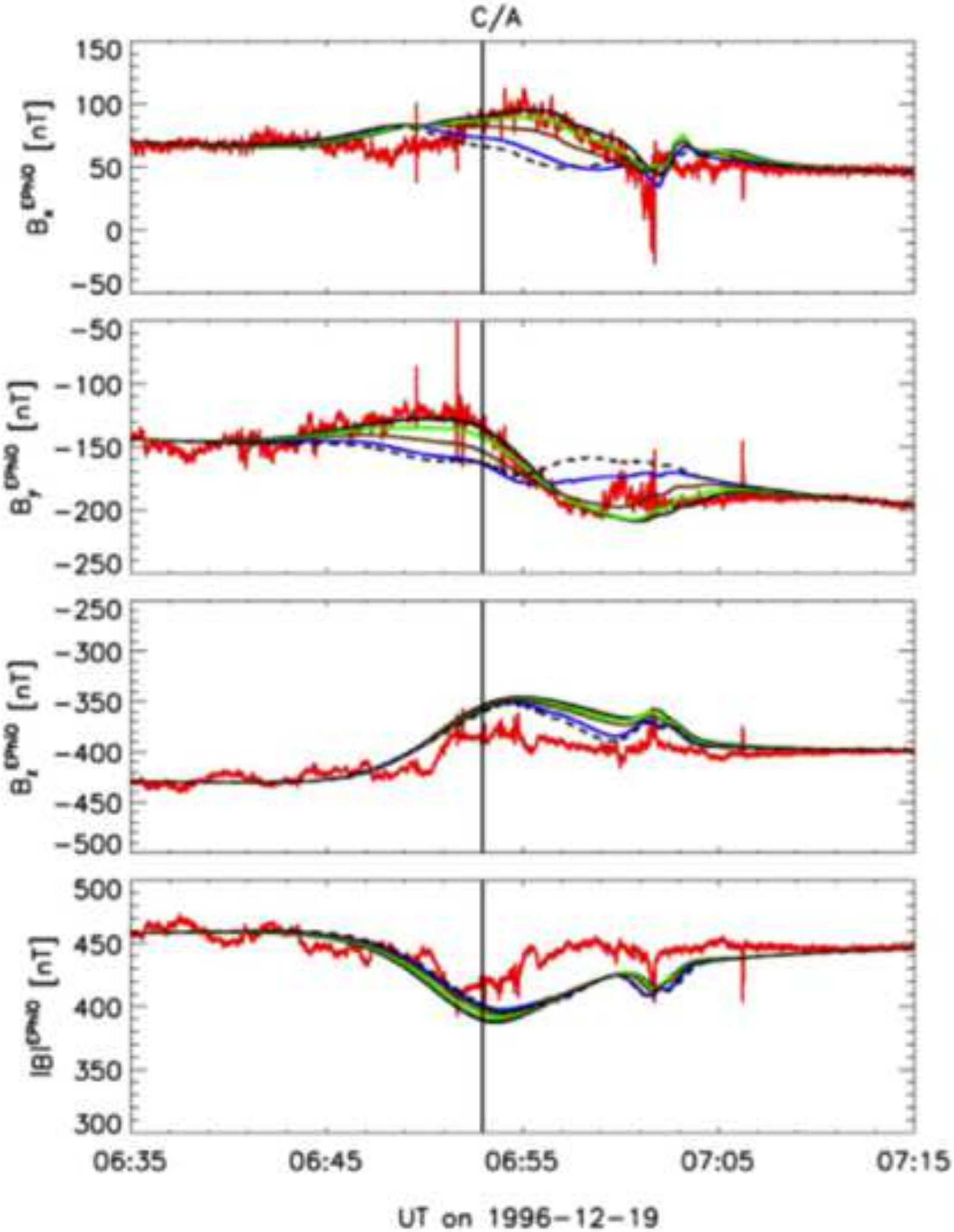

figure 17

Click here to download figure Figure_17.tiff

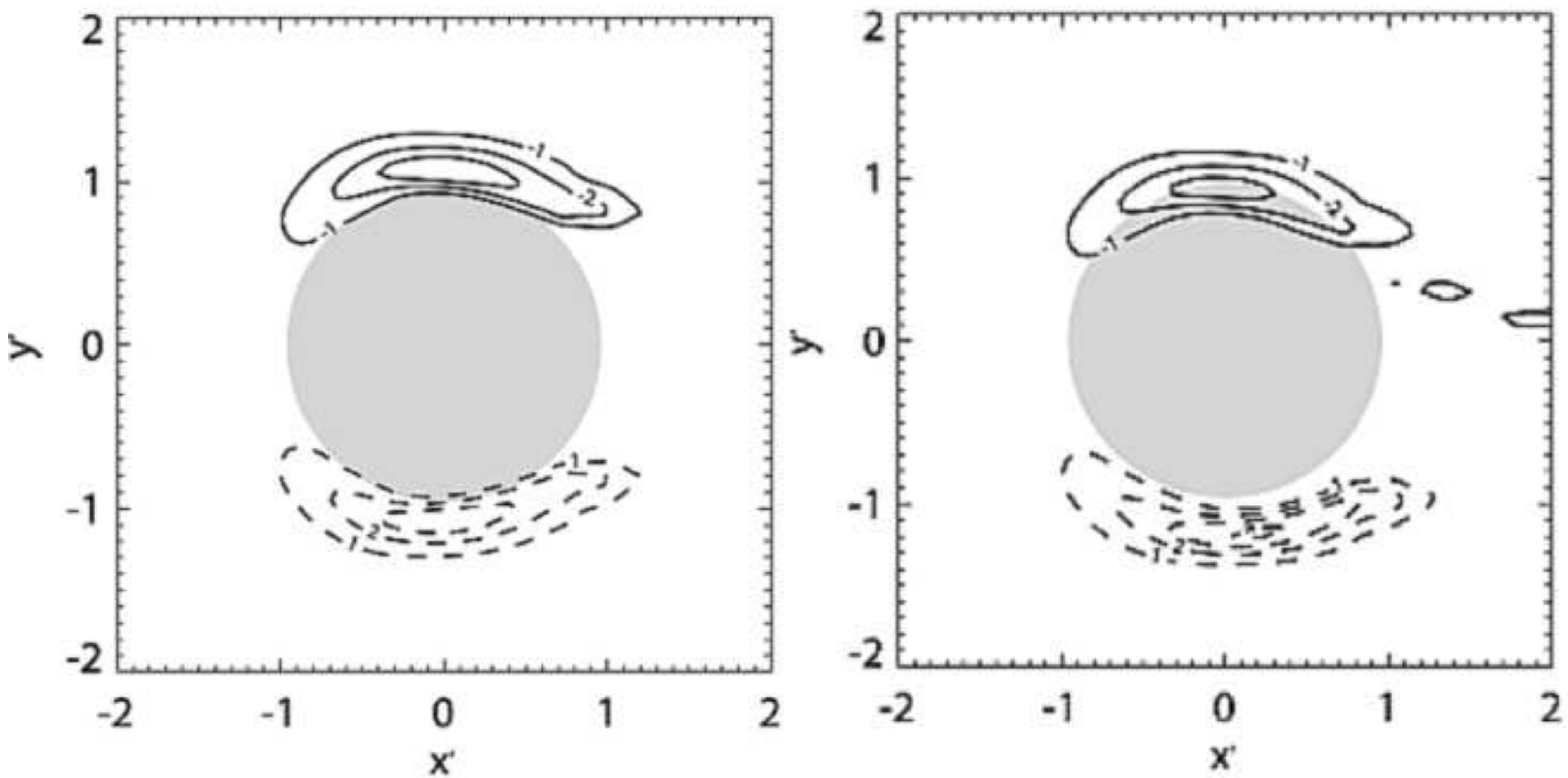

figure 18

Click here to download figure Figure_18.png

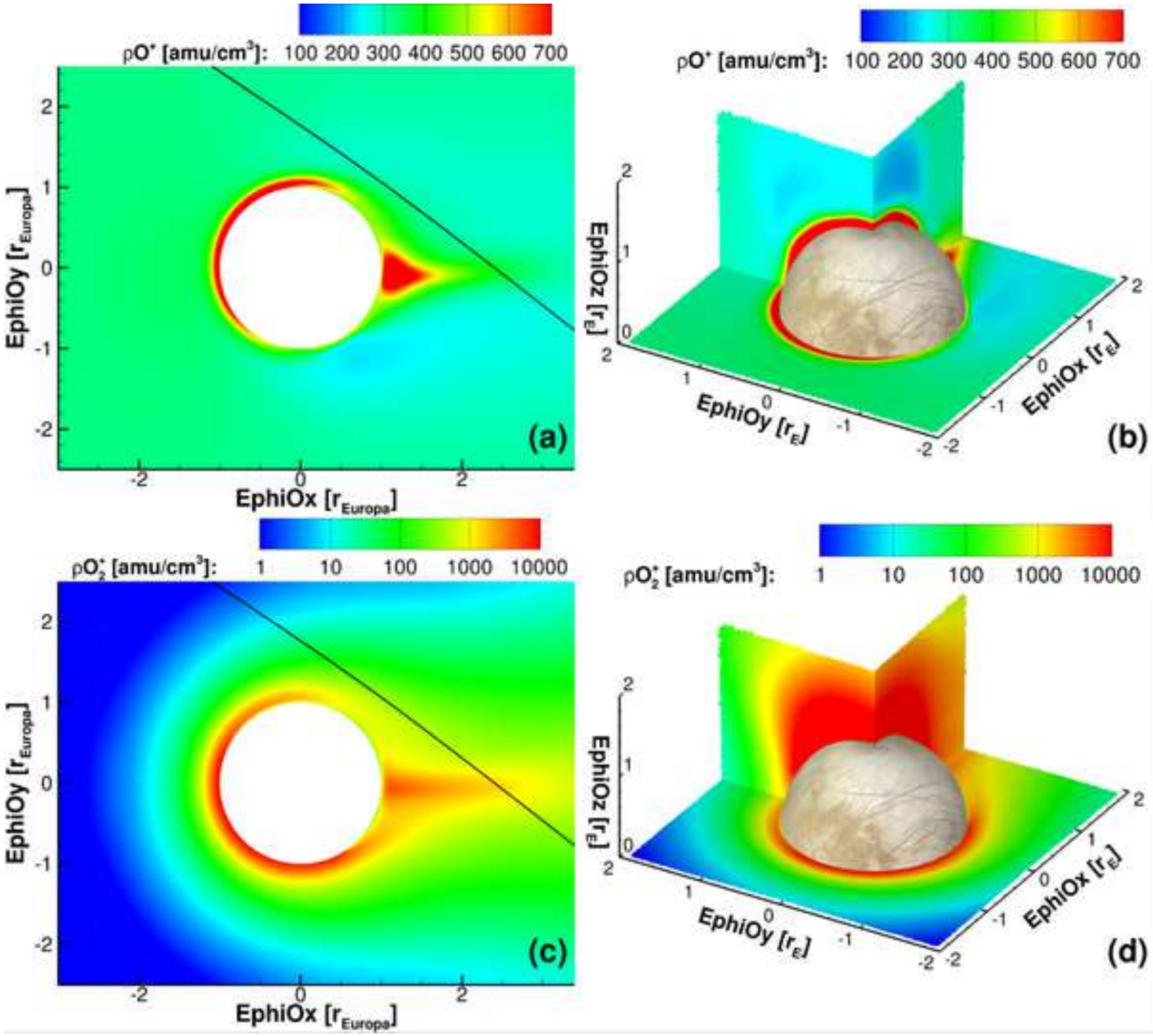

figure 19

Click here to download figure Figure_19.tiff

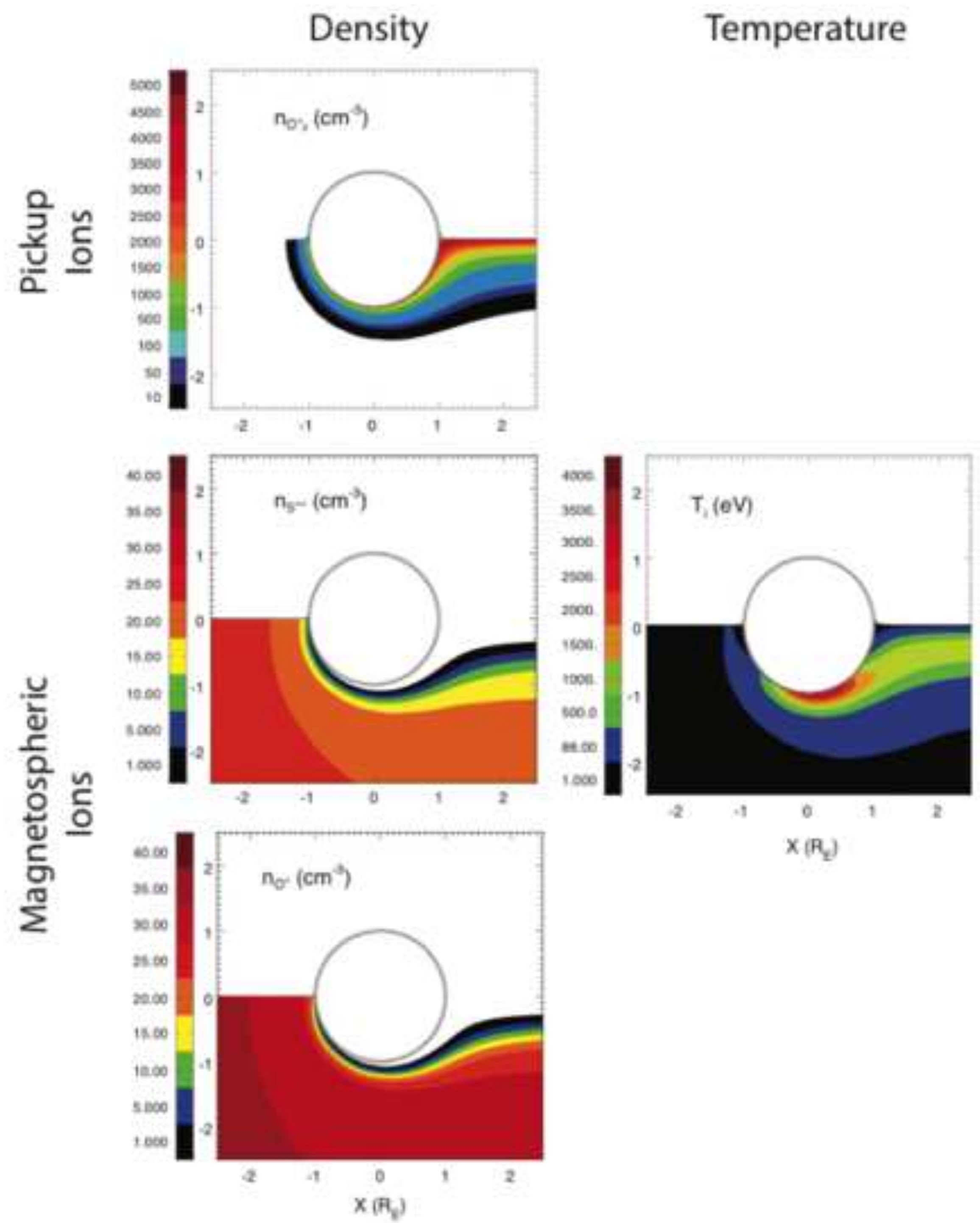

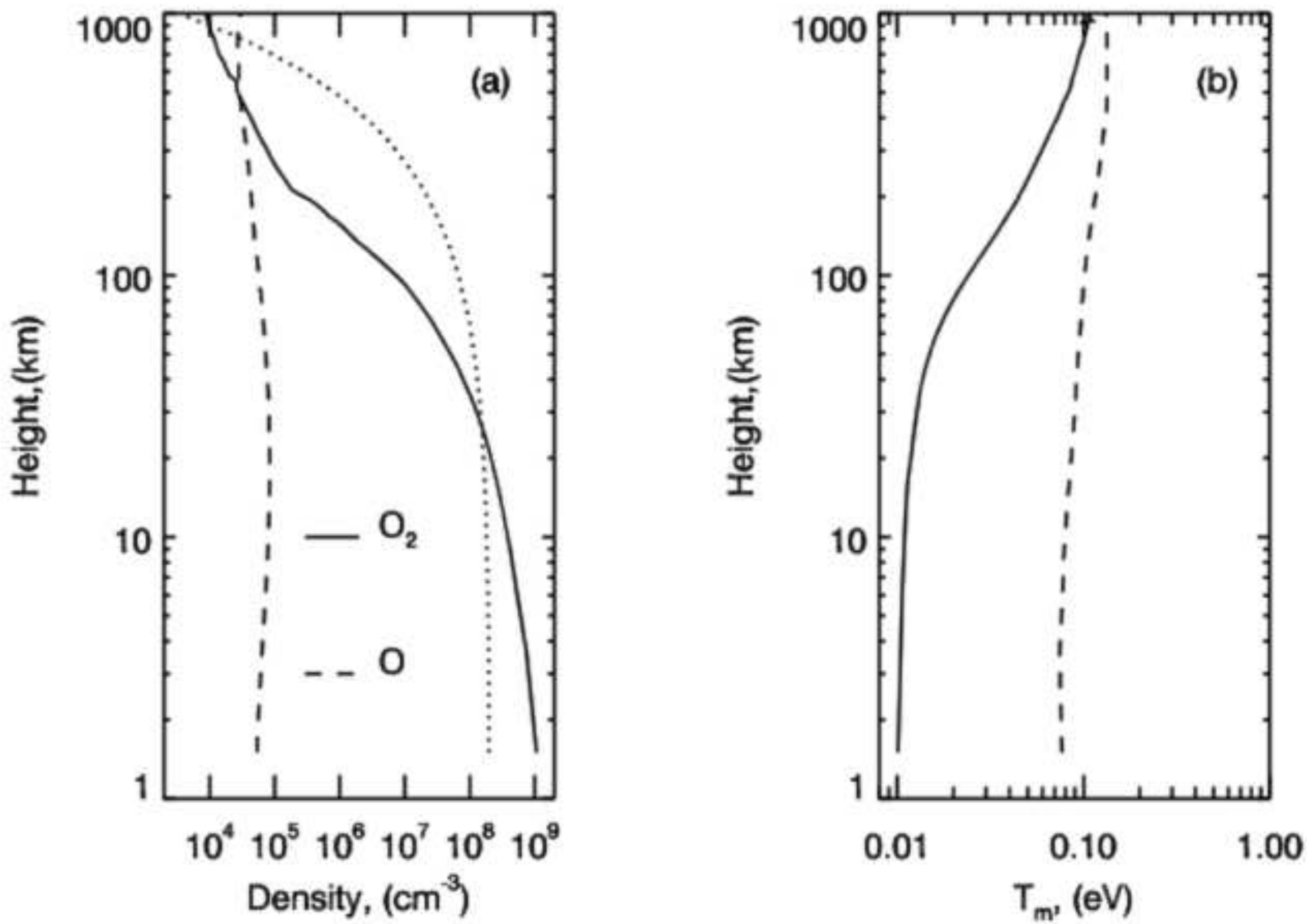
(a)
(b)
Height,(km)
1000
100
10
1
O2
O
10^4 10^5 10^6 10^7 10^8 10^9
Density, (cm^-3)
0.01
0.10
1.00
Tm, (eV)

figure 21 Click here to download figure Figure_21_new.tif

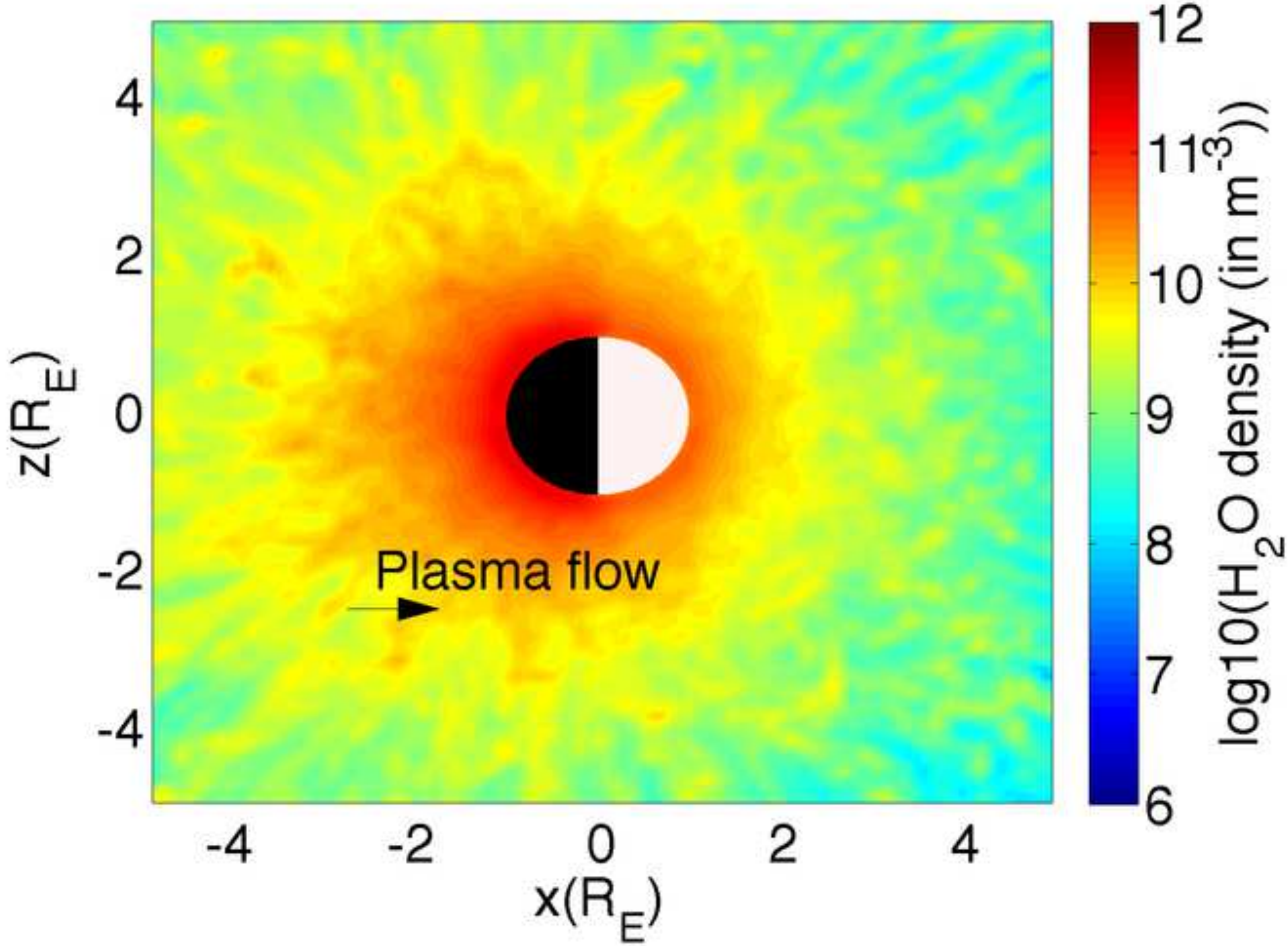

figure 22

Click here to download figure Figure_22.tiff

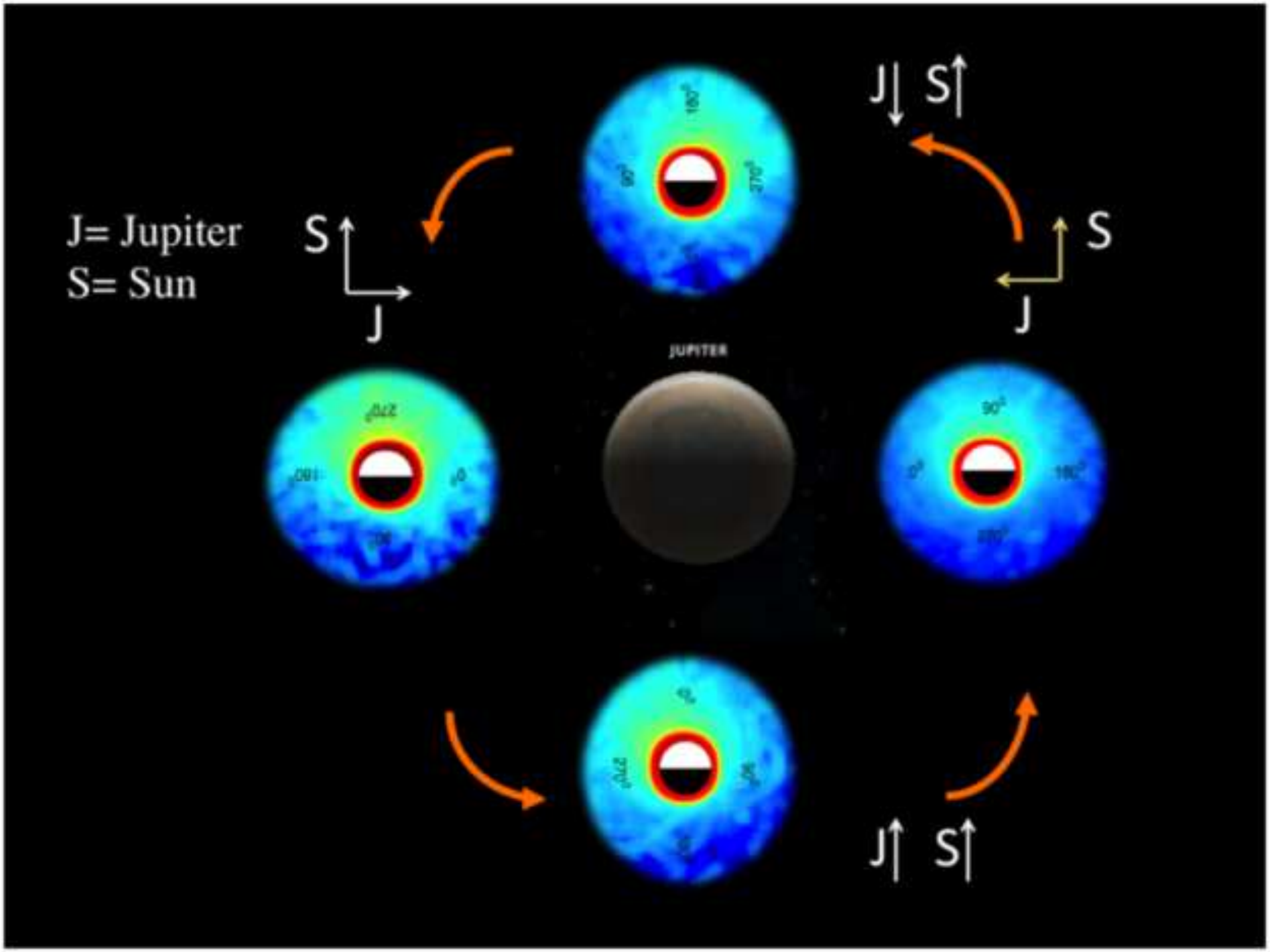

figure 23 Click here to download figure Figure_23.tiff

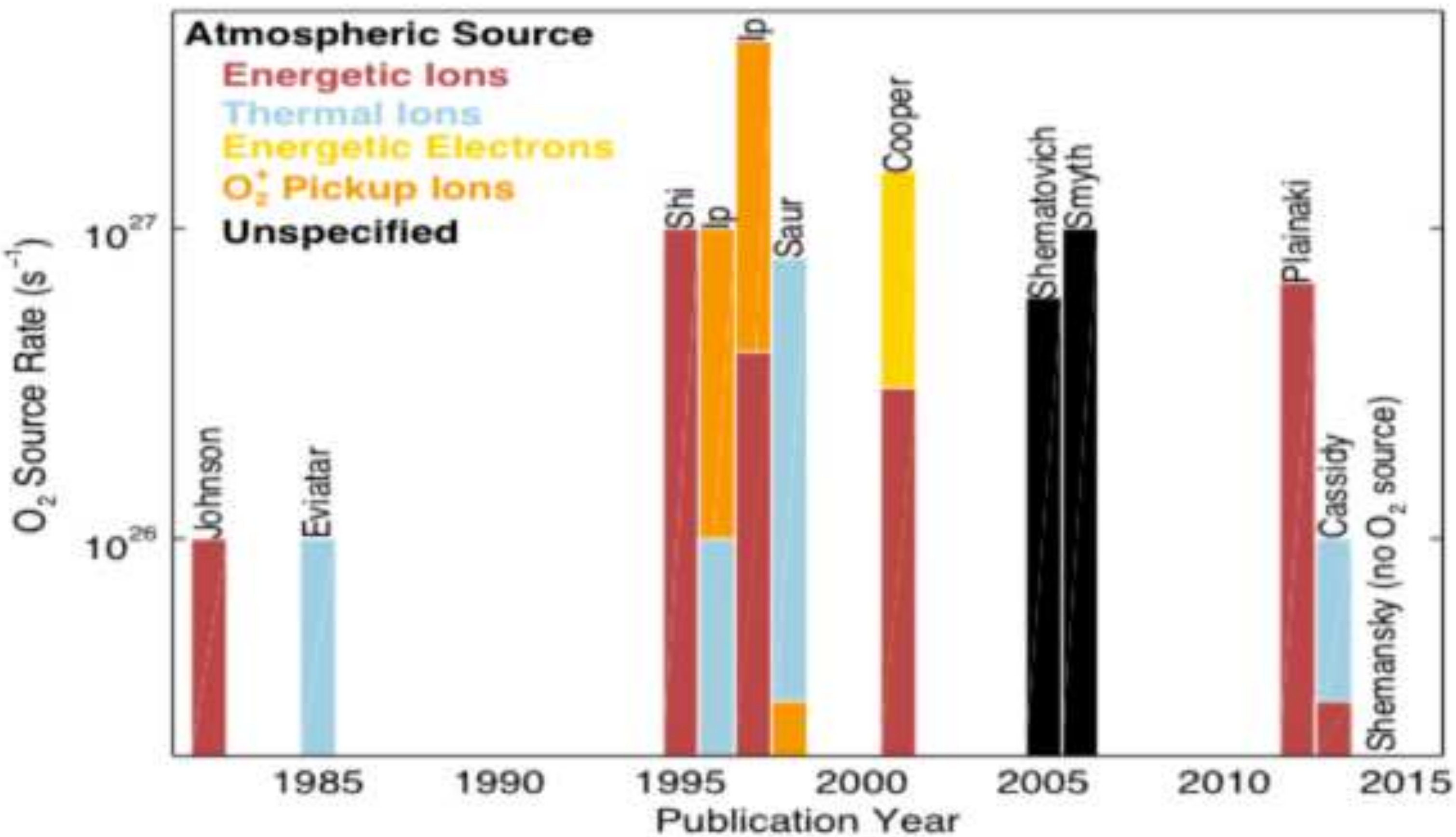

figure 24

Click here to download figure Figure_24.eps

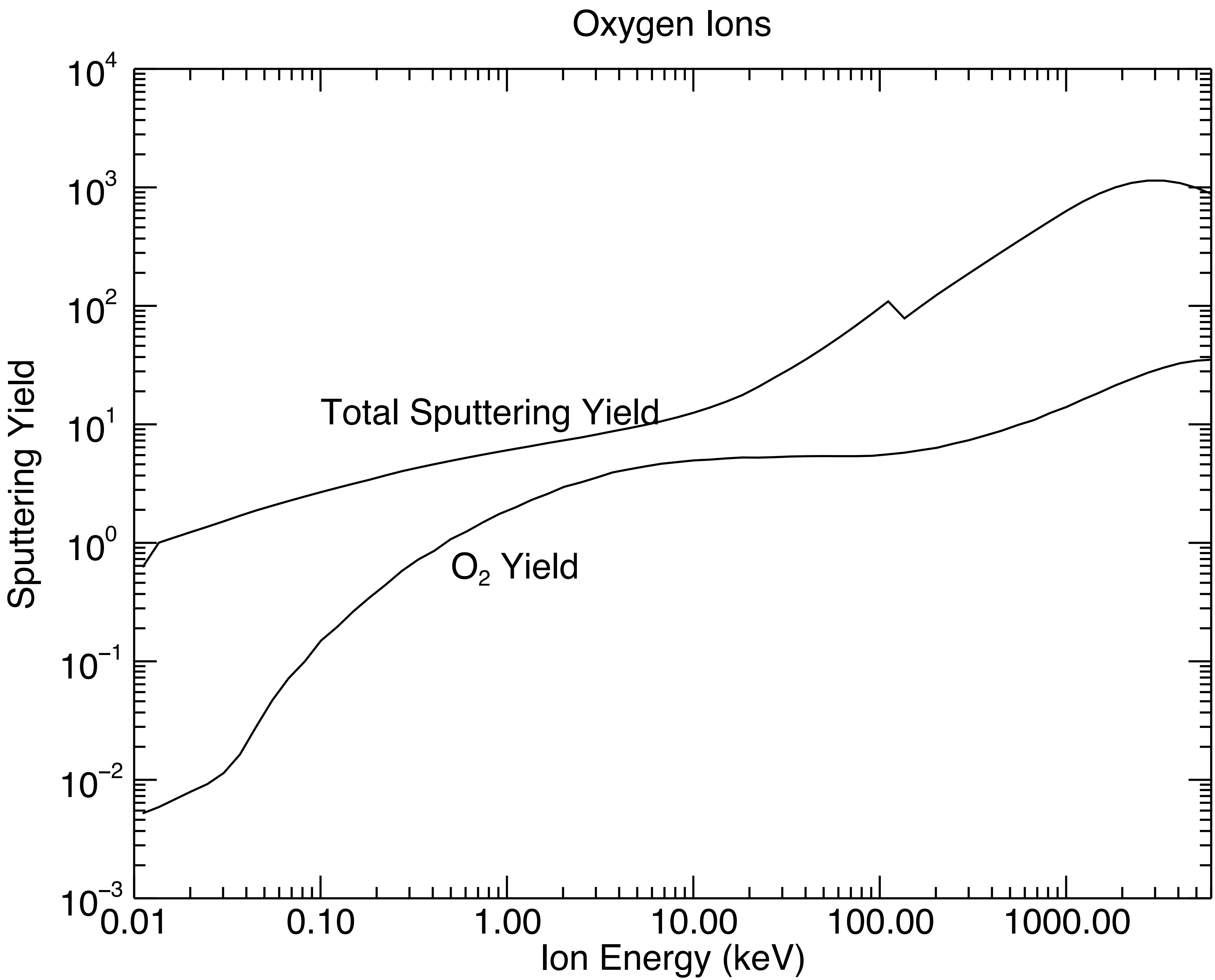

figure 25

Click here to download figure Figure_25.tiff

Table 1: Overview of the observations of Europa's tenuous atmosphere

Oxygen atmosphere	**Related publications**	**Years**	**Obs. days / visits**	**Total integration time**	**Main findings on Europa's atmosphere**
HST/GHRS *	Hall et al. 1995; 1998	1994 / 1996	3	337 min	- First detection of oxygen atmosphere- - O_2 main species
HST/STIS #1 *	McGrath et al. 2004	1999	1	156 min	- First images of oxygen emissions - Irregular oxygen aurora morphology
Cassini UVIS *	Hansen et al. 2005 / Shemansky et al. 2014	2001	2	967 min	- Extended atomic oxygen cloud
NH/Alice	Retherford et al. 2007	2007	~6	104 min	- Confirm ratio of 2 for O_2 main species
HST/ACS	Saur et al. 2011 / Sparks et al. 2010 / Retherford et al. 2007	2007 - 2008	3	343 min	- Correlation of oxygen brightness to Europa's magnetospheric position (Saur et al. 2011)
HST/STIS #2	Roth et al. 2014a,b; 2016	2012 / 2014 - 2015	19	2639 min	- Transient H_2O plume outgassing activity - Systematic correlation of aurora morphology and brightness to the magnetosphere - Consistently brighter dawn side aurora - Differing oxygen line ratio between upstream and downstream hemispheres - Oxygen aurora unchanged in eclipse
Trace species					
Mt. Bigelow *	Brown and Hill, 1996	1995	1	20 min	- First detection of sodium
Keck HIRES *	Brown 2001	1998	2	10, 20, 600, 1800 sec	- First detection of potassium, and contemporary measurements of sodium and potassium in the region 5-15 R_E - First Na/K ratio (similar to cosmic abundance)
Keck HIRES *	Leblanc et al. 2002	1999	1	4, 15 min	- Sodium vertical profiles up to 40 R_E
KPNO McMath*	Leblanc et al. 2005	2000	3	600, 1800 sec	- Sodium velocity profiles
Cassini ISS *	Porco et al. 2003 / Cassidy et al. 2008	2001			- Visible auroral emissions in eclipse detected
HST/FOS	Horst and Brown 2013	1994	2	35, 924, 1100 sec	- No detection of Magnesium, only upper limit

*see McGrath et al. 2009 for a more detailed review of these observations

Table 2: Comparison among the plasma model assumptions.

	Saur et al. (1998)	Kabin et al. (1999)	Liu et al. (2000)	Schilling et al. (2007, 2008)	Rubin et al. (2015)
Modeling approach	Numerical solution to Ohm's law, 3D two-fluid plasma model, fixed B field	3D single-fluid MHD model	2 species ideal MHD model	3D single fluid MHD	3D multifluid MHD
Simulation domain	Cartesian grid with 20 km resolution	Cartesian grid variable grid size.	Cartesian, extending $-192R_E \leq x \leq 64R_E$; $-128R_E \leq y$; $z \leq 128R_E$, variable grid size.	Cartesian, +/- 10 R_E extent in x-y plane, +/- 60 along z. Variable grid size.	Spherical, -32 R_E to 32 R_E extent on all axes and variable grid size
Electron modeling	Separate magnetospheric and ionospheric electrons	Single electron population	Single electron population	Single electron population	Single electron population
Electron heat conduction	Included	Not included	Not included	Not included	Included
Modeled ion species	Single ion species stands in for both O^+ and O_2^+	Single ion species stands in for O^+ and O_2^+	Magnetospheric O^+ and pickup O_2^+	Single ion species stands in for O^+ and O_2^+	Magnetospheric O^+ and pickup O_2^+
Inner boundary conditions	Electric potential determined by ionospheric conductivity.	2 cases: perfectly conducting sphere and a perfectly absorbing sphere	Magnetospheric ion density set to 0, velocity set to 0, field set to sum of background Jovian and induced dipole.	Solid body is described by the concept of virtual plasma	Floating boundary condition; field inside of moon set to sum of background Jovian and induced dipole. Boundary permits plasma flow into surface.
Ocean induction	Not included: assumed constant homogenous Jovian background field (not self-consistent)	Included	Included	Included	Included
Neutral atmosphere model (surface density, scale height, column density)	single fluid of O_2 molecules, asymmetric atmospheric surface dens. (ratio surface density trailing/leading hemisphere~2.3), H=150 km, column density: $5\cdot10^{18}m^{-2}$	None	hydrostatic O_2 atmosphere (surface dens.:$2.85\cdot10^7$ cm^{-3}, scale height:175 km, column density: $5\cdot10^{18}m^{-2}$)	Similar to Saur et al.	Similar to Saur et al., but includes two scale heights to model extended atmospheric corona.
Ionization source and total rate	Electron impact ionization	Electron impact ionization	Electron impact ionization	Electron impact ionization	Electron impact ionization
Collisions between particles	Ion-neutral collisions	Ion-neutral collisions	Estimated to be neglible	Ion-neutral collisions	Ion-neutral
Plasma loss	Dissociative recombination, absorption by moon, and, implicitly, charge exchange	Dissociative recombination and absorption by moon	Dissociative recombination and absorption by moon	Dissociative recombination	Dissociative recombination and absorption by moon
modeled data	HST oxygen emission observations	E4	E4 (density, plasma temperature, speed, magnetic field)	E4 (magnetic field)	E4, E26

Table 3

Click here to download table Table_03_exo_models_v08.pdf

Table 3: Comparison among the atmosphere model assumptions.

	Ip et al. 1996; 1998	Saur et al. 1998	Shematovich and Johnson 2001	Shematovich et al. 2005	Tiscareno and Geissler 2003	Smyth and Marconi 2006	Cassidy et al. 2007	Cassidy et al. 2009	Plainaki et al. 2012; 2013; Milillo et al. 2016	Wurz et al. 2014	Shemansky et al. 2014
Validity range (vertical altitude coverage)	6 R_E	Up to a few Europa radii	up to ~1000 km from the surface	up to ~1000 km from the surface	N/A	up to ~1000 km from the surface	8R_E	400 km	up to 4 R_E; infinity (Hill radius) (2016)	exobase - infinity (Hill radius)	not described
Spatial resolution	Not specified	20 km	1.5 km	1.5 km	10° latitude	Not described	N/A	N/A	0.1R_E	> 1km (variable : > mean free path)	not described
Included species	H_2O, O_2, H_2	O_2	O_2 and O	H_2O,OH,O_2, O, H_2,H	H_2O	O_2, H_2O, H_2, OH, O, H	O_2	H_2O, Na, CO_2, SO_2	H_2O, O_2, H_2	H_2O, OH, O_2, O, H, H_2, various volatiles, various minerals	O_2, H_2O, H_2, OH, O, H
Included source process:											
surface sputtering	Yes	yes	yes	yes	yes	yes	yes	yes	Yes	Yes	Yes
radiolysis	No	no	no	yes	no	yes	yes	no	Yes	Yes	No
sublimation			no				no	yes	Estimation	Yes	
PSD	No	no	no	no	no	no	no	no	No	Yes	No
MIV	No	no	no	no	no	no	no	no	Estimation	Yes	No
O_2^+ dissociative	No	no	yes	yes	no	no	no	no	No	no	yes

recombination											
Other	pickup-ion sputtering (1996)	Adjustable source rate	Yes (O_2, photo- and electron impact dissociation)	Yes (H_2O, O_2, and OH photo- and electron impact dissociation)							Includes process called "Exchange sputtering"
Included Loss processes											
Ionization/dissociation from particles (ions, e)	yes	yes	Yes,	Yes,	yes	yes	yes	yes	Yes	ions: no, e: yes	yes
Elastic collisions (moment transfer) between magnetosph. ions and neutrals	no	yes	yes	yes	no	yes	no	no	No	No	yes
Ionization/dissociation from UV photons	no	No (estimated to be negligible)	yes	no	no	no	yes	yes	No	Yes	no
Charge exchange with magnetospheric ions	no	yes	yes	yes	no	yes	no	no	Estimated	No	yes
Charge exchange with pickup ions	no	no	Yes	yes	no	no	no	no	No	No	No
Particle multiple bouncing	O_2, (1998)	O_2	O_2,	O_2, H_2	No	O_2, H_2	O_2	O_2, H_2	O_2, H_2	No	No
Gravitational escape	Yes (1996)	no	Yes	yes	yes	yes	yes	yes	Yes	Yes	No
Radiation pressure	no	no	No	no	no	no	no	no	No	No	No

Neutral/Neutral collisions	no	no	Yes	yes	no	yes	no	no	No	No	No
Chemistry included	no	no	No	no	no	yes	no	no	No	No	yes
Dimensionality	2D	3D	1D spatial configuration, 3D velocity space configuration	1D spatial configuration, 3D velocity space configuration	2D	1D	3D	3D	3D	1D spatial configuration, 2D velocity space config.	1D
Orbital configuration	Not specified	Not specified	Not specified	Not specified	Not specified	Not specified	Not specified	Not specified	O_2	Not specified	Not specified
Surface release yield	Variety of experiments from mid-1980s and Johnson (1990) www.people.virginia.edu/~rej	N/A	free parameter	free parameter	Shi et al. (1995), Johnson (1990)	free parameter	free parameter	Johnson 1990 www.people.virginia.edu/~rej	Famà et al. 2008 formula	Cassidy et al. (2010), Shi et al. (1993), and Famà et al. (2008)	Aumayr and Winter (2004), Shemansky (2003)
Energy Distribution Function	O_2 sputtering distribution, thermal accommodation	N/A		H_2O and O_2 sputtering distribution, thermal accommodation	H_2O sputtering distribution	not described	O_2 sputtering distribution, thermal accommodation	See paper	H_2O: sputtering distribution (Sigmund, 1969); O2, H2: Johnson et al., 1983.Thermal accomodation for O_2 and H_2 re-impacting the surface	H_2O: sputtering distribution (Sigmund, 1969; Wurz and Lammer 2003); Sublimated H_2O: Maxwellian distribution;	not described

										PSD-ed H_2O: Johnson (2002)	
Plasma Flow Geometry	2D MHD solution to flow around cylinder	2D electric field calculati on. Fixed B field.	Not applicable	Not applicable	Lunar-like	Lunar-like	Lunar-like	Lunar -like	Lunar-like	Not applicable	Lunar-like
Model free (tunable) parameters	Not specified	O2 surface density/ depletio n length scale	Not specified	Source rate	Ion bomba rdmen t patter n	Source rate	Stickin g coeffici ent, source rate	N/A	energetic ion spectrum, precipitation map, surface Temperature, orbital position	Not specified	Not specified

Table 4 Click here to download table Table_04_exo_models_v07.pdf

Table 4: Comparison among the atmosphere model outputs

	Ip et al. 1996; 1998	Saur et al. 1998	Shematovich and Johnson 2001	Shematovich et al. 2005	Tiscareno and Geissler 2003	Smyth and Marconi 2006	Cassidy et al. 2007	Cassidy et al. 2009	Plainaki et al. 2012; 2013; Milillo et al. 2016	Bern model	Shemansky et al. 2014
Density spatial distribution H_2O	no	Not applicable	Not applicable	average case	2D	1D	Not applicable	3D	3D	1D	Not applicable
Density spatial distribution O_2	2D (1996)	3D	average case	average case	Not applicable	1D	3D	no	3D	1D	Not applicable
Density spatial distribution H_2	no	Not applicable	Not applicable	Average case	Not applicable	1D	Not applicable	no	3D	1D	Not applicable
Density spatial distribution minor species	Not applicable	Not applicable	average case (O)	average case (O, OH)	Not applicable	1D	Not applicable	3D	Not applicable	1D	average case (O)
Near-surface O_2 scale height	~20 km	145 km	~ 20 km	~ 20 km	Not applicable	~ 20 km	~ 20 km	Not applicable	~ 20 km	~20 km (sublimated) ~600 km (sputtered)	Not applicable
Neutral supply to the torus	Yes (1998)	no	Yes (O)	Yes (H,H2,O)	yes (H_2O)	yes	no	no	Yes	yes	No
Ion supply to the magnetosphere (mass loading)	yes	yes	yes	yes	no	no	no	no	Yes	yes	No
Energy spectrum of the released neutrals	no	no	yes	yes	yes	no	no	yes	Yes	yes	No

self-consistent ionosphere creation	Yes(1996)	yes	no	no	no	no	no	no	No	no	No

Table 5: Interdisciplinary science goals, objectives and requirements related to the Europa atmospheric science

Notes: The JUICE Science Objectives related to Europa as defined in the Red Book, were numbered as follows: 1. Determine the composition of the non-ice material at Europa, especially as related to habitability; 2. Search for liquid water under the most active sites at Europa; 3. Study the recently active processes at Europa; 4. Understand the moons as sources and sinks of Jupiter's magnetospheric plasma.

Interdisciplinary Science Goal of the current proposal	Science objective of the current proposal	Related JUICE Science Objectives	Requirements	
			JUICE Payload Instruments in simultaneous operation	Notes
G1. Characterization of the atmospheric environments of Europa	G1.1. Identify the local composition and determine the density spatial and energy distribution of the main constituents of Europa's exosphere	1;3	JANUS, MAJIS, PEP-JDC, PEP-JNA, PEP-NIM, SWI, UVS	phase 2.b (Europa flybys)
	G1.2. Search for residuals in the exosphere of recent plume activity	2;3		
G2. Investigation of the interactions between the tenuous atmosphere of Europa and the Jovian magnetosphere, with respect to the relation between the time-scales of their variations	G2.1. Determine the neutral escape and the ion-supply to the Jovian magnetosphere	4	PEP-JDC, PEP-JEI, PEP-JNA, PEP-JoEE, RPWI	phase 2.b (Europa flybys)
	G2.2. Identify the variability of Europa's gas cloud with changes of the Jovian plasma conditions and to the moon's induced magnetic field	4	J-MAG, PEP-JDC, PEP-JoEE, PEP-JEI, PEP-JENI, RPWI, UVS	phase 2.b (Europa flybys) phase 2.c (Jupiter inclined orbit)?
	G2.3. Determine the role of Io in supplying plasma to the tenuous atmosphere of Europa and investigate the related temporal variability	4	MAJIS, PEP-JENI, RPWI, UVS	phase 2.c (Jupiter inclination orbit)
G3. Study of the moon atmosphere - surface coupling as a main agent for both the exosphere generation and surface weathering	G3.1. Determine local plasma composition at Europa above the surface regions with major concentration in non-icy components; determine their relation with the exosphere composition	1; 2; 3	MAJIS, PEP-JDC, PEP-JEI, PEP-JNA, PEP-JoEE, PEP-NIM, RPWI, SWI, UVS	phase 2.b (Europa flybys)
	G3.2. In case of the existence of plumes at Europa, identify their implications to the moon's local surface composition	2; 3	JANUS, MAJIS, PEP-NIM, UVS	phase 2.b (Europa flybys)